MODELLING OF ACOUSTIC EMISSION GENERATED IN SPUR GEAR PAIR AND ROLLING ELEMENT BEARING

Ph.D. Thesis

By

RAM BIHARI SHARMA

DISCIPLINE OF MECHANICAL ENGINEERING

INDIAN INSTITUTE OF TECHNOLOGY INDORE

SEPTEMBER 2017

MODELLING OF ACOUSTIC EMISSION GENERATED IN SPUR GEAR PAIR AND ROLLING ELEMENT BEARING

A THESIS

Submitted in partial fulfillment of the requirements for the award of the degree
of

DOCTOR OF PHILOSOPHY

by

RAM BIHARI SHARMA

DISCIPLINE OF MECHANICAL ENGINEERING

INDIAN INSTITUTE OF TECHNOLOGY INDORE

SEPTEMBER 2017

INDIAN INSTITUTE OF TECHNOLOGY INDORE

CANDIDATE'S DECLARATION

I hereby certify that the work which is being presented in the thesis entitled **MODELLING OF ACOUSTIC EMISSION GENERATED IN SPUR GEAR PAIR AND ROLLING ELEMENT BEARING** in the partial fulfillment of the requirements for the award of the degree of **DOCTOR OF PHILOSOPHY** and submitted in the **DISCIPLINE OF MECHANICAL ENGINEERING, INDIAN INSTITUTE OF TECHNOLOGY INDORE**, is an authentic record of my own work carried out during the time period from **January 2014** to **September 2017** under the supervision of **Dr. Anand Parey**, Associate Professor, IIT Indore

The matter presented in this thesis has not been submitted by me for the award of any other degree of this or any other institute.

Signature of the student with date

(RAM BIHARI SHARMA)

This is to certify that the above statement made by the candidate is correct to the best of my/our knowledge.

Signature of Thesis Supervisor with date
(Dr. ANAND PAREY)

RAM BIHARI SHARMA has successfully given his/her Ph.D. Oral Examination held on **………..**

Signature of Thesis Supervisor
Date:

Convener, DPGC
Date:

Signature of PSPC Member #1
Date:Date:

Signature of PSPC Member #2
Date:

Signature of External Examiner
Date:

ACKNOWLEDGEMENTS

First and everlasting, I would like to express my all praise and thanks for GOD, who gave me the strength and patience to carry out this research work in this good manner.

I would like to express my sincere gratitude to my supervisor **Dr. Anand Parey** for his splendid guidance, support, and encouragement during these several years of research work. I wish to have his valuable support in future as well. I am very thankful for his dedicated supervision and without him the work reported in this thesis would not have been possible. I appreciate the time he spent with me on realizing this work both theoretically and experimentally.

I express my sincere thanks to **Prof. Pradeep Mathur**, Director, IIT Indore, and Deans of Academic Affair, Research and Development and Student Affairs for their kind support and providing appropriate facilities.

I would like to thank my PSPC committee members, **Dr. Ritunesh Kumar** and **Dr. Ram Bilas Pachori**, for their valuable suggestions right from the beginning of my research work.

I express my sincere thanks to **Dr. Anil Kumar Emadabathuni** and **Dr. Devendra Deshmukh,** Former and Present Head of the department, Mechanical Engineering for providing me an opportunity and necessary infrastructure to carry out my research work.

I express my very sincere thanks to **Prof. N. Tandon** and technical staff of Dynamics Laboratory of IIT Delhi for kind support and guidance during the experimental investigation on IEA gear lubrication testing machine.

I am indebted to the technical staff of the Solid Mechanics Laboratory, Metrology Laboratory, Advance Manufacturing Process Laboratory, Central Workshop, and Smart Manufacturing Laboratory of IIT Indore for their valuable support for conducting the experiments. I would like to express my special thanks to **Mr. Sandeep Patil, Mr. Kailash Patel, Mr.**

Santosh Sharma, Mr. Anand Petare, **Mr. Amit Jain**, and **Mr. Deepak Rathore.**

I extend my thanks to all the staff members of Discipline of Mechanical Engineering, Central library, Academic section, Accounts section, and all disciplines of IIT Indore for their kind cooperation.

I would like to thank all of my friends who have been extremely supportive, especially, **Mr. Naresh Kumar Raghuvanshi, Mr. Vikas Sharma, Mr. Ankur Saxena, Mr. Pavan Gupta, Mr. Dada Saheb Ramteke, Mr. Amit Kumar Jain, Mr. Vinod Singh,** and **Mr. Saurav Yadav** for their endless support and encouragement.

I would like to special thank to **Mr. Sandeep Patil,** Deputy Manager of Solid Mechanics Lab for his support throughout my research work.

And last, but not least, my most especial gratitude is to my **parents**, to all my **family members** and **friends** for trusting in me and for their support and encouragement during all these years.

I would like to heartfelt thanks to my mother **Mrs. Leelabati Sharma**, my father **Mr. Mayaram Sharma**, (who are at the root of every effort embedded in my whole life) my best friend and wife **Mrs. Sangeeta Sharma,** and my daughter **Ms. Anika Sharma** for their continuous support, love and affection during all these years of research work.

Once again, I would like to express my sincere thanks to all those people who have helped me a lot in the accomplishment of this PhD thesis.

Ram Bihari Sharma

ABSTRACT

Gears and bearings are the most important components which are widely used in various applications such as automobiles, industrial machines, power plants, etc. The failure of these components is one of the most frequent causes of the machine breakdown. Hence, health monitoring or fault diagnosis of gearboxes and bearings is an important aspect to prevent unwanted shutdowns/catastrophic failures of the machines in advance and to ensure reliability and low operating cost. Various techniques like vibration monitoring, acoustic measurements, thermography, ultrasonic testing, acoustic emission (AE), and wear debris analysis etc. are used for condition monitoring of gearboxes and bearings.

AE is a very effective technique for the health monitoring and diagnostics of rotating machine components. Several experimental investigations have been found in the literature which show the effectiveness of AE in identifying the fault/defect in gears and bearings.

The literature reviewed has revealed that gear operating parameters as well as bearing operating parameters such as speed, load, specific film thickness of lubrication, and temperature strongly influence the AE energy during the operation of gears and bearings. It has also been identified that the presence of the defect on the gear tooth and bearing elements as well as defect size strongly affects to the AE level. Furthermore, it has been concluded in the experimental studies that asperity contact is a potential source of AE generation during the operation of gears and bearings. A fine correlation between asperities contact and AE value has been reported. But, there is no theoretical or mathematical model available to comprehend the physical mechanism of AE generated during the gear and bearing operation. In this thesis, the theoretical or mathematical models are developed for spur gear pair and rolling element bearing for healthy as well as defected condition by using approaches of contact mechanics and linear elastic fracture mechanics. These mathematical models correlate the energy of AE to operational parameters of gears and bearings as well as parameters related to defect. The mathematical models are developed for AE generated in healthy spur gear pair, spur gear pair with crack, spur gear pair with pitting. The mathematical models are also developed for AE generated in rolling element bearing in healthy as well as defected condition i.e. defect on inner-race, outer-race, and rolling element. The developed models were validated on the basis of experimental studies and satisfactory results have been observed. It shows the potential of the developed models to perceive the AE generated during the gear and bearing operation which is the significant factor in the condition monitoring of spur gear and rolling element bearing.

Keywords: Acoustic emission; gear; bearing; modelling; asperity contact; gear operating parameters; bearing operating parameters; friction; load sharing factor; lubrication; dynamic factor; crack; crack propagation; fracture; stress intensity; defect; surface topography; pitting; protrusion contact.

TABLE OF CONTENTS

Table of Contents (continued) **Page No.**

Table of Contents (continued) **Page No.**

Table of Contents (continued) **Page No.**

LIST OF FIGURES

LIST OF TABLES

NOMENCLATURE

a	crack length in gear tooth
a_i	radius of Hertzian contact area for inner race-rolling element contact
a_o	radius of Hertzian contact area for outer race-rolling element contact
a_r	radius of Hertzian contact area for gear teeth contact
A_c	total apparent contact area of one pair of teeth during meshing of gears
A_{ci}	total apparent contact area between rolling element and inner race during the load zone
A_{co}	total apparent contact area between rolling element and outer race during the load zone
A_d	the portion of contact area of gear tooth surface which is having protrusions around the produced defect
A_{di}	total apparent contact area of defect exist on inner race
A_{do}	total apparent contact area of defect exist on outer race
A_{dr}	total apparent contact area of defect exist on rolling element
A_r	the contact area of gear tooth surface excluding the contact area A_d and the area of defect (pit)
AE rms	root mean square value of acoustic emission
B	width of gear tooth
C	distance between the contact point and the central line of the tooth
C_e	part of the total elastic strain energy which alters into AE pulses
C_m	part of the total elastic strain energy received by the AE sensors/ AE measurement instruments

d	separation between smooth surface of gear tooth and the reference plane in the rough surface of another gear tooth
d_i	separation between smooth surface of rolling element and the reference plane in the rough surface of inner race
d_{id}	separation between smooth surface of rolling element and the reference plane in the rough surface of defect exist on inner race
d_o	separation between smooth surface of rolling element and the reference plane in the rough surface of outer race
d_{od}	separation between smooth surface of rolling element and the reference plane in the rough surface of defect exist on outer race
d_{rid}	separation between smooth surface of inner race and the reference plane in the rough surface of defect exist on rolling element when contact with inner race
d_{rod}	separation between smooth surface of outer race and the reference plane in the rough surface of defect exist on rolling element when contact with outer race
D	diameter of defect (pit) on the pitch line of gear tooth surface
D_e	pitch diameter in bearing
D_i	diameter of inner race-rolling element contact
D_o	diameter of outer race-rolling element contact
D_r	diameter of rolling element of bearing
E_{ei}	stored elastic energy in the contact of individual asperity for inner race-rolling element contact
E_{eo}	stored elastic energy in the contact of individual asperity for outer race-rolling element contact
E_i	stored elastic energy in the contact of individual asperity for gear teeth surface contact

$\bar{E}_{ia}$	stored mean elastic energy in the contact of individual asperity
E_r	energy release rate available for growth of crack extension
E_{AE}	total elastic strain energy accumulated by the AE instrument in the form of AE signal during the duration ΔT
E_T	total elastic energy stored due to the asperity contacts in N_r number of revolutions of gears
E_{Ti}	total elastic energy stored due to the asperity contacts in N_{r_b} number of revolutions of bearing for the inner race-rolling element contact
E_{To}	total elastic energy stored due to the asperity contacts in N_{r_b} number of revolutions of bearing for outer race-rolling element contact
E'	Hertzian contact modulus
E'_{AE}	elastic energy rate of AE produced by total asperity contacts
E'_{AE_d}	elastic energy rate of acoustic emission produced by total protrusion contacts in contact area A_d
E'_{AE_r}	elastic energy rate of acoustic emission produced by total asperity contacts in contact area A_r
E'_T	elastic strain energy rate released by asperity contacts
F_r	total radial load in bearing
F_ψ	theoretical radial contact load received by each rolling element at angle ψ during the loading zone
h	standardized separation
$J_r(\epsilon)$	radial integral
k_v	dynamic factor
k_t	mesh stiffness
K_I	stress intensity factor

L	distance between the contact point and the edge crack situated on tooth root
$LSF_{DEPSTC(1)}$	load sharing factor corresponding to defect with protrusion end point (at respective defect diameter) of single tooth contact for the new tooth pair
$LSF_{DSPSTC(1)}$	load sharing factor corresponding to defect with protrusion start point (at respective defect diameter) of single tooth contact for the new tooth pair
$LSF_{HPDTC(1)}$	load sharing factor corresponding to highest point of double tooth contact for the new tooth pair during engagement
$LSF_{HPDTC'(2)}$	load sharing factor corresponding to highest point of double tooth contact for the previous tooth pair during disengagement
$LSF_{HPDTC(3)}$	load sharing factor corresponding to highest point of double tooth contact for the next tooth pair during engagement
$LSF_{HPDTC'(1)}$	load sharing factor corresponding to highest point of double tooth contact for the new tooth pair during disengagement
$LSF_{HPSTC(1)}$	load sharing factor corresponding to highest point of single tooth contact for the new tooth pair
$LSF_{LPSTC(1)}$	load sharing factor corresponding to lowest point of single tooth contact for the new tooth pair
$LSF_{TD(1)}$	load sharing factor corresponding to the tooth disengagement for the new tooth pair
$LSF_{TD(2)}$	load sharing factor corresponding to the tooth disengagement for the previous tooth pair
$LSF_{TE(1)}$	load sharing factor corresponding to the tooth engagement for the new tooth pair
$LSF_{TE(3)}$	load sharing factor corresponding to the tooth engagement for the next tooth pair
N	count rate of AE signal

N_a	asperity density i.e. asperities in the unit contact area of a one pair of teeth during meshing of gears
N_{ai}	asperity density i.e. asperities in the unit contact area of inner race-rolling element contact during load zone
N_{ai_d}	asperity density i.e. asperities in the unit contact area of defect exist on inner race
N_{ao}	asperity density i.e. asperities in the unit contact area of outer race-rolling element contact during load zone
N_{ao_d}	asperity density i.e. asperities in the unit contact area of defect exist on outer race
N_{ari_d}	asperity density i.e. asperities in the unit contact area of defect exist on rolling element when contact with inner race
N_{aro_d}	asperity density i.e. asperities in the unit contact area of defect exist on rolling element when contact with outer race
N_e	total number of rolling elements in bearing
N_r	number of revolutions of gear
N_{r_b}	number of revolutions of bearing
N_T	total number of asperity contacts during the meshing of gears
$N_{T_{(1EH)}}$	total number of asperity contacts in the meshing of gears during the contact area between tooth engagement and highest point of double tooth contact for the new tooth pair
$N_{T_{(1HD)}}$	total number of asperity contacts in the meshing of gears during the contact area between the highest point of double tooth contact and tooth disengagement for the new tooth pair
$N_{T_{(1LH)}}$	total number of asperity contacts in the meshing of gears during the contact area between the lowest point of single

tooth contact and highest point of single tooth contact for the new tooth pair

$N_{T_{(1LH)_d}}$ total number of asperity contacts in the meshing of gears during the contact area between the lowest point of single tooth contact and highest point of single tooth contact for the new tooth pair excluding the contact area $(\mathrm{A_d} + \pi/4(\mathrm{D})^2)$ at respective defect diameter.

$N_{T_{(2HD)}}$ total number of asperity contacts in the meshing of gears during the contact area between the highest point of double tooth contact and tooth disengagement for the previous tooth pair

$N_{T_{(3EH)}}$ total number of asperity contacts in the meshing of gears during the contact area between the tooth engagement and highest point of double tooth contact for the next tooth pair

p_a load shared by asperities for respective area

p_i load supported by the pair of teeth at particular local contact during mesh cycle

p_p load shared by protrusions

P normal load acting on surface of gear tooth

$P(z)$ probability of randomly selected variable z

r total number of rolling elements in the load zone of bearing

r_b radius of rolling element in bearing

r_s radius of spherical asperity for gear teeth surface contact

r_{si} radius of spherical asperity for inner race-rolling element contact

r_{so} radius of spherical asperity for outer race-rolling element contact

$r^{'}$ reduced radius of the curvature during Hertzian contact area for gear teeth surface contact

r'_i	reduced radius of the curvature during Hertzian contact area for inner race-rolling element contact
r'_{id}	reduced radius of the curvature during Hertzian contact area for the defect exist on inner race-rolling element contact
r'_o	reduced radius of the curvature during Hertzian contact area for outer race-rolling element contact
r'_{od}	reduced radius of the curvature during Hertzian contact area for the defect exist on outer race-rolling element contact
r'_{rid}	reduced radius of the curvature during Hertzian contact area for the defect exist on rolling element- inner race contact
r'_{rod}	reduced radius of the curvature during Hertzian contact area for the defect exist on rolling element- outer race contact
r_1	radius of assumed plane surface during asperity contact at any point on the involute surface of gear
$r_{1DEPSTC(1)}$	radius of tooth surface of gear at the point of contact (at respective defect diameter) corresponding to the defect with protrusion end point of single tooth contact for the new tooth pair
$r_{1DSPSTC(1)}$	radius of tooth surface of gear at the point of contact (at respective defect diameter) corresponding to the defect with protrusion start point of single tooth contact for the new tooth pair
$r_{1HPDTC(1)}$	radius of tooth surface of gear at the point of contact corresponding to the highest point of double tooth contact for the new tooth pair during engagement

$r_{1HPDTC'(2)}$	radius of tooth surface of gear at the point of contact corresponding to the highest point of double tooth contact for the previous tooth pair during disengagement
$r_{1HPDTC(3)}$	radius of tooth surface of gear at the point of contact corresponding to the highest point of double tooth contact for the next tooth pair during engagement
$r_{1HPDTC'(1)}$	radius of tooth surface of gear at the point of contact corresponding to the highest point of double tooth contact for the new tooth pair during disengagement
$r_{1HPSTC(1)}$	radius of tooth surface of gear at the point of contact corresponding to the highest point of single tooth contact for the new tooth pair
$r_{1LPSTC(1)}$	radius of tooth surface of gear at the point of contact corresponding to the lowest point of single tooth contact for the new tooth pair
$r_{1TD(1)}$	radius of tooth surface of gear at the point of contact corresponding to the tooth disengagement for the new tooth pair
$r_{1TD(2)}$	radius of tooth surface of gear at the point of contact corresponding to the tooth disengagement for the previous tooth pair
$r_{1TE(1)}$	radius of tooth surface of gear at the point of contact corresponding to the tooth engagement for the new tooth pair
$r_{1TE(3)}$	radius of tooth surface of gear at the point of contact corresponding to the tooth engagement for the next tooth pair
R_1	radius of pitch circle of pinion
R_2	radius of pitch circle of gear
S	distance from the boundary of defect (pit) corresponding to

	the area of the protrusions around the defect
S_t	gear tooth thickness at tooth root
t_c	transducer proportionality constant
$\bar{t}$	mean release time of the elastic energy due to asperity deformation for gear teeth surface contact
$\overline{t'_i}$	mean release time of the elastic energy due to asperity deformation for the inner race-rolling element contact
$\overline{t'_o}$	mean release time of the elastic energy due to asperity deformation for the outer race-rolling element contact
v	sliding velocity along the line of contact of the gear
v_i	linear velocity of rotating inner ring
v_r	linear velocity of rotating rolling element
v_{ri}	relative velocity between inner race and rolling element
v_{ro}	relative velocity between outer race and rolling element
$V(t)$	AE electrical signal
V_{rms}	root mean square value of acquired AE signal
$V_{rms(F)}$	total AE rms when load sharing during the one gear mesh is considered
$V_{rms(F)_b}$	total root mean square value of AE when contact load distribution during the load zone is considered
$V_{rms(FL)}$	total AE rms when load sharing and lubrication phenomenon during the one gear mesh are considered
$V_{rms(FL)_b}$	total root mean square value of AE when contact load distribution and lubrication effect during the load zone is considered
$V_{rms(FL)_{b_i}}$	total root mean square value of the generated AE by incorporating the effect of defect exists on inner race
$V_{rms(FL)_{b_o}}$	total root mean square value of the generated AE by incorporating the effect of defect exists on outer race

$V_{rms(FL)_{b_r}}$	total root mean square value of the generated AE by incorporating the effect of defect exists on rolling element
$V_{rms(FLD)}$	total AE rms when load sharing, lubrication and dynamic effect , all three phenomenon during the one gear mesh are considered
W	working depth of gear tooth
x	fractional constant for the contact load at an angle ψ i.e. F_{ψ}
x_g	number of teeth in gear
y	fractional constant for the radial load due to lubrication effect
$z(x)$	height of the rough surface profile i.e. asperities at a distance x from the mean line
z_d	height of the protrusions around the defect from the mean line

Greek Symbols

θ	angle of meshing
$\theta_{DEPSTC(1)}$	angle of meshing corresponding to defect with protrusion end point (at respective defect diameter) of single tooth contact for the new tooth pair
$\theta_{DSPSTC(1)}$	angle of meshing corresponding to defect with protrusion start point (at respective defect diameter) of single tooth contact for the new tooth pair
$\theta_{HPDTC(1)}$	angle of meshing corresponding to highest point of double tooth contact for the new tooth pair during engagement
$\theta_{HPDTC'(2)}$	angle of meshing corresponding to highest point of double tooth contact for the previous tooth pair during disengagement
$\theta_{HPDTC(3)}$	angle of meshing corresponding to highest point of double tooth contact for the next tooth pair during engagement

$\theta_{HPDTC'(1)}$	angle of meshing corresponding to highest point of double tooth contact for the new tooth pair during disengagement
$\theta_{HPSTC(1)}$	angle of meshing corresponding to highest point of single tooth contact for the new tooth pair
$\theta_{LPSTC(1)}$	angle of meshing corresponding to lowest point of single tooth contact for the new tooth pair
$\theta_{TD(1)}$	angle of meshing corresponding to the tooth disengagement for the new tooth pair
$\theta_{TD(2)}$	angle of meshing corresponding to the tooth disengagement for the previous tooth pair
$\theta_{TE(1)}$	angle of meshing corresponding to the tooth engagement for the new tooth pair
$\theta_{TE(3)}$	angle of meshing corresponding to the tooth engagement for the next tooth pair
θ_{T}	total angle of meshing during one mesh cycle
$\emptyset(z)$	probability density function (PDF) of randomly selected variable z i.e. the asperity heights for gear teeth surface contact
$\emptyset(z)_{i}$	probability density function (PDF) of the asperity heights for inner race-rolling element contact
$\emptyset(z)_{id}$	probability density function (PDF) of the asperity heights for the defect exist on inner race and rolling element contact
$\emptyset(z)_{o}$	probability density function (PDF) of the asperity heights for outer race-rolling element contact
$\emptyset(z)_{od}$	probability density function (PDF) of the asperity heights for the defect exist on outer race and rolling element contact

$\emptyset(z)_{rid}$	probability density function (PDF) of the asperity heights for the defect exist on rolling element and inner race contact
$\emptyset(z)_{rod}$	probability density function (PDF) of the asperity heights for the defect exist on rolling element and outer race contact
δ	maximum Hertzian deflection of the asperity at the point of contact for gear teeth surface contact
δ_i	maximum Hertzian deflection of the asperity at the point of contact for inner race-rolling element contact
δ_o	maximum Hertzian deflection of the asperity at the point of contact for outer race-rolling element contact
μ	mean of the distribution of the asperity heights
σ	standard deviation of distribution of the asperity heights
β	characteristic radius of spherical asperity summits
φ	pressure angle
ρ	density of lubricant
τ	operating temperature of gears
η_0	viscosity of lubricant
α_0	pressure viscosity coefficient
ω_1	angular velocity of gear
ω_i	rotational speed of shaft or inner ring in bearing
ϵ	dimensionless load parameter
Δ_r	radial clearance
Δa	crack propagation length
ΔA	crack progressive area
$\Delta r'_{(1EH)}$	variation of reduced radius of Hertzian curvature between tooth engagement and highest point of double tooth contact for the new tooth pair

$\Delta r'_{(1HD)}$	variation of reduced radius of Hertzian curvature between the highest point of double tooth contact and tooth disengagement for the new tooth pair
$\Delta r'_{(1LH)}$	variation of reduced radius of Hertzian curvature between the lowest point of single tooth contact and highest point of single tooth contact for the new tooth pair
$\Delta r'_{(2HD)}$	variation of reduced radius of Hertzian curvature between the highest point of double tooth contact and tooth disengagement for the previous tooth pair
$\Delta r'_{(3EH)}$	variation of reduced radius of Hertzian curvature between the tooth engagement and highest point of double tooth contact for the next tooth pair
ψ_{dei}	angle of rotation corresponding to end point of defect area exist on inner race
ψ_{deo}	angle of rotation corresponding to end point of defect area exist on outer race
ψ_{deri}	angle of rotation corresponding to end point of defect area exist on rolling element when contact with inner race
ψ_{dero}	angle of rotation corresponding to end point of defect area exist on rolling element when contact with outer race
ψ_{dsi}	angle of rotation corresponding to starting point of defect area exist on inner race
ψ_{dso}	angle of rotation corresponding to starting point of defect area exist on outer race
ψ_{dsri}	angle of rotation corresponding to starting point of defect area exist on rolling element when contact with inner race
ψ_{dsro}	angle of rotation corresponding to starting point of defect area exist on rolling element when contact with outer race
ψ_l	angle of rotation corresponding to end point of load zone
$-\psi_l$	angle of rotation corresponding to starting point of load zone

ψ_T	total angle of rotation of bearing during load zone
α	angle of rotation
$\alpha_{DEPSTC(1)}$	angle of rotation corresponding to the defect with protrusion end point (at respective defect diameter) of single tooth contact for the new tooth pair
$\alpha_{DSPSTC(1)}$	angle of rotation corresponding to the defect with protrusion start point (at respective defect diameter) of single tooth contact for the new tooth pair
$\alpha_{HPDTC(1)}$	angle of rotation corresponding to the highest point of double tooth contact for the new tooth pair during engagement
$\alpha_{HPDTC'(2)}$	angle of rotation corresponding to the highest point of double tooth contact for the previous tooth pair during disengagement
$\alpha_{HPDTC(3)}$	angle of rotation corresponding to the highest point of double tooth contact for the next tooth pair during engagement
$\alpha_{HPDTC'(1)}$	angle of rotation corresponding to the highest point of double tooth contact for the new tooth pair during disengagement
$\alpha_{HPSTC(1)}$	angle of rotation corresponding to the highest point of single tooth contact for the new tooth pair
$\alpha_{LPSTC(1)}$	angle of rotation corresponding to the lowest point of single tooth contact for the new tooth pair
$\alpha_{TD(1)}$	angle of rotation corresponding to the tooth disengagement for the new tooth pair
$\alpha_{TD(2)}$	angle of rotation corresponding to the tooth disengagement for the previous tooth pair
$\alpha_{TE(1)}$	angle of rotation corresponding to the tooth engagement for the new tooth pair

$\alpha_{TE(3)}$	angle of rotation corresponding to the tooth engagement for the next tooth pair

ABBREVIATION

AB	Path of contact
AE	Acoustic emission
AGMA	American gear manufacturers association
AX	Path of approach
DEPSTC	Defect with protrusion end point of single tooth contact at respective defect diameter
DSPSTC	Defect with protrusion start point of single tooth contact at respective defect diameter
EDM	Electrical discharge machining
EHL	Elastohydrodynamic lubrication
HPDTC	Highest point of double tooth contact during engagement
HPDTC′	Highest point of double tooth contact during disengagement
HPSTC	Highest point of single tooth contact
IAE	Institute of automotive engineers
LPSTC	Lowest point of single tooth contact
LSF	Load sharing factor during meshing of gears
TD	Tooth disengagement
TE	Tooth engagement
XB	Path of recess

CHAPTER 1

INTRODUCTION AND LITERATURE REVIEW

1.1 Introduction

Gears and rolling element bearings are most extensively used components which play a vital role in machines. The failure of the gears and bearings is one of the most frequent causes of the machine breakdown. Hence, the condition monitoring or fault diagnosis of gearboxes and bearings are very important to prevent unwanted shutdowns/catastrophic failures. Various techniques like vibration measurements, acoustic measurements, temperature measurements, ultrasonic testing and wear debris analysis, are used for condition monitoring of gearboxes and bearings. The application of acoustic emission (AE) for the health monitoring and diagnostics of rotating machine components is very effective technique.

AE technique has become the most focusing research topic in the fault diagnosis and condition monitoring of the gearboxes as well as bearings. Several experimental investigations have been conducted to assess the effectiveness of AE in identifying the fault/defect in gears and bearings.

The mathematical model of any mechanical system is very useful to comprehend the concrete physical mechanism of the system. A mathematical model expresses the relationship among the various parameters involved in that system. With the help of mathematical modeling of AE generated in gears and bearings, the effect of various operational parameters as well as defects on AE can be understood.

1.1.1 Acoustic emission

AE is defined as the transient elastic wave that is spontaneously generated by the rapid release of strain energy caused by structural amendment within a material or on its surface under the stresses [1-4]. The typical frequency range of AE takes place between 100 kHz and 1 MHz. AE is initiated at the microscopic level; it is much sensitive to detect the loss of any mechanical veracity, thus it provides the condition of fault/defect at early stages of growth or at just initiation of the fault/defect. Since AE is non-directional technique, AE sensor can be fixed in any direction to acquire the signal. However, attenuation of the AE signal during its propagation over spaces and particularly across the interfaces is the main drawback of this technique. Therefore, AE sensors should be mounted very close to the AE source to overcome this limitation. Mostly, the AE parameters which are used for the diagnosis are amplitude, counts, rms (root mean square) energy, and events. The sources of AE in rotating machinery consist of asperities contact, impacting, friction, cyclic fatigue, material loss, cavitation, leakage, crack initiation, crack propagation, plastic deformation etc [5]. AE is the useful technique for the health monitoring of rotating machine components such as bearings, gears etc. [6-10]. Rao et al. [11] prescribed a detailed review on the application of AE technique for the condition monitoring and diagnosis of rotating machine elements. The AE technique provides better fault identification sensitivity as compared to other fault analysis techniques like vibration analysis [12-14].

1.2 Literature review

The detailed literature review on the AE generated in gear pair and bearing is presented and discussed in the forthcoming subsections.

1.2.1 Gear operating parameters and AE

Several researchers have investigated experimentally that gear operating parameters such as speed, load, specific film thickness, and temperature influence the energy of AE generated during meshing of the gears. It is also investigated experimentally that asperity interaction is the potential source of AE in gears [15-21]. Each of these experimental studies is briefly discussed in the following paragraphs.

Tan et al. [15] established the relationship between vibration and AE indicators of condition monitoring of gear and the gearbox operating parameters (load, speed, oil film thickness and temperature) by conducting experiments. It is postulated that the source of AE mechanism during gear mesh is endorsed to asperities contact. Toutountzakis et al. [16] presented the behaviour of AE in terms of AE rms and energy values to changes in rotational speed of gear. Hamzah and Mba [17] presented the correlation between AE activity and various load and speed conditions for the spur and helical gears on the basis of experimental study. The experimental investigations suggested that AE is sensitive to any variation in specific film thickness due to changes in load conditions. Tan et al. [18] performed fatigue gear testing experimentally on spur gears and detailed that the value of AE rms increases with increasing torque. They also determined the increased sensitivity of the AE level with more asperity contacts. Tandon and Mata [19] performed an experimental study on spur gears in a back-to-back gearbox test rig and measured three AE parameters viz. peak amplitude, energy, and counts. They concluded that the AE parameters increase in accordance with the increased load. Tan and Mba [20] investigated experimentally the influence of operational variables like load, speed and lubricating condition to identify the source of AE during meshing of gears under isothermal conditions. They found that load and speed influence the AE rms level, in which speed is having more impact on AE and asperity contact is the main source for AE during gear mesh. It was also concluded that sliding contact during gear mesh is responsible for the continuous AE waveform while rolling contact is responsible for high amplitude AE transient burst. Hamzah and Mba [21] presented experimental results which indicate that specific film thickness influences the AE level during the operation of spur gears for a range of load and speed conditions, a direct consequence of asperities interaction and also concluded that asperity contact is the primary cause for AE activity during the gear meshing. Vicuna [22] has investigated the effects of operating conditions such as lubricant temperature, load, and speed on AE generated during gear meshing in non-faulty planetary gearbox based on experimental results. It was concluded that rotational speed is the most important parameter which influences the AE value. Temperature affects the film thickness and accordingly asperity contacts have two contrary effects on AE value. Eftekharnejad and Mba [23] performed an experimental investigation on helical gears and detailed the direct association of volume of removed material with AE and also mentioned that presence of protrusions is responsible for the generation of AE activity. Hamzah et al. [24] presented the experimental investigation on AE levels with variation in specific film thickness and oil temperature for both spur and helical gears, where it has been found that AE rms value decreased as the specific film thickness increased and vice versa due to the level of asperity contact. Hamel et al. [25] demonstrated from an experimental study on defective helical gear that the value of AE may not be identified due to the existence of fault, if the oil film thickness separates the asperities of gears completely. Hence, asperity contact between gear surfaces is the key source for the generation of AE.

These above mentioned experimental studies clearly illustrate that gear operating parameters affect the AE energy generated in gear operation. The asperity interaction has also been investigated as the primary source of AE generation during gear mesh.

1.2.1.1 Sliding contact and AE

The various studies also illustrate that the asperity contact is responsible for AE generation during sliding contact due to friction or wear and the relationship between AE characteristics (rms value, count rate) and wear mechanism has been also recognized. Boness et al. [26] and Boness and McBride [27] detailed that asperity contact was the responsible source for AE rms signals acquired from the sliding contacts. They also obtained an empirical rapport between AE rms value and wear volume removed from the test ball in a ball-on-cylinder test apparatus. Benabdallah and Aguilar [28] investigated the relationship between wear properties and friction and the AE rms level under pure sliding contact at varying sliding speed. Lingard et al. [29] have shown an efficient relationship between AE and the wear rates, wear regimes in a pure sliding test on metallic specimens. Hanchi and Klamecki [30] presented experimental results which show the changes in AE count rates with respect to change in the behaviour of wear rate in the sliding of metals. Sun et al. [31] examined the AE signals produced by bearing steel contact within sliding situations in experimental tests on pin-on-disc tribometer and found a good relationship between AE rms and wear rates and friction levels. Price et al. [32] have detected the severe sliding and pitting fatigue wear regimes by application of AE.

Hence, it is clear from the above mentioned literature that AE generates due to asperity interaction during sliding contact between the surfaces.

1.2.2 Statistical analysis and modelling of contact of surfaces

As mentioned in section 1.2.1, asperity contact is the main cause of generation of AE. In this section, a detailed literature review has been done to understand asperity contact. The analysis and modelling of contact of surfaces have been comprehensively performed by many researchers. Each of these works is briefly described in the upcoming paragraph.

Greenwood and Williamson [33] have developed the model for the contact of two nominally flat surfaces based upon the mainly Hertzian contact concept, in which the asperity height distribution is assumed as Gaussian and asperities tip radius is assumed spherical and constant. They developed a theoretical model for the total real area of contact, the number of asperity contacts and most important the contact load of the asperity interaction between two surfaces. This model has been extended using model developed by Greenwood and Tripp [34] in which they mentioned that modelling of contact between two rough surfaces may be done by a contact between a single rough surface (which is having an asperity distribution equivalent to composite asperity height distributions of the both meshing surfaces) and a smooth one. Gupta and Cook [35] have presented a statistical analysis of the interaction of rough surfaces. They developed an analytical model to investigate the contact problem of a pair of rough surfaces. The topography of the rough surface has been detailed by the statistical distribution of peak heights and radius of curvature of the peaks. The distribution of peak heights of the surfaces has been identified to be closely Gaussian. They developed empirical relationships to estimate the sizes and densities of microcontacts as a function of topographic index and the normal load. Archard [36, 37] has examined the contact areas and temperature between sliding surfaces by conducting the experimental study. He found that the real areas of contact between sliding surfaces are shaped by elastic deformation of the contacting protuberance. Iwaki and Mori [38] have investigated the change of the distribution of the surface roughness when two surfaces are pressed using a given pressure. They found that the contacting points may be evaluated by the distribution of surface profiles. They also found that the gap between two surfaces is distributed according to that of the difference of the variables of both surface profiles. Kimura [39] presented a statistical analysis of the geometrical nature of contacting surfaces. He proposed mathematical expressions for estimation of the number and the mean area of the real contact points formed between rough surfaces on the basis of profiles of contacting surfaces. Ling [40] proposed a distribution of surface asperities during the mating of two rough surfaces. He suggested form of the asperities on the basis of roughness measurements of ground steel, brass, and aluminium by stylus traversing parallel, 45°, and perpendicular to lay. Mikic [41] investigated analytically the effect of previous loading on the surface parameters i.e. contact area, number of contact prints, their size distribution, and value of thermal contact conductance for two nominally flat surfaces during contact. Gaussian distribution of surface heights has been considered in the model. Thomas and Probert [42] have examined the variation of the true contact area between a rough surface and smooth surface as a function of load. The effects of load and orientation on surface profiles have been investigated by conducting experiments for anisotropic and several isotropic surfaces having randomly distributed surface heights. Whitehouse and Archard [43] presented a model of surface contact consisting of asperities having a statistical distribution of both heights and curvatures. They mentioned that the surfaces, consisting of a random structure, may be defined by the height distribution and the auto correlation function.

It is clear from the above mentioned studies that statistical analysis of the interaction of rough surfaces is detailed by the statistical distribution of asperity heights and radius of tip of the asperities. The distribution of asperity heights has been identified to be closely Gaussian. The elastic deformation of the asperities has been found during the contact between sliding surfaces.

1.2.3 Modelling of the parameters of AE

Literature shows that attempts have been made for modelling of the parameters of AE by different approaches. Baranov et al. [44] developed a model for the characteristics of AE under sliding friction of solids on the basis of deviation theory of a random function. They developed theoretical expressions for the amplitude distribution, its parameters, and count rate of AE. Fan et al. [45] developed a model of the AE generated by elastic asperity contact of materials during sliding friction. The mathematical model was validated by conducting the experiments. Bosia et al. [46] presented a phenomenological model to investigate the relationship of damage progression and AE using energy balance considerations in a fibre bundle model approach. The model describes the appropriate amount of energy dissipation due to development of micro-cracks and other formation of surfaces under the external load condition in a material. Saini and Park [47] developed a model to establish the relationship between AE rms value, cutting parameters, geometry of tool and work piece material in orthogonal cutting operations. They examined the effect of parameters of the turning operation on AE and found that AE rms value increases as value of cutting speed, cutting force and shear plane angle is increased. Hamzah and Mba [17] developed a numerical model to evaluate the deviations in AE with speed and load variation for both spur and helical gears.

Hence, the above mentioned studies show the modelling of the parameters of AE using different methods.

1.2.4 Bearing operating parameters and AE

Several experimental investigations have been conducted to assess the effectiveness of AE in identifying the defect in bearings. The results of these studies illustrate the capability of AE to diagnose the defect and effective condition monitoring of bearings. Rogers [48] detailed the application of AE technique to measure the slow speed anti-friction slew bearings on cranes of offshore gas production. Yoshioka and Fujiwara [49, 50] have shown that defects on bearings may be identified by AE parameters before they appear in the vibration acceleration range. Holroyd and Randall [51] presented the diagnosis of defect on bearings using modulation of AE signatures at bearing defect frequencies. Some researchers presented the experimental investigation on the application of AE parameters for the bearing fault diagnosis with simulated defects on the different elements of bearing. Mostly, the AE parameters which are used for the diagnosis are amplitude, counts, rms energy, and events [52]. Tandon and Nakra [53] described a study to detect the defects in radially loaded ball bearing by using AE parameters like count and peak amplitude. Kakishima et al. [54] presented a comparative experimental study on the evaluation of AE and vibration to identify the defect on the inner race of a roller as well as ball bearing. They concluded that AE technique was able to detect the defect and it was also noted that an increase in defect size resulted in an increase of AE levels. The defects in the form of scratch on the raceway of angular contact ball bearing have been identified with AE signals [55, 56]. Bansal et al. [57] demonstrated the quality inspection of rolling element bearing using distribution of events by counts and peak amplitude of AE. Tan [58] detailed the drawbacks of the AE count technique and proposed that defects in rolling element bearings may be identified by measurement of the area under the amplitude time curve. Some researchers detailed the study on the application of AE to natural fault diagnosis in bearings. Yoshioka [59] described the usefulness of AE for identification of the onset of natural degradation in bearings. The work of Elforjani and Mba [60-62] also details about the investigation of potential of the AE technique in identifying and locating the natural defects in rolling element bearings. Some studies [63-66] have shown the application of demodulated AE signals to detect the defects in rolling element bearings.

It has been reported in the literature on the application of AE to bearing defect analysis that bearing operating parameters such as rotational speed, load, etc. strongly influence the AE values during the bearing operating condition. It has been noted from publications to date that the presence of defect on the elements of bearing and defect size strongly contributes to the level of AE energy. Al-Ghamd and Mba [67] presented the experimental investigation on the application of AE technique and vibration analysis to identify the presence of defect and its size in a radially loaded roller bearing for the different load and speed conditions. They concluded that asperity interaction is the primary source for the generation of AE and the value of AE rms increased with increase in the speed and load for defect free condition as well as for the all defect of various sizes. In addition, the relationship between AE values for a range of defect conditions is also investigated and found that the value of AE rms increases as size of defect increases. Choudhury and Tandon [68] investigated the usefulness of AE technique to identify defects in radially loaded cylindrical roller bearings. They measured the value of AE of bearings without defect and with defects of different sizes. They concluded that the value of AE parameter increases with increasing speed for the bearings without defect and with defects. Tandon and Nakra [53] presented the experimental study for the effectiveness of AE technique to detect the defects in radially loaded ball bearings. They found that the value of AE parameter increases with increasing speed and load conditions for the bearings without defect and with defects. Tan [58] also reported the similar findings. Al-Dossary et al. [69] presented an experimental investigation on the application of AE technique to characterize the defect sizes on a radially loaded bearing at varying speed and load conditions. They noted that AE parameters value increased with increasing load and speed for various defects. They also noted the AE parameters value increases as size of defect increases. Morhain and Mba [70] presented an experimental investigation on radially loaded roller bearing with seeded defects of different size at varying speed and load conditions. They concluded that changes in operational indicators such as load and speed have direct effects on the AE parameters like AE rms. The AE rms increases with increasing rotational speed, load and defect size. Mba [71] reported in an experimental study on the health monitoring of bearing that AE rms value increases with increasing rotational speed and radial load. Mba [72] detailed the experimental study to establish a relationship between AE activity and increasing defect size. Mirhadizadeh et al. [73] presented an experimental investigation on the influence of operational variables i.e. speed, load, etc on the generation of AE in bearing. It was concluded that the operational variables affect the value of AE.

The primary source of AE activity is investigated during the experimental investigation on the application of AE for bearing defect identification [67, 70-72]. It is found that AE is generated due to the interaction of two surfaces in relative motion during frictional contact and the dominant AE source mechanism is asperity contacts. The material protrusions above the surface roughness have been also investigated as the fundamental source of AE in seeded defect [67, 72]. Some studies are also available on the insight of bearing vibration and faults which may contribute to AE modelling of bearings [74-76].

Hence, the above mentioned literature has revealed that operational parameters of bearing, presence of defect on the bearing elements and defect size strongly influence the value of AE. It has also been reported in the experimental studies that asperity contact is a potential source of AE generation during bearing operation.

1.2.5 Influence of defect in gear tooth on AE

It has been mentioned in the researches that the presence of defect in the gears strongly influences the AE during the meshing of gears. In addition, it is also noted that size of defect contributes to the level of AE measured. Toutountzakis et al. [77] presented an experimental investigation to find out the effectiveness of AE for detection of gear defect. It is concluded that the protrusions are responsible for AE activity during the meshing of gears. Tandon and Mata [19] performed an experimental study to investigate the presence of defect in spur gears by AE in back-to-back gearbox test rig and measured three AE parameters viz. peak amplitude, energy, and ring-down counts. The defects, simulated pits, were introduced on the pitch-line of gear tooth with varying diameters using spark erosion method. They observed that the monitored AE parameters increase with increased gear defect size i.e. diameter of pit. Singh et al. [79] performed an experimental study for application of AE to gear fault diagnosis and noted that AE activity increases with the pitting spreads over the teeth. Tan et al. [18] performed an experimental investigation on spur gears using fatigue gear testing to observe the influence of natural pitting on the surface of gears in generation of AE. They concluded that the value of AE rms increases with the increasing gear pitted area at all load condition. It is postulated that consequence of the increase in pitted area is more asperity contacts and friction, resulting in increased AE levels. Eftekharnejad and Mba [23] performed an experimental investigation on helical gears to assess the effectiveness of AE to detect the seeded defects. They concluded that the AE rms levels increase for increasing defect size for all test load conditions and also detailed the direct relationship between volume of removed material with AE rms levels. They mentioned that presence of protrusions around the edge of seeded defect is responsible for the generation of more AE activity. Tan et al. [15] presented an experimental study on spur gears. They concluded that the source of AE mechanism which generates the gear mesh bursts during gear mesh is the asperity contacts. The amplitude of each AE transient burst at the mesh varies due to the changing nature of the asperities contact with time. Elforjani et al. [78] presented the experimental study for monitoring seeded defects on worm gears using AE technique. They concluded that AE parameters such as AE rms and energy are capable of the detection of defects in worm gears. AE transient increases due to the presence of defects. Toutountzakis et al. [16] presented the observations on AE activity due to misalignment and natural pitting during the experimental study of gear defect diagnosis. They concluded that the AE rms and energy level increases with gear deterioration i.e. increased pit size. Sentoku [80] presented an experimental investigation on the spur gear defect detection using AE activity. They associated gear tooth surface damage i.e. pitting to AE and concluded that AE amplitude and energy increases as pitting increases. Siores et al. [81] postulated that the AE activity can be correlated with different defect conditions.

These above mentioned experimental studies show that AE energy increases with increasing size of defect. It has also been shown in these studies that asperity and protrusion contacts are the potential source of AE generation during gear mesh.

1.2.6 Crack parameters and AE

The crack growth from a perspective of fracture is one of the major concerns. During the initiation and propagation of the crack, the detectable elastic stress waves release away from the crack which can offer an early cautioning of imminent failure of gear. The detection of crack formation or propagation is a critical step during the condition monitoring of machine components. AE measurement is quite sensitive towards the crack as AE signal is engendered at the incipient stage of crack initiation or propagation.

Scruby [82] mentioned that AE is used as a diagnostic technique for the investigation of fracture because it provides the information regarding the growth of defect. Cracking and fracture processes generally produce high levels of amplitude of burst AE signals [83]. It has been noted from publications to date that there is a possibility of the diagnosis of crack initiation, propagation and fracture using the AE technique in the various components viz gear, bearing, shaft, compact tension specimen etc. [84-96]. It has also been found that there is a good relationship between crack parameters and AE energy. Singh et al. [84] have investigated the gear tooth cracking using AE technique. They established the viability of AE, released during crack initiation and propagation, to detect the growing crack in gear tooth. They presented experimental findings on the crack initiation and propagation in gear tooth using AE by single tooth bending fixture. It has been postulated that as the crack propagates with growing number of cycles, the amplitude of the identified AE signal increases with enhanced frequency. Sentoku and Tokuda [85] have conducted the experimental investigation using AE technique for bending fatigue process of carburized spur gear. They measured the AE signals and crack length and concluded that the change in crack length for the spur gear results in the change in amplitude of AE. Sentoku and Yamato [86] have accomplished the AE source location in bending fatigue process of carburized spur gear and determined the AE characteristics by various analyses of experimental data. They postulated that the change in crack length results in the change of AE amplitude, AE energy and event count rate for the spur gear. Pullin et al. [87] detailed the capability of AE for the detection of cracking in gear teeth. A novel test rig was designed to determine the onset of cracking and fatigue fractures in gear teeth by allowing the fatigue loading of an individual gear tooth. Obata et al. [88] estimated the fatigue crack growth rate of spur gear teeth by AE technique on a spur gear test machine. It has been concluded that the crack growth rate of the spur gear can be determined using the relation between the AE event counts and distribution of inter granular fractures on the crack surface of gear. The increasing pattern of AE event counts has been allied with the intergranular fractures area through crack propagation on the cracked surface of gear teeth. Miyachika et al. [89] has also performed the experimental research on the effect of fatigue crack propagation on the AE characteristics in the bending fatigue process of spur gear teeth and established a relationship between AE parameters and the fatigue crack propagation under different tooth loads. It has been concluded that the values of AE parameters change with variation in crack length as well as a number of cycles. Masuyama et al. [90] presented the experimental analysis on fatigue crack growth in a carburized gear tooth using AE technique and mentioned that the AE energy rate is proportional to the stress intensity factor range, crack growth rate, and crack length. Elforjani and Mba [60-62] concluded that sub-surface initiation and subsequent crack propagation may be identified with data analysis techniques on AE which is generated from accelerated natural degradation of a bearing raceway. They demonstrated a perfect relationship between creation and propagation of bearing defects on rolling element bearings races during operation and increasing AE energy levels. Moriwaki [91] has investigated the tool failure by monitoring the amplitude of detected AE signal. The AE signals with large amplitudes were detected during cracking, chipping and fracture of the cutting tools. Yu et al. [92] presented the correlation of AE signal characteristics with crack growth behaviour. The study has been performed using compact tension (CT) specimens based upon AE absolute energy, count rate and crack length and it was found that AE parameters are related to crack growth. Elforjani and Mba [93] presented an experimental investigation on detecting crack initiation and growth in slow speed shafts by AE technique. It has been demonstrated that there is a vibrant correlation between increasing AE levels and development and propagation of shaft defects. It has been found in the literature [19, 23, 80-81, 94] that AE is applied for identifying bending fatigue in spur gears and there is a good relationship between AE and fault/crack propagation. It is also found that AE is very sensitive towards the defects which exist in gear. The relationship between AE signal characteristics and crack growth behavior in metals is detailed in previous research [95-103]. It is mentioned that AE monitoring is able to predict the fatigue crack growth.

The various studies also illustrate the theoretical relationships between AE and crack parameters by using different techniques of fracture mechanics. Lysak [104] has presented the analytical dependencies between parameters of crack and AE signal parameters acquired in the investigation of crack initiation and growth from the perspective of fracture. Diei and Dornfeld [105] presented a study on high amplitude AE signal generated during crack propagation and proposed a quantitative model which relates the peak value of AE rms to the fractured area and the resultant cutting force during fracture of a machine tool. Desai and Gerberich [106] have presented the analysis of incremental cracking for the CT specimen using stress wave emission. They derived a relationship between stress wave amplitude, incremental fracture area, and stress intensity. Malen and Bolin [107] have developed a theoretical estimation of the amplitude of stress wave emitted due to the local variation in the inelastic strain which may occur by the various source e.g. crack propagation, dislocation motion etc. Ono [108] presented a theoretical model for AE due to cracking in relation to the amplitude distribution analysis of burst type AE signal in his critical review. Sano and Fujimoto [109] presented a review on AE during the fracture of metals; in which the effects on the AE accompanied with the crack growth in elastic materials has been detailed. Harris and Dunegan [110] proposed a model to establish the relationship between AE count rate and stress intensity range. This model is modified by Lindley et al. [111] by considering the effect of fracture events in the zone ahead of the crack tip.

Hence, these experimental studies for gear tooth cracking using AE technique illustrate that the parameters related to crack propagation in gear tooth influence AE energy. The theoretical correlations of AE characteristics with crack parameters have also been shown by different methods.

1.3 Motivation of the research

The literature reviewed has revealed that gear operating parameters as well as bearing operating parameters such as speed, load, specific film thickness, and temperature strongly influence the AE energy during the operation of gears and bearings. A good relationship has been found between operational parameters and AE. It has also been noted that the presence of the defect on the gear tooth and bearing elements and parameters related to defect such as defect size strongly affects to the AE level. Furthermore, it has been found in the experimental studies that asperity/ protrusion contact is a potential source of AE generation in gears and bearings. A fine correlation between asperity contact and AE value has been reported due to friction or wear. But, to the best knowledge of the author, there is no theoretical or mathematical model available to comprehend the physical mechanism of AE generated during the gear and bearing operation i.e. how the gear and bearing operational parameters as well as the presence of defect and defect size on gear tooth and bearing elements influence the AE. Therefore, in this thesis, the mathematical models are developed to correlate the energy of AE to operational parameters of gears and bearings as well as parameters related to defect by using approaches of contact mechanics and linear elastic fracture mechanics.

1.4 Objectives of the research

The aim of this research work is to develop the theoretical or mathematical models of AE generated during operating condition of spur gear pair and rolling element bearing. The developed models correlate the energy of AE to operating parameters of healthy gears and bearings as well as defected condition. The objectives are as follows:

1. To develop the theoretical model of AE generated in involute spur gear pair.
2. To develop the theoretical model of AE generated in rolling element

bearing.

3. To develop the theoretical model of AE generated during crack propagation in spur gear.

4. To develop the theoretical model of AE generated due to pitting on the spur gear.

1.5 Outline of the thesis

The thesis work is mainly based on development of the theoretical models of AE generated in gears and bearings. These mathematical models are discussed in separate chapters of the thesis. Chapter 1 is about the introduction and literature review of AE generated during operation of gears and bearings. Chapters 2 to Chapter 5 are for the mathematical modeling of AE for healthy as well as defected spur gear pair and rolling element bearing. The last chapter is about the conclusions and scope for future work.

Chapter 1: Introduction and literature review

Chapter 1 presents the brief introduction which is essential to understand the further investigations and analyses in the thesis. The detailed literature on AE generated in gears and bearings has been presented. Furthermore, motivation of the research and thesis objectives is discussed.

Chapter 2: Modelling of acoustic emission generated in involute spur gear pair

Chapter 2 describes the mathematical model of AE generated in involute spur gear pair. The theoretical model establishes a rapport between gear operating parameters and energy of AE. Further, an experimental study, conducted on gear lubricant testing machine, has been presented for the validation of developed theoretical model. In the last, the summary of the chapter is presented.

Chapter 3: Modelling of acoustic emission generated by crack propagation in spur gear

Chapter 3 discusses the development of a theoretical model to correlate the AE energy, generated by crack propagation in gear tooth, to the parameters allied with crack by using approaches of linear elastic fracture mechanics. Further, validation of the developed theoretical model is presented with the results of an experimental investigation. In the last, the summary of the chapter is presented.

Chapter 4: Modelling of acoustic emission generated due to pitting on spur gear

Chapter 4 presents a theoretical model to establish a relationship between size of fault/defect and energy of AE generated during gear meshing on the basis of interaction of asperity and protrusion around the defect. The developed theoretical model is validated with the experimental study performed on gear lubrication testing machine. Then after, the summary of the chapter is presented.

Chapter 5: Modelling of acoustic emission generated in rolling element bearing

Chapter 5 presents a theoretical model to understand the influence of operating parameters on energy of AE generated in rolling element bearing. The model is extended for the defected bearing by considering the defect on inner race, outer race and rolling element to understand the physics of the influence of defect on AE during the bearing operation. Further, the validation of developed model has been presented with the experimental studies. In the last, the summary of the chapter is presented.

Chapter 6: Conclusions and scope of future work

Chapter 6 concludes the research work of the thesis with valuable observations from the theoretical modeling and experimental investigations. Furthermore, the scope for future work is suggested.

CHAPTER 2

MODELLING OF ACOUSTIC EMISSION GENERATED IN INVOLUTE SPUR GEAR PAIR

2.1 Introduction

AE is an important technique for the condition monitoring and diagnostics of various mechanical system components like gear, bearing, machine tool etc. Several researchers have found experimentally that gear operating parameters such as speed, load, specific film thickness, and temperature influence the energy of AE generated during meshing of the gears as discussed in Chapter-1. But, there is lack of theoretical or mathematical model to comprehend the actual physical mechanism of AE during the meshing of gears i.e. how the gear operating parameters influence the AE when the surfaces of teeth of gears mesh together.

In this chapter, a theoretical model has been developed to establish a rapport between gear operating parameters and energy of AE on the basis of asperity contact and friction between involute surfaces of gear teeth. The model has been developed using Hertzian contact approach, statistical concepts, and varying sliding velocity of gear tooth mechanism as described in section 2.2. The effects of load sharing, lubrication, and dynamic load condition during the gear mesh cycle are also considered in the developed model as presented in subsection of section 2.2. i.e. 2.2.1, 2.2.2, and 2.2.3 respectively. An experimental study has been performed for validation of developed theoretical model as presented in section 2.3. The value of AE measured by experimental investigation is presented in subsection 2.3.1 and the value of AE calculated by developed theoretical model is presented in subsection 2.3.2. The results obtained by experiments are compared with the results evaluated by developed model and discussed in section

2.4. Finally, in section 2.5, the summary of the work of this chapter is presented.

2.2 Mathematical model of AE in involute spur gear pair

The model is developed based on following assumptions:

a. Only sliding contact speed has been taken into consideration when two gears mesh together.
b. Gears are assumed to have zero pitch error, unbalance, and shaft misalignment.
c. Only elastic deformation of asperities has been considered.
d. Temperature of gear pair is assumed to be constant during operation.

The model has been developed on the basis of statistical concepts, Hertzian contact approach and varying sliding velocity of gear tooth mechanism, in which, rough surface has been assumed to consist of asperities whose heights (z) vary in some statistical manner and all asperity summits have been considered as spherical and have the same characteristic radius. Let the separation between the involute smooth surface of gear tooth and the reference plane in the rough surface of another gear tooth is d as shown in Fig. 2.1 which is constant at line of action.

For the investigation of contact between the surfaces of gear teeth, those are having asperities with different summit heights, all deformable surface roughness can be considered on one surface such that it is having an asperity distribution equivalent to composite asperity height distributions of the both meshing surfaces of gears and the second surface can be considered as smooth surface.

The model has been developed as shown in Fig. 2.1 based on the model of Greenwood and Williamson [33] and model of Fan et al. [45]. In Fig. 2.1, the contact of two surfaces of gear teeth at the point of contact has been extracted from the meshing of gears.

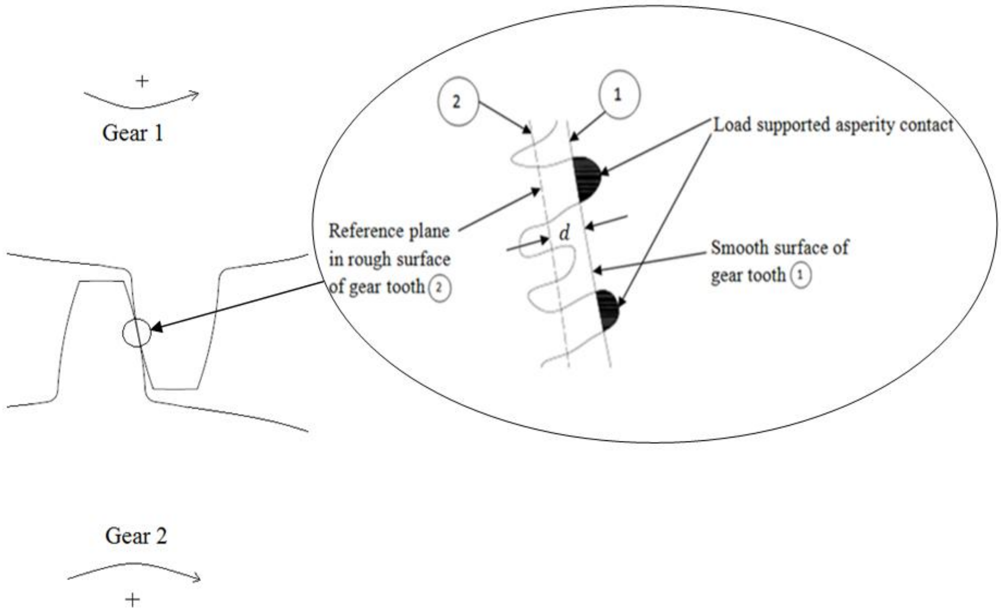

Fig. 2.1 Deformation of asperities at the point of contact during contact between smooth surface and rough surface in involute gear teeth meshing

The probability $P(z)$ that an asperity has a summit between z and $z + dz$ above reference plane in rough surface is [33,112]

$$P(z) = \emptyset(z)dz \tag{2.1}$$

where, z is the random variable for the heights of asperity summits which vary randomly, $\emptyset(z)$is the probability density function (PDF) of the asperity height which describe the distribution and for the incorporation of all the asperities heights, it should be such that [113]

$$\int_{-\infty}^{+\infty} \emptyset(z)dz = 1 \tag{2.2}$$

When a load is applied, the smooth surface shift towards the mean level of the asperities so that, it will make contact with all the asperities for which the heights are greater than the separation i.e. $z > d$. Thus, the probability of making contact at any particular asperity of height z is [33,112]

$$P\ (z > d) = \int_{d}^{\infty} \emptyset(z)dz \tag{2.3}$$

If there are N_a asperities in the unit contact area of one pair of teeth during meshing of gears, the number of such asperity contacts in this area is given by

$$n = N_a \int_d^{\infty} \emptyset(z)dz \tag{2.4}$$

If two surfaces are brought together into contact by applying the load, the true contact area due to asperities contact is much smaller than apparent contact area as prescribed in Eq. (2.5) which is most responsible for friction and stored elastic energy for the asperity contact. Hence, the true area of one asperity contact is extremely small. Each asperity contact can be considered as distinct Hertzian contact, if the contact is purely elastic [113]. Consequently, assume the smooth surface of gear is plane through a zone of Hertzian radius of the asperity contact at point of contact through line of action.

The total (elastic) true area of contact is given by [33]

$$A_{tr} = \pi N_a r_s \int_d^{\infty} (z-d)\emptyset(z)dz \tag{2.5}$$

The resulting stress distribution $\sigma_a(r)$ is semielliptical during contact of spherical asperities as shown in Fig. 2.2. This is a characteristic of Hertzian contacts. The maximum stress σ_m which occurs on the axis of symmetry is known as the Hertz stress [113].

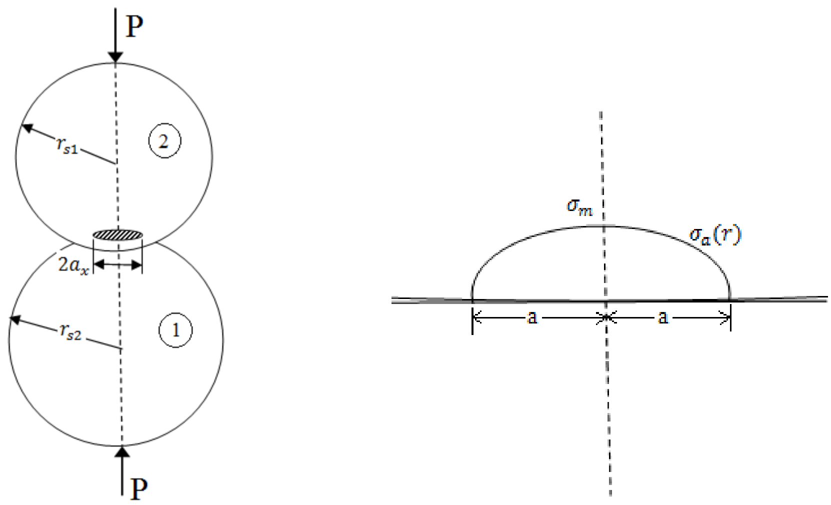

(a) (b)

Fig. 2.2 (a) Spheres in elastic contact (b) The resulting semi-elliptical stress distribution [113]

In Fig. 2.2, two elastic spheres 1 and 2 of radii r_{s1} and r_{s2} are pressed into contact with force P.

The stored elastic energy (E_i) for the asperities contact between the surfaces can be given by [114]

$$E_i = \int P d\delta \tag{2.6}$$

The elastic energy, in Eq. (2.6), can be considered for the contact of pair of asperities for one pair of teeth during meshing of gears. Where, P is the load and $\delta = z - d$, is the deformation of asperity at the point of contact which is given by [115]

$$\delta = \left(\frac{9P^2}{16E'^2 r'}\right)^{1/3} \tag{2.7}$$

where, r' is reduced radius of Hertzian curvature given by

$$\frac{1}{r'} = \frac{1}{r_1} + \frac{1}{r_s} \tag{2.8}$$

where, r_s is radius of spherical asperity and r_1 is the radius of assumed plane surface during asperity contact at any point on the involute surface of gear.

E' is the Hertzian contact modulus which is given by

$$\frac{1}{E'} = \frac{1-{\nu_1}^2}{E_1} + \frac{1-{\nu_2}^2}{E_2} \tag{2.9}$$

E_1 and E_2 are the Yong's modulus and ν_1 and ν_2 are the Poisson's ratios of the materials of both gears.

Using Eqs. (2.6) and (2.7),

$$E_i = \left(\frac{9}{16}\right)^{1/3} \frac{2}{3E'^{2/3} r'^{1/3}} \int P^{2/3} dP = \frac{2}{5} P\delta \tag{2.10}$$

The total elastic energy stored due to the asperity contacts in the unit area for one pair of teeth during meshing of gears is

$$E_{ia} = \int \left(\frac{2}{5} P \left(\frac{9P^2}{16E'^2 r'}\right)^{1/3}\right) dr' = \frac{3}{5} P\delta\Delta r' \tag{2.11}$$

where, $\Delta r'$ is the variation of reduced radius of Hertzian curvature during unit area. Since, maximum deformation (δ) depends upon the value of z ($\delta = z - d$), the stored mean elastic energy ($\bar{E}_{ia}$) i.e. the stored elastic energy for one asperity contact is given by

$$\bar{E}_{ia} = \frac{\int_d^\infty \left(\frac{3}{5} P\delta\Delta r'\right) \emptyset(z) dz}{\int_d^\infty \emptyset(z) dz} = \frac{\frac{3}{5} P\Delta r' \int_d^\infty (z-d) \emptyset(z) dz}{\int_d^\infty \emptyset(z) dz} \tag{2.12}$$

Thus, the total elastic energy stored due to the asperity contacts in N_r number of revolutions of gears, E_T, is

$$E_T = N_r x_g A_c n \bar{E}_{ia} \tag{2.13}$$

where, x_g is the number of teeth in gear, n is the number of asperity contacts in the unit contact area of one pair of teeth, A_c is the total apparent contact area of one pair of teeth during meshing of gears.

Substitute the value of n and $\bar{E}_{ia}$ from Eqs. (2.4) and (2.12) respectively into Eq. (2.13), the total elastic energy is

$$E_T = \frac{3}{5} N_r x_g A_c N_a P \Delta r' \int_d^{\infty} (z-d)\emptyset(z) dz \tag{2.14}$$

Now, the time for the asperity deformation has been calculated by considering the varying sliding velocity of gear. For this purpose, assume the sliding velocity between the surfaces of teeth of gears is v. The time required for deformation and release of distinct asperity contacting through a zone of Hertzian radius can be evaluated as [44]

$$t' = \frac{a_r}{v} \tag{2.15}$$

where, a_r is defined as Hertzian radius of the resultant circular asperity contact area which is given by

$$a_r = \left(\frac{3Pr'}{4E'}\right)^{1/3} \tag{2.16}$$

In gear mechanism, the sliding velocity varies along the line of contact continuously and it is given by

$$v = \omega_1 r_1 - \omega_2 r_2 \tag{2.17}$$

where, ω_1 and ω_2 are the angular velocities of gear 1 and gear 2 respectively. r_1 and r_2 are the radii of tooth surfaces of gear 1 and gear 2 respectively at the point of contact as shown in Fig. 2.3 [116].

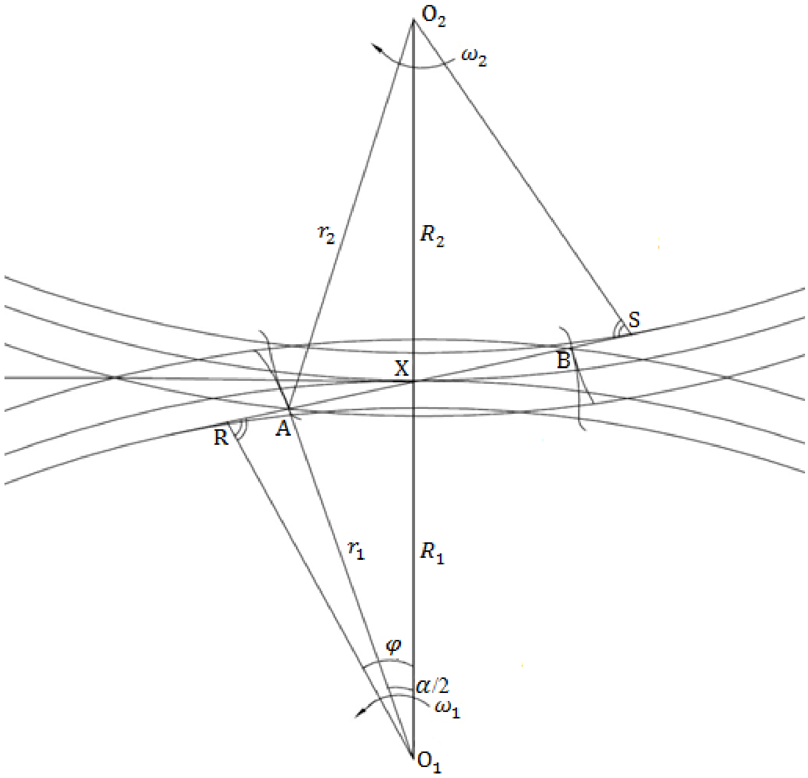

Fig. 2.3 Meshing of involute gears [116]

In Fig. 2.3, R_1 and R_2 are the radii of pitch circle of gear 1 and 2 respectively, X is the pitch point, A and B are the point of tooth engagement and tooth disengagement respectively.

Substitute Eq. (2.16) & (2.17) into Eq. (2.15) and using Eq. (2.7), the total time is expressed as:

$$t = \int \frac{\left(\delta r'\right)^{1/2}}{\omega_1 r_1 - \omega_2 r_2}\, dr_1 \tag{2.18}$$

In Fig. 2.3, by using geometry of $\Delta\, O_2AS$ and similarity between $\Delta\, O_1XR$ and $\Delta\, O_1XS$, the value of r_2 is expressed as

$$r_2 = \sqrt{\left(\frac{O_2X}{O_1X} O_1R\right)^2 + \left[XR\left\{\left(\frac{O_2X}{O_1X}\right) + 1\right\} - RA\right]^2} \tag{2.19}$$

From the geometry in Fig. 2.3, substitute the value of O_1R, XR & RA into Eq. (2.19), the value of r_2 is

$$r_2 = r_1\sqrt{\left(\frac{R_2}{R_1}\right)^2 \{cos(\varphi-\alpha/2)\}^2 + \left[\{tan\,\varphi\, cos(\varphi-\alpha/2)\}\left\{\left(\frac{R_2}{R_1}\right)+1\right\} - sin(\varphi-\alpha/2)\right]^2} \tag{2.20}$$

where, φ is pressure angle and α is angle of rotation during one mesh period.

Using the value of r_2 from Eq. (2.20), Eq. (2.18) is expressed as follows:

$$t = \iint \frac{1}{r_1} \frac{(\delta r')^{1/2}}{\omega_1 - \omega_2\sqrt{\left(\frac{R_2}{R_1}\right)^2 (cos(\varphi-\alpha/2))^2 + \left[(tan\,\varphi\, cos(\varphi-\alpha/2))\left\{\left(\frac{R_2}{R_1}\right)+1\right\} - sin(\varphi-\alpha/2)\right]^2}} dr_1 d\alpha \tag{2.21}$$

Hence, the total time for the asperities deformation is

$$t = \int \frac{(\delta)^{\frac{1}{2}}[\int\left(\frac{r_s}{r_1(r_1+r_s)}\right)^{1/2} dr_1]}{\omega_1 - \omega_2\sqrt{\left(\frac{R_2}{R_1}\right)^2 (cos(\varphi-\alpha/2))^2 + \left[(tan\,\varphi\, cos(\varphi-\alpha/2))\left\{\left(\frac{R_2}{R_1}\right)+1\right\} - sin(\varphi-\alpha/2)\right]^2}} d\alpha \tag{2.22}$$

The integral of Eq. (2.22) is calculated numerically for the initial and final values of r_1 and α during the particular area of asperities deformation.

Since, maximum deformation (δ) depends upon the value of z $(\delta = z - d)$, the mean release time of asperity contact during deformation is given by

$$\bar{t} = \frac{\int_d^\infty [\int\left(\frac{r_s}{r_1(r_1+r_s)}\right)^{1/2} dr_1]\left[\int \frac{1}{\omega_1 - \omega_2\sqrt{\left(\frac{R_2}{R_1}\right)^2 (cos(\varphi-\alpha/2))^2 + \left[(tan\,\varphi\, cos(\varphi-\alpha/2))\left\{\left(\frac{R_2}{R_1}\right)+1\right\} - sin(\varphi-\alpha/2)\right]^2}} d\alpha\right](z-d)^{1/2}\emptyset(z)dz}{\int_d^\infty \emptyset(z)dz} \tag{2.23}$$

Using Eqs. (2.14) and (2.23), the elastic strain energy rate released by asperity contact/deformation is

$$E'_T = \frac{E_T}{\bar{t}} =$$

$$\frac{3N_r x A_c \Delta \mathbf{r}' N_a P \omega_1 \int_d^{\infty}(z-d)\emptyset(z)dz \int_d^{\infty}\emptyset(z)dz}{5[\int\left(\frac{r_s}{r_1(r_1+r_s)}\right)^{1/2}dr_1]\int_d^{\infty}(z-d)^{1/2}\emptyset(z)dz} \frac{1}{\left[\int\left[1/\left(1-R_1/R_2\sqrt{\left(\frac{R_2}{R_1}\right)^2(\cos(\varphi-\alpha/2))^2+\left[(\tan\varphi\cos(\varphi-\alpha/2))\left\{\left(\frac{R_2}{R_1}\right)+1\right\}-\sin(\varphi-\alpha/2)\right]^2}\right)\right]d\alpha\right]} \tag{2.24}$$

It can be noted that the total number of asperity contacts during the meshing of gears can be specified as,

$$N_T = N_r x_g A_c N_a \int_d^{\infty}\emptyset(z)dz \tag{2.25}$$

Substitute Eq. (2.25) into Eq. (2.24), the elastic strain energy rate is

$$E'_T = \frac{E_T}{\bar{t}} =$$

$$\frac{3N_T \Delta \mathbf{r}' P \omega_1 \int_d^{\infty}(z-d)\emptyset(z)dz}{5\left[\int\left(\frac{r_s}{r_1(r_1+r_s)}\right)^{1/2}dr_1\right]\left[\int_d^{\infty}(z-d)^{1/2}\emptyset(z)dz\right]\left[\int\left[1/\left(1-R_1/R_2\sqrt{\left(\frac{R_2}{R_1}\right)^2(\cos(\varphi-\alpha/2))^2+\left[(\tan\varphi\cos(\varphi-\alpha/2))\left\{\left(\frac{R_2}{R_1}\right)+1\right\}-\sin(\varphi-\alpha/2)\right]^2}\right)\right]d\alpha\right]} \tag{2.26}$$

But, some part of this energy is lost due to conversion of this energy into AE pulses and then after, some part of the energy is lost due to receiving capacity of AE instruments. Therefore, the elastic energy rate of the AE is given by

$$E'_{AE} =$$

$$\frac{3C_e C_m N_T \Delta \mathbf{r}' P \omega_1 \int_d^{\infty}(z-d)\emptyset(z)dz}{5\left[\int\left(\frac{r_s}{r_1(r_1+r_s)}\right)^{1/2}dr_1\right]\left[\int_d^{\infty}(z-d)^{1/2}\emptyset(z)dz\right]\left[\int\left[1/\left(1-R_1/R_2\sqrt{\left(\frac{R_2}{R_1}\right)^2(\cos(\varphi-\alpha/2))^2+\left[(\tan\varphi\cos(\varphi-\alpha/2))\left\{\left(\frac{R_2}{R_1}\right)+1\right\}-\sin(\varphi-\alpha/2)\right]^2}\right)\right]d\alpha\right]} \tag{2.27}$$

where, C_e is the part of the total elastic strain energy, mentioned in Eq. (2.26), which alters into AE pulses and C_m is the part which is received by the AE sensors/ AE measurement instruments.

Hence, the total elastic strain energy accumulated by the AE sensor/ AE instrument during the specific duration ΔT is given by

$$E_{AE} = \int_0^{\Delta T} E'_{AE}\, dt \tag{2.28}$$

If $V(t)$ is the electrical signal which has been measured, the total energy of the AE signals is given by

$$E_{AE'} = \int_0^{\Delta T} V^2(t)\, dt \tag{2.29}$$

It may be noted that the energy given in Eqs. (2.28) and (2.29) will be equal.

The rms value of AE signal during the specific duration $\Delta T$of AE signal is described as [47]

$$V_{rms} = \sqrt{\frac{1}{\Delta T}\int_0^{\Delta T} V^2(t)\,dt} \tag{2.30}$$

Using Eqs. (2.28), (2.29) and (2.30), the rms value of AE signal is expressed as

$$V_{rms} = \sqrt{\frac{1}{\Delta T}\int_0^{\Delta T} E'_{AE}\,dt} \tag{2.31}$$

Substituting Eq. (2.27) into Eq. (2.31), the rms value of the AE signal energized by the asperity interaction during the meshing of gears is

$$V_{rms} = \left[\frac{1}{\Delta T}\int_0^{\Delta T} \frac{3C_eC_mN_T\Delta \boldsymbol{r}' P\omega_1\int_d^{\infty}(z-d)\phi(z)dz}{5\left[\int\left(\frac{r_s}{r_1(r_1+r_s)}\right)^{1/2}dr_1\right]\left[\int_d^{\infty}(z-d)^{1/2}\phi(z)dz\right]\left[\int\left[1/\left(1-R_1/R_2\sqrt{\left(\frac{R_2}{R_1}\right)^2(cos(\varphi-\alpha/2))^2+\left[(tan\,\varphi\, cos(\varphi-\alpha/2))\left\{\left(\frac{R_2}{R_1}\right)+1\right\}-sin(\varphi-\alpha/2)\right]^2}\right)\right]d\alpha\right]}\,dt\right]^{1/2} \tag{2.32}$$

The elastic strain energy rate released by asperity contact/deformation (E'_T) will be constant and accordingly the energy rate of the AE (E'_{AE}) will be also constant, if the sliding in the involute gears is steady during meshing of gears for particular contact load, speed and particular gear profile, gear surface. Hence, by Eq. (2.32), the rapport between AE rms and the gear parameters based on elastic asperity contact is specified as

$$V_{rms} = \left[\frac{3C_eC_mN_T\Delta \boldsymbol{r}' P\omega_1\int_d^{\infty}(z-d)\phi(z)dz}{5\left[\int\left(\frac{r_s}{r_1(r_1+r_s)}\right)^{1/2}dr_1\right]\left[\int_d^{\infty}(z-d)^{1/2}\phi(z)dz\right]\left[\int\left[1/\left(1-R_1/R_2\sqrt{\left(\frac{R_2}{R_1}\right)^2(cos(\varphi-\alpha/2))^2+\left[(tan\,\varphi\, cos(\varphi-\alpha/2))\left\{\left(\frac{R_2}{R_1}\right)+1\right\}-sin(\varphi-\alpha/2)\right]^2}\right)\right]d\alpha\right]}\right]^{1/2} \tag{2.33}$$

Define, $C_c = \left[\frac{3}{5}C_eC_m\right]^{1/2}$, Eq. (2.33) is expressed as

$$V_{rms} = C_c \left[\frac{N_T \Delta \boldsymbol{r}' P \omega_1 \int_d^{\infty} (z-d) \emptyset(z) dz}{\left[\int \left(\frac{r_s}{r_1(r_1+r_s)}\right)^{1/2} dr_1\right] \left[\int_d^{\infty} (z-d)^{1/2} \emptyset(z) dz\right] \left[\int \left[1/\left(1 - R_1/R_2 \sqrt{\left(\frac{R_2}{R_1}\right)^2 (cos(\varphi-\alpha/2))^2 + \left[(tan\,\varphi\, cos(\varphi-\alpha/2))\left\{\left(\frac{R_2}{R_1}\right)+1\right\} - sin(\varphi-\alpha/2)\right]^2}\right)\right] d\alpha\right]} \right]^{1/2} \tag{2.34}$$

It can be noted that, a portion

$$\left[\frac{\Delta r' \int_d^{\infty} (z-d) \emptyset(z) dz}{\left[\int \left(\frac{r_s}{r_1(r_1+r_s)}\right)^{1/2} dr_1\right] \left[\int_d^{\infty} (z-d)^{1/2} \emptyset(z) dz\right] \left[\int \left[1/\left(1 - R_1/R_2 \sqrt{\left(\frac{R_2}{R_1}\right)^2 (cos(\varphi-\alpha/2))^2 + \left[(tan\,\varphi\, cos(\varphi-\alpha/2))\left\{\left(\frac{R_2}{R_1}\right)+1\right\} - sin(\varphi-\alpha/2)\right]^2}\right)\right] d\alpha\right]} \right]^{1/2}$$

in Eq. (2.34), can be determined by topographic characteristics of the gear tooth surface and specifications/profile of gears.

2.2.1 Influence of load sharing during the total length of contact

The model is extended by considering the influence of load sharing during the total length of contact. The asperity interaction is the phenomenon which is related to local contact mechanics and the actual applied load for the deformation of asperities will be different during the mesh cycle due to load sharing during total length of contact. Hence, the value of AE generated due to deformation of asperities by the specific load at particular local contact will vary during the mesh cycle. In this section, the load sharing effect is considered in the model using analytical study mentioned in [117-120] for the load sharing of spur gears during the mesh.

The concept of load sharing of spur gears is explained here briefly based on [117-120]. As gear teeth mesh in double contact of gear tooth pair with contact ratio lower than 2, the contact will occur between a single pair of teeth and two pairs of teeth during the path of contact. The total load, transmitted between the gears, is shared between the meshing tooth pairs and this can be measured by load sharing factor (LSF) as follows:

$$\text{LSF} = p_i/P \tag{2.35}$$

where, p_i is the load supported by the pair of teeth at particular local contact during mesh cycle and P is the total load along the path of contact. According to the AGMA standard [120] for spur gears, the theoretical LSF with respect to meshing angle is shown in Fig. 2.4. It is clear from Fig. 2.4, that pair of teeth support 1/3 (33.33%) of the total load at the instant of TE (tooth engagement) and this load increases linearly to 2/3 (66.66%) of the total transmitted load at the HPDTC (highest point of double tooth contact during engagement). The load is increased to 3/3 (100%) of the total load when only one gear pair is in mesh at the LPSTC (lowest point of single tooth contact) and remains constant up to HPSTC (highest point of single tooth contact). The load changes again to 2/3(66.66%) of the total transmitted load at the HPDTC' (highest point of double tooth contact during disengagement) and decreases linearly to 1/3 of the total load at the TD i.e. tooth disengagement.

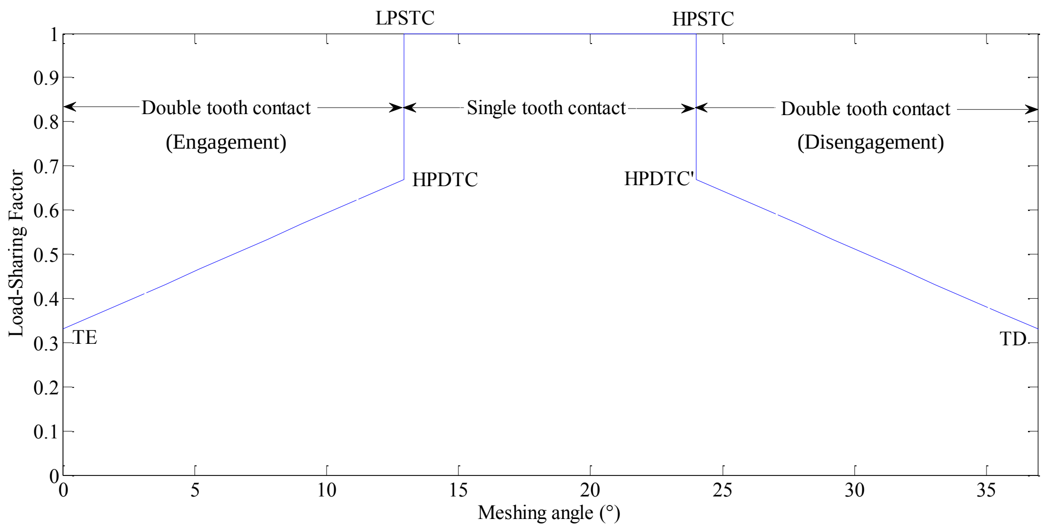

Fig. 2.4 Load Sharing Factor with meshing angle during mesh cycle [119, 120]

If the load sharing during the mesh cycle is taken into consideration, the load at the local contact of asperities will be as per the LSF as described above. Hence, the energy rate of the AE generated by deformation of asperities of local contact due to load, p_i, during mesh cycle is expressed as follows by using Eq. (2.27):

$$E'_{AE_i} = \frac{3C_e C_m N_T \Delta r' p_i \omega_1 \int_d^{\infty}(z-d)\emptyset(z)dz}{5\left[\int\left(\frac{r_s}{r_1(r_1+r_s)}\right)^{1/2} dr_1\right]\left[\int_d^{\infty}(z-d)^{1/2}\emptyset(z)dz\right]\left[\int\left[1/\left(1-R_1/R_2\sqrt{\left(\frac{R_2}{R_1}\right)^2(cos(\varphi-\alpha/2))^2+\left[(tan\,\varphi\,cos(\varphi-\alpha/2))\left\{\left(\frac{R_2}{R_1}\right)+1\right\}-sin(\varphi-\alpha/2)\right]^2}\right)\right]d\alpha\right]} \quad (2.36)$$

It is clear from Eqs. (2.35) and (2.36), the value of AE will vary during the total length of contact according to LSF. The total AE evaluation during the mesh cycle is described as follows:

(i) The total AE generated during the TE to HPDTC is calculated by summation of AE generated during the TE to HPDTC by new tooth pair and AE generated during the HPDTC' to TD by previous tooth pair. During this section of mesh cycle, both pairs of teeth are simultaneously engaged.

(ii) The total AE generated during the LPSTC to HPSTC by new tooth pair.

(iii) The total AE generated during the HPDTC' to TD is calculated by summation of AE generated during the HPDTC' to TD by new tooth pair and AE generated during TE to HPDTC by next tooth pair. Two pairs of teeth are again simultaneously engaged.

Hence, the total rms value of the generated AE is calculated as follows by using Eq. (2.36):

$$V_{rms(F)} = C_c\left[\frac{1}{\theta_T}\left[\int_{\theta_{TE(1)}}^{\theta_{HPDTC(1)}}[A.P.B]\,d\theta + \int_{\theta_{HPDTC'(2)}}^{\theta_{TD(2)}}[C.P.D]\,d\theta + \int_{\theta_{LPSTC(1)}}^{\theta_{HPSTC(1)}}[E.P.F]\,d\theta + \int_{\theta_{HPDTC'(1)}}^{\theta_{TD(1)}}[G.P.H]\,d\theta + \int_{\theta_{TE(3)}}^{\theta_{HPDTC(3)}}[I.P.J]\,d\theta\right]\right]^{1/2} \quad (2.37)$$

In Eq. (2.37), values of $A, B, C, D, E, F, G, H, I,$ and J are given by Eq. (2.37 A), (2.37 B), (2.37 C), (2.37 D), (2.37 E), (2.37 F), (2.37 G), (2.37 H), (2.37 I), and (2.37 J) respectively as follows:

$$A = LSF_{TE(1)} + \frac{\left(LSF_{HPDTC(1)} - LSF_{TE(1)}\right)}{\left(\theta_{HPDTC(1)} - \theta_{TE(1)}\right)}\left(\theta - \theta_{TE(1)}\right) \tag{2.37 A}$$

$$B = \frac{N_{T_{(1EH)}} \Delta \boldsymbol{r'}_{(1EH)} \omega_1 \int_d^{\infty} (z-d) \emptyset(z) dz}{\left[\int_{r_{1TE(1)}}^{r_{1HPDTC(1)}} \left(\frac{r_S}{r_1(r_1+r_S)}\right)^{1/2} dr_1\right]\left[\int_d^{\infty} (z-d)^{1/2} \emptyset(z) dz\right]\left[\int_{\alpha_{TE(1)}}^{\alpha_{HPDTC(1)}}\left[1/\left(1 - R_1/R_2 \sqrt{\left(\frac{R_2}{R_1}\right)^2 (cos(\varphi-\alpha/2))^2 + \left[(tan\,\varphi\, cos(\varphi-\alpha/2))\left\{\left(\frac{R_2}{R_1}\right)+1\right\} - sin(\varphi-\alpha/2)\right]^2}\right)\right] d\alpha\right]} \tag{2.37 B}$$

$$C = LSF_{HPDTC'(2)} + \frac{\left(LSF_{TD(2)} - LSF_{HPDTC'(2)}\right)}{\left(\theta_{TD(2)} - \theta_{HPDTC'(2)}\right)}\left(\theta - \theta_{HPDTC'(2)}\right) \tag{2.37 C}$$

$$D = \frac{N_{T_{(2HD)}} \Delta \boldsymbol{r'}_{(2HD)} \omega_1 \int_d^{\infty} (z-d) \emptyset(z) dz}{\left[\int_{r_{1HPDTC'(2)}}^{r_{1TD(2)}} \left(\frac{r_S}{r_1(r_1+r_S)}\right)^{1/2} dr_1\right]\left[\int_d^{\infty} (z-d)^{1/2} \emptyset(z) dz\right]\left[\int_{\alpha_{HPDTC'(2)}}^{\alpha_{TD(2)}}\left[1/\left(1 - R_1/R_2 \sqrt{\left(\frac{R_2}{R_1}\right)^2 (cos(\varphi-\alpha/2))^2 + \left[(tan\,\varphi\, cos(\varphi-\alpha/2))\left\{\left(\frac{R_2}{R_1}\right)+1\right\} - sin(\varphi-\alpha/2)\right]^2}\right)\right] d\alpha\right]} \tag{2.37 D}$$

$$E = LSF_{LPSTC(1)} + \frac{\left(LSF_{HPSTC(1)} - LSF_{LPSTC(1)}\right)}{\left(\theta_{HPSTC(1)} - \theta_{LPSTC(1)}\right)}\left(\theta - \theta_{LPSTC(1)}\right) \tag{2.37 E}$$

$$F = \frac{N_{T_{(1LH)}} \Delta \boldsymbol{r'}_{(1LH)} \omega_1 \int_d^{\infty} (z-d) \emptyset(z) dz}{\left[\int_{r_{1LPSTC(1)}}^{r_{1HPSTC(1)}} \left(\frac{r_S}{r_1(r_1+r_S)}\right)^{1/2} dr_1\right]\left[\int_d^{\infty} (z-d)^{1/2} \emptyset(z) dz\right]\left[\int_{\alpha_{LPSTC(1)}}^{\alpha_{HPSTC(1)}}\left[1/\left(1 - R_1/R_2 \sqrt{\left(\frac{R_2}{R_1}\right)^2 (cos(\varphi-\alpha/2))^2 + \left[(tan\,\varphi\, cos(\varphi-\alpha/2))\left\{\left(\frac{R_2}{R_1}\right)+1\right\} - sin(\varphi-\alpha/2)\right]^2}\right)\right] d\alpha\right]} \tag{2.37 F}$$

$$G = LSF_{HPDTC'(1)} + \frac{\left(LSF_{TD(1)} - LSF_{HPDTC'(1)}\right)}{\left(\theta_{TD(1)} - \theta_{HPDTC'(1)}\right)}\left(\theta - \theta_{HPDTC'(1)}\right) \quad (2.37\ \mathrm{G})$$

$$H = \frac{N_{T_{(1HD)}} \Delta \boldsymbol{r'}_{(1HD)} \omega_1 \int_d^\infty (z-d)\emptyset(z)dz}{\left[\int_{r_{1HPDTC'(1)}}^{r_{1TD(1)}} \left(\frac{r_s}{r_1(r_1+r_s)}\right)^{1/2} dr_1\right]\left[\int_d^\infty (z-d)^{1/2}\emptyset(z)dz\right]\left[\int_{\alpha_{HPDTC'(1)}}^{\alpha_{TD(1)}} \left[1/\left(1 - R_1/R_2\sqrt{\left(\frac{R_2}{R_1}\right)^2 (cos(\varphi-\alpha/2))^2 + \left[(tan\,\varphi\,cos(\varphi-\alpha/2))\left\{\left(\frac{R_2}{R_1}\right)+1\right\} - sin(\varphi-\alpha/2)\right]^2}\right)\right] d\alpha\right]} \quad (2.37\ \mathrm{H})$$

$$I = LSF_{TE(3)} + \frac{\left(LSF_{HPDTC(3)} - LSF_{TE(3)}\right)}{\left(\theta_{HPDTC(3)} - \theta_{TE(3)}\right)}\left(\theta - \theta_{TE(3)}\right) \quad (2.37\ \mathrm{I})$$

$$J = \frac{N_{T_{(3EH)}} \Delta \boldsymbol{r'}_{(3EH)} \omega_1 \int_d^\infty (z-d)\emptyset(z)dz}{\left[\int_{r_{1TE(3)}}^{r_{1HPDTC(3)}} \left(\frac{r_s}{r_1(r_1+r_s)}\right)^{1/2} dr_1\right]\left[\int_d^\infty (z-d)^{1/2}\emptyset(z)dz\right]\left[\int_{\alpha_{TE(3)}}^{\alpha_{HPDTC(3)}} \left[1/\left(1 - R_1/R_2\sqrt{\left(\frac{R_2}{R_1}\right)^2 (cos(\varphi-\alpha/2))^2 + \left[(tan\,\varphi\,cos(\varphi-\alpha/2))\left\{\left(\frac{R_2}{R_1}\right)+1\right\} - sin(\varphi-\alpha/2)\right]^2}\right)\right] d\alpha\right]} \quad (2.37\ \mathrm{J})$$

and 1, 2, and 3 stands for the new tooth pair, previous tooth pair and next tooth pair respectively.

2.2.2 Influence of lubrication

Lubrication film thickness plays an important role in the gear AE generation mechanism. The researchers explained the importance of lubrication in AE during gear operation [17, 21, 24, 25]. They detailed the effect of film thickness of lubrication on the AE by conducting the experimental studies and explained that the value of AE rms increases as film thickness of lubrication decreases. In this section, the lubrication effect is presented on the model using the theory of load sharing of Johnson and Greenwood [121] for the asperity contact in elastohydrodynamic lubrication (EHL).

In the gear operation, a condition of partial EHL is said to exist [122-123]. A model to explain the load sharing by the lubricating film pressure, ${p_h}'$, and the asperity contact pressure, ${p_a}'$, of Johnson and Greenwood [121] is shown in Fig. 2.5. In which, the load shared by asperities per unit area is defined. Hence, the load shared by asperities is:

$$p_a = \frac{2}{3} E'(N_a \beta \sigma) \left({}^{\sigma}/_{\beta} \right)^{1/2} F_{3/2}(d/\sigma) a_a \qquad (2.38)$$

where, σ is the standard deviation of distribution of the asperities height and β is the characteristic radius of spherical asperity summits, and a_a is the respective area. For the Gaussian distribution of asperity heights, the function $F_{3/2}(d/\sigma)$ is obtained by the following definition

$$F_n(h) = 1/\sqrt{2\pi} \int_h^{\infty} (t-h)^n \, exp(-t^2/2) dt \qquad (2.39)$$

where, h is the standardized separation and it is given as, $h = d/\sigma$.

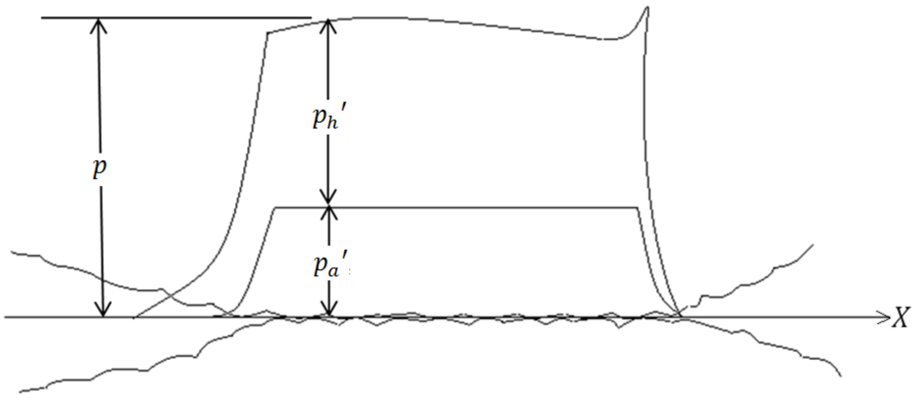

(a)

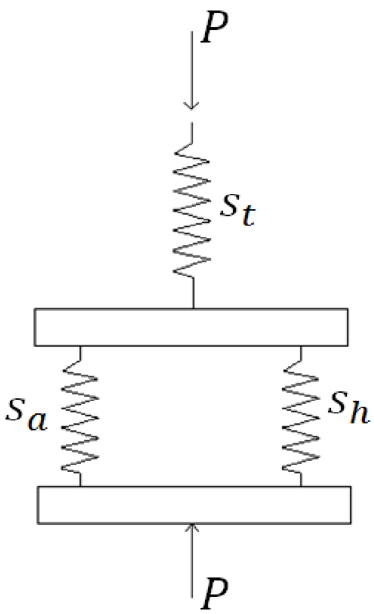

(b)

Fig. 2.5 An EHL contact between two rough surfaces: (a) Total pressure (p) shared by oil film pressure (p_h') and the asperity contact pressure (p_a') (b) Spring model of the flexible elements in an EHL contact in which total load (P) shared by spring s_h (hydrodynamic action of the oil film) and spring s_a (elastic stiffness of the asperities). The spring, s_t, signifies the total Hertz deformation of both bodies which act in parallel configuration[121]

Since, the main source of AE is asperity interactions during gear operation. The load given by Eq. (2.38) is the responsible for the deformation of the asperities and generation of AE accordingly.

Hence, if the lubrication effect is considered in the proposed model, the effect on AE due to load shared by asperities is defined as follows using Eqs. (2.37) and (2.38):

$$V_{rms(FL)} = C_c \left[\frac{1}{\theta_T} \left[\int_{\theta_{TE(1)}}^{\theta_{HPDTC(1)}} [A.p_a.B]\, d\theta + \int_{\theta_{HPDTC\prime(2)}}^{\theta_{TD(2)}} [C.p_a.D]\, d\theta + \int_{\theta_{LPSTC(1)}}^{\theta_{HPSTC(1)}} [E.p_a.F]\, d\theta + \int_{\theta_{HPDTC\prime(1)}}^{\theta_{TD(1)}} [G.p_a.H]\, d\theta + \int_{\theta_{TE(3)}}^{\theta_{HPDTC(3)}} [I.p_a.J]\, d\theta \right] \right]^{1/2} \quad (2.40)$$

2.2.3 Influence of dynamic effect

The dynamic factor is used to account for transmission error in the gear mechanism. Transmission error produces deviation from the uniform angular velocity of the gear pair. As per the AGMA standard ANSI/AGMA 2001-D04, the dynamic factor, k_v, is defined by the following equation:

$$k_v = \left(\frac{A + \sqrt{200V}}{A} \right)^B \quad (2.41)$$

where,

$$A = 50 + 56(1 - B)$$

$$B = 0.25(12 - Q_v)^{2/3}$$

Q_v is the AGMA transmission accuracy-level number which is unified in the ANSI/AGMA 2015-1-A01. V is the pitch line velocity in SI units (m/s). So, due to the dynamic factor, the load, P_d, is given as follows:

$$P_d = k_v P \quad (2.42)$$

Hence, if the dynamic effect is also taken into consideration, the AE rms of the model is expressed as follows by using Eqs. (2.40) and (2.42):

$$V_{rms(FLD)} = C_c\left[\frac{1}{\theta_T}\left[\int_{\theta_{TE(1)}}^{\theta_{HPDTC(1)}}[A.k_v.p_a.B]\,d\theta + \int_{\theta_{HPDTC'(2)}}^{\theta_{TD(2)}}[C.k_v.p_a.D]\,d\theta + \int_{\theta_{LPSTC(1)}}^{\theta_{HPSTC(1)}}[E.k_v.p_a.F]\,d\theta + \int_{\theta_{HPDTC'(1)}}^{\theta_{TD(1)}}[G.k_v.p_a.H]\,d\theta + \int_{\theta_{TE(3)}}^{\theta_{HPDTC(3)}}[I.k_v.p_a.J]\,d\theta\right]\right]^{1/2} \tag{2.43}$$

2.3 Experimental validation of the model

2.3.1 Experimental setup and data acquisition system

The experimental investigation was performed on IAE (Institute of Automotive Engineers) gear lubrication testing machine (S/No. 87870) at ITMMEC (Industrial Tribology, Machine Dynamics, and Maintenance Engineering Centre), IIT Delhi as shown in Fig. 2.6. The machine comprises the test head including test gears and power return gearbox on a bed plate which coupled together by means of a torque shaft. The test head assembly comprises of two test gear spindles mounted on anti-friction bearings. There is spigot for locating the test gears behind the front cover of the test head assembly. The gears are located after removing the front cover. Lubrication on the test gears is accomplished by a jet of oil. The power assembly comprises of two double helical power gears mounted on the antifriction bearing with driving pulley. Load on the test gears is applied by a detachable arm onto which different weights can be added. A schematic diagram of the gear test rig is shown in Fig. 2.7.

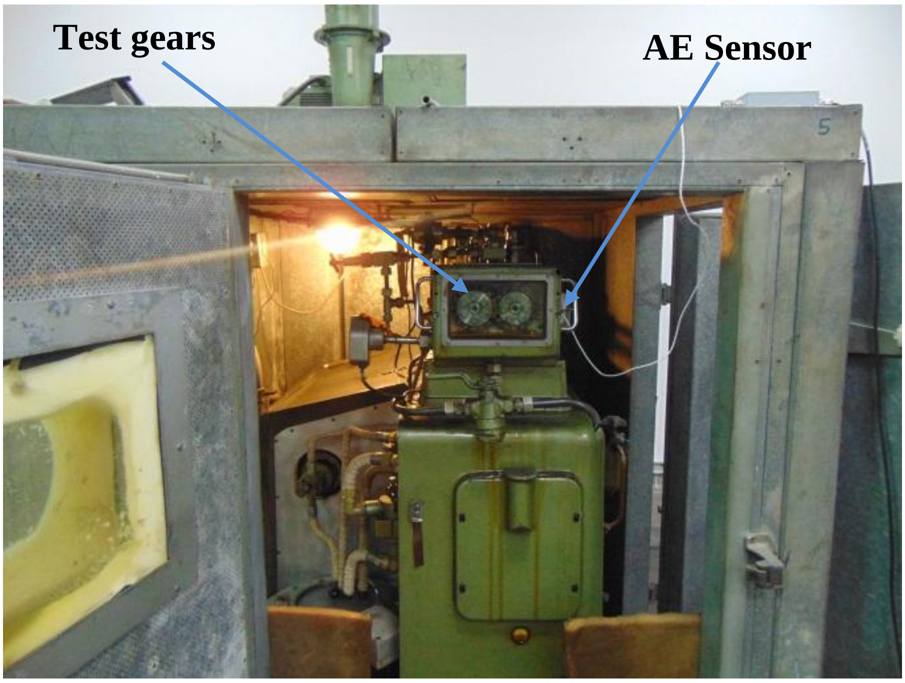

(a)

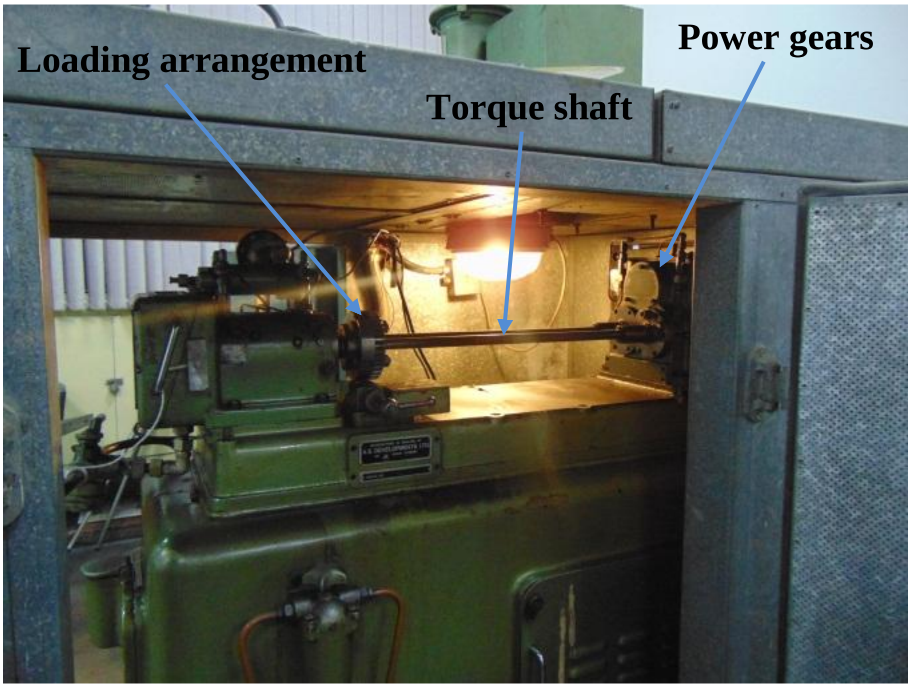

(b)

Fig. 2.6 Gear testing machine (a) Front view (b) Side view

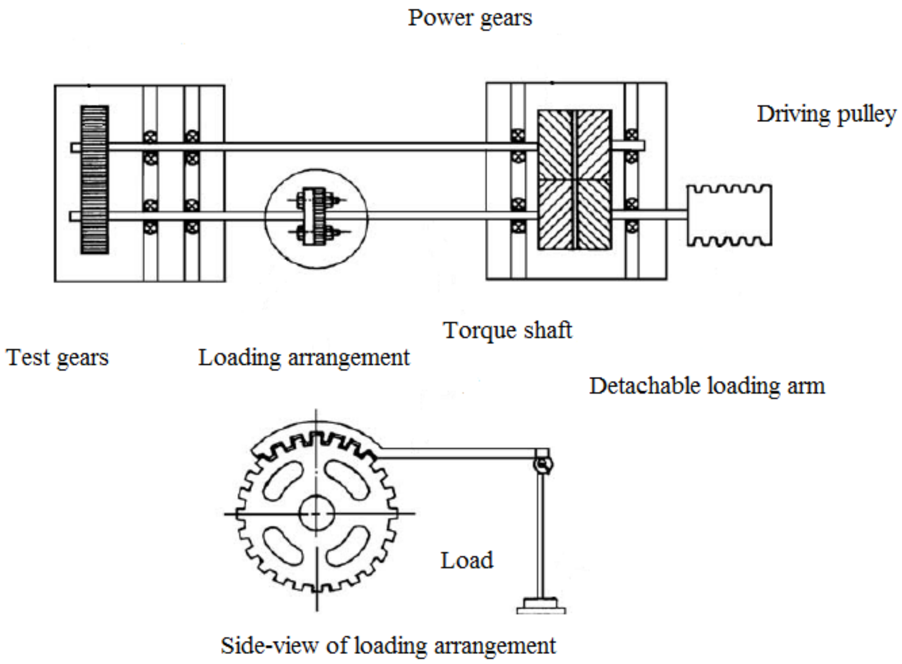

Fig. 2.7 A schematic diagram of gear testing machine

The measurements were performed on spur gears. The gears had an involute profile. Table 2.1 summarises the test gears specifications.

Table 2.1: Test gears specifications

No. of teeth, pinion	15
No. of teeth, gear	16
Pitch diameter, pinion (mm)	75
Pitch diameter, gear (mm)	80
Module (mm)	5
Pressure angle (°)	20
Face width (mm)	5.1
Depth of tooth (mm)	10.15

AE was sensed using a piezoelectric transducer (RI5D AD59). The sensor was attached near to the test gear as shown in Fig. 2.8. The AE sensor had a resonant frequency of 144.53 kHz and was followed by a preamplifier (AET 160) with an appropriate plug-in filter (FL-25). The AE signal was post-amplified prior to analysis in AET 5000 mainframe AE processor.

The calibration of AE system has been performed using Pencil Lead Break (PLB) test. In this teat, an AE event is simulated using the fracture of a brittle graphite lead in an appropriate fitting. This test is conducted by breaking a 0.5 mm (or 0.3mm) diameter pencil lead approximately 3 mm (+/- 0.5 mm) from its tip by pressing it against the surface of the element. An intense AE signal occurs due to this phenomenon which is quite similar to a natural AE source and that the sensors detect as a strong burst. There are basically two purpose of this test. First, it provides the sensitivity of transducer i.e. it makes sure that the transducer is in fine AE contact with the part being tested. Second, it detects the accuracy of the source location setup by determining the actual value of the wave speed for the object being tested. AE signal amplitude measurement and power spectral density measurement have been performed for the calibration of AE system. ASTM- E 1106 standard is followed for primary calibration of AE transducer. A factor has been used to account for the sensitivity of AE sensor.

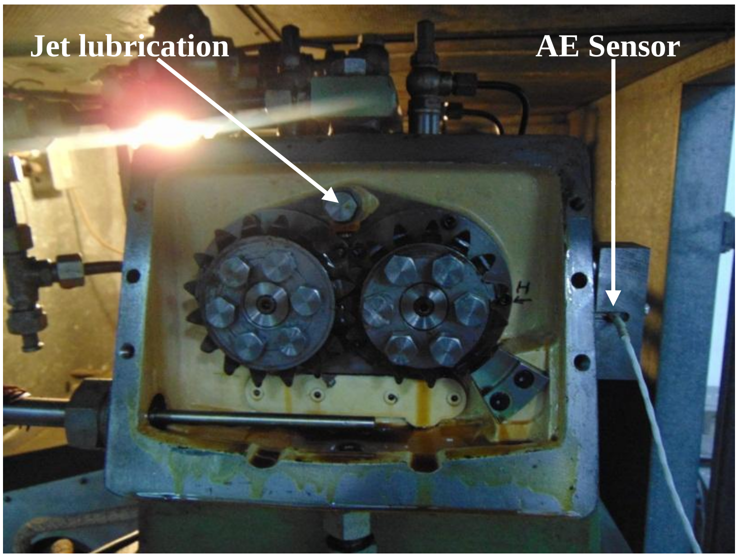

Fig. 2.8 AE sensor location near to test gear

The AE signal was measured close to the test gear. The condition of test gears was healthy. All the measurements were performed at 1000 rpm. The tests were conducted for the different load i.e. 0.305, 0.764, 1.529, 1.835, 2.294, and 3.059 kN. Appropriate threshold level of detection and the level of post amplification were set up to obtain maximum discernment between signal and background noise and to maintain the sensitivity of the AE monitoring system. The AE parameter measured was rms of the AE data.

2.3.2 AE by developed model

In order to evaluate the value of AE by the proposed model, the parameters allied with Eq. (2.43) are determined and prescribed in the Table C.1 of Appendix C.

The surface topography characteristics of the contact surface of the gear tooth are determined experimentally by using Marsurf LD 130 which is combined contour and roughness measurement system. The specification of this experimental setup is specified in Appendix A. The surface topography of the gear tooth is measured over an area of 4.0 mm^2 using Marsurf LD 130 as shown in Fig. 2.9. An image, depicting the surface topography of the spur gear tooth, is shown in Fig. 2.10. The surface topography characteristics of the contact surface of the gear tooth consist of the asperity peak density, N_a, asperity peak radius, β, and standard deviation of asperity heights, σ. These surface topography characteristics are determined by using spectral moment method as described by McCool [124] which is detailed in Appendix B1 and MountainsMap_v7 surface imaging topography software. The evaluated values of these surface topography characteristics are mentioned in Table C.1 of Appendix C.

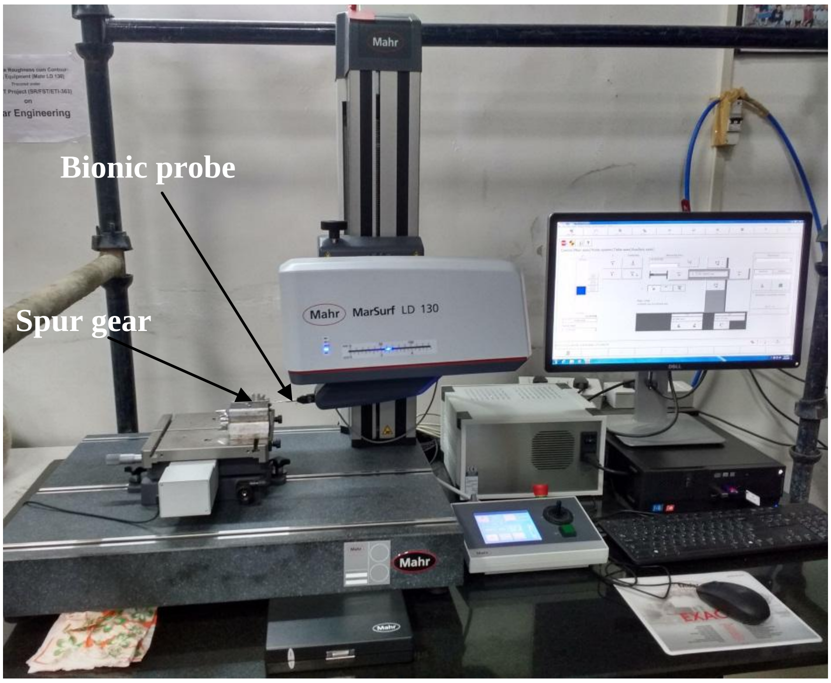

Fig. 2.9 Measurement of surface topography of the spur gear tooth using Marsurf LD 130

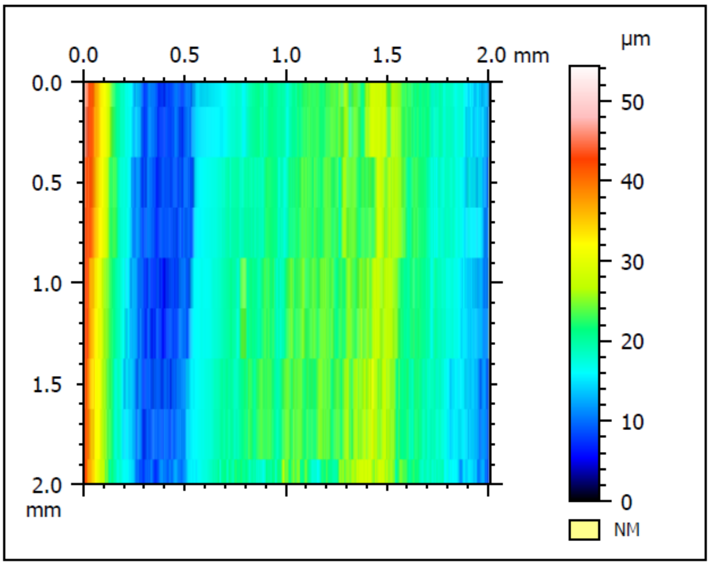

Fig. 2.10 Surface topography image of test area of surface of spur gear tooth

The distribution of asperity heights is considered as Gaussian distribution hence the PDF is prescribed by

$$\emptyset(z) = \frac{1}{\sigma\sqrt{2\pi}} exp\left(-\frac{1}{2}\left(\frac{z-\mu}{\sigma}\right)^2\right) \tag{2.44}$$

where, μ is mean of the distribution and σ is the standard deviation.

The meshing duration of the double/single tooth pair within one mesh period (θ_d and θ_s) and the total angle of meshing (θ_T) during one mesh period is calculated by using the equations detailed in [125] which are mentioned in Appendix B2 and then after, the angular displacements for the various positions during one mesh period i.e. $TE, HPDTC, LPSTC, HPSTC, HPDTC', TD$ for the different tooth pair i.e. new, previous and next tooth pair are calculated according to position and mentioned in Table C.1 of Appendix C.

The values of LSF for the various positions during the one mesh period i.e. $TE, HPDTC, LPSTC, HPSTC, HPDTC', TD$ for the different tooth pair i.e. new, previous and next tooth pair are calculated as per AGMA standard [120] for spur gears and mentioned in Table C.1 of Appendix C.

The total number of asperity contacts during the one mesh period for the different zone of contact areas of meshing for the different tooth pair i.e. $N_{T_{(1EH)}}, N_{T_{(2HD)}}, N_{T_{(1LH)}}, N_{T_{(1HD)}}, N_{T_{(3EH)}}$ are calculated by using Eq. (2.25) and mentioned in Table C.1 of Appendix C.

The dynamic factor is calculated by using Eq. (2.41), where the AGMA transmission accuracy-level number, Q_v, is considered as 6 as prescribed by [126] and mentioned in Table C.1 of Appendix C.

The separation between an involute smooth flat surface of gear tooth and the reference plane of the mean peak height in the rough surface of another gear tooth, d, is calculated by using the equations described in [121] and [122] which are detailed in Appendix B3. The value of separation, d, is calculated for different load conditions and mentioned in Table C.1 of Appendix C.

The load shared by asperities, p_a, for the different separation condition, d , during the one mesh period is calculated by using Eqs. (2.38) and mentioned in Table C.1 of Appendix C.

The radius of assumed plane surface during asperity contact at any point on the involute surface of gear, r_1, for the various position during one mesh period i.e. $TE, HPDTC, LPSTC, HPSTC, HPDTC', TD$ for the different tooth pair i.e. new, previous and next tooth pair is calculated by using the theoretical length of line of action of involute gear pair, AB, path of approach, AX, path of recess, XB, (referring to the Fig. 2.3), and simple mathematical equations of sine law and cosine law, which are detailed in Appendix B4 and geometry of Fig. 2.3. The obtained values of r_1 are mentioned in Table C.1 of Appendix C.

The variation of reduced radius of Hertzian curvature, $\Delta r'$, during the one mesh period for the different zone of contact areas of meshing for the different tooth pair i.e. $\Delta r'_{(1EH)}, \Delta r'_{(2HD)}, \Delta r'_{(1LH)}, \Delta r'_{(1HD)}$, $\Delta r'_{(3EH)}$ are calculated by using Eq. (2.8) and mentioned in Table C.1 of Appendix C.

It is assumed that the part of the total elastic strain energy which alters into AE pulses, C_e, is 95% and the part which is received by the AE sensors/ AE measurement instruments, C_m , is also 95%.

2.4 Results and discussion

To validate the developed AE model of gear, the AE data was obtained from an experimental investigation conducted on gear test rig and the AE data was evaluated by the developed model under the same conditions.

Experimental findings have been presented on the influence of load in generating AE for operating the gears. The experimental findings suggest that change in load condition results in a change in AE rms for the spur gears. The experimental results for effect of load variation on AE rms values at a constant speed (1000 rpm) during the test have been given in Table 2.2. With the help of these experimental data, the influence of load on the generation of AE activity is presented in Fig. 2.11, which illustrates that the increase in load resulted in an increase in AE levels.

The AE is calculated through developed model by putting all values of concerned parameters, given in Table C.1 of Appendix C, at constant speed of 1000 rpm with five different load conditions of 0.305, 0.764, 1.529, 1.835, 2.294, and 3.059 kN which is same as experimental investigation. The results of AE rms evaluated by the developed model have been given in Table 2.2. The variation in AE rms for different load condition on the spur gear set is illustrated in Fig. 2.11. The plot shows that the increase in load results in the increase of AE rms level for spur gear.

It can be observed that the AE rms values evaluated by the developed model are close to the AE rms values obtained from experimental investigation under the same conditions.

Table 2.2: Comparative results of the AE observed by experimental study and developed model in healthy spur gear pair

Type of test gears	Contact load (kN)	AE rms by experimental investigation (V)	AE rms by developed model (V)
Spur	0.305	0.0065	0.0058
	0.764	0.0089	0.008
	1.529	0.0103	0.01
	1.835	0.011	0.0105
	2.294	0.0119	0.0113
	3.059	0.0133	0.0121

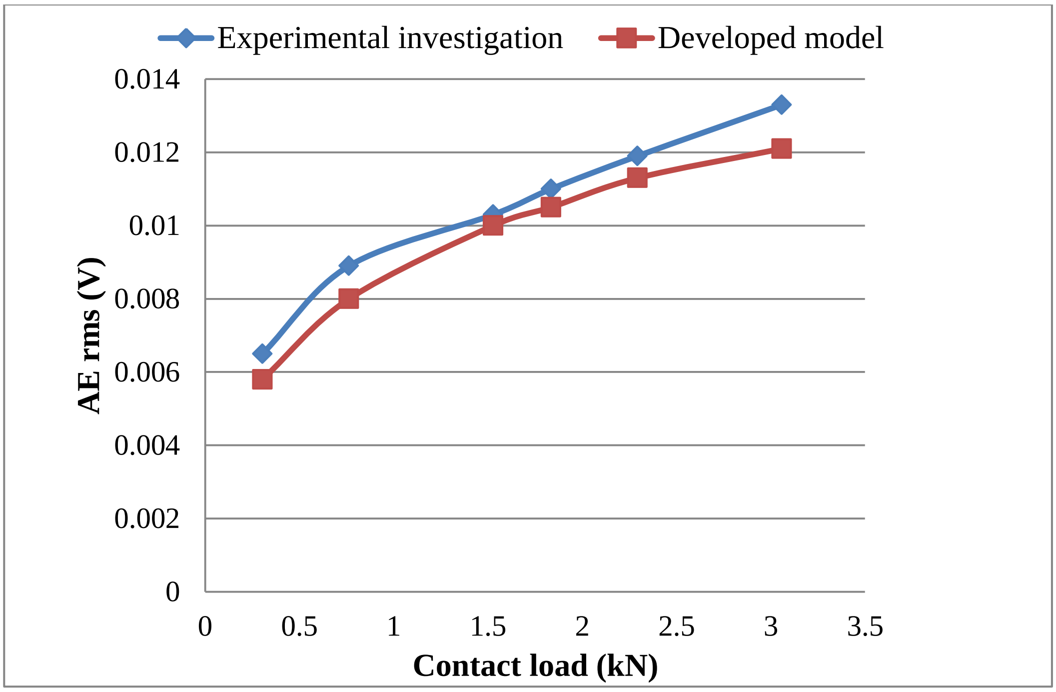

Fig. 2.11 AE rms from spur gear running at different loads by experimental investigation and developed model

2.5 Summary

Modelling of AE in gears is very intricate due to various aspects which influence the gear process. Hence, using appropriate assumptions, related to involute gear tooth meshing and asperities deformation process during asperity contact and also based upon experimental studies accomplished by researches, a mathematical model has been developed to predict the AE engendered by asperity interaction between the involute surfaces of gear teeth during gear pair mesh.

The developed model correlates AE to gear parameters which demonstrates that the level of AE is influenced by the load, speed, number of asperity contacts, gear teeth surface topographies and specifications/profile of gears. The model has been developed by considering the effect of load sharing during the mesh cycle, lubrication, and dynamic load condition which play the vibrant role in generating of the AE during the gear mesh. The developed relationship between gear parameters and AE energy level was validated on the basis of an experimental study conducted on gear lubricant testing machine and satisfactory results have been observed. It shows the potential of the developed model to perceive the AE generated during the meshing of spur gears.

CHAPTER 3

MODELLING OF ACOUSTIC EMISSION GENERATED BY CRACK PROPAGATION IN SPUR GEAR

3.1 Introduction

A lot of experimental studies are available in the literature for fault diagnosis of gear using AE as discussed in Chapter-1. In this chapter, a theoretical model to correlate the AE energy, generated by crack propagation in gear tooth, to the parameters allied with crack has been proposed based on linear elastic fracture mechanics. The developed theoretical model is validated with the results of experimental investigation.

The mathematical modelling is presented in section 3.2. The effect of load sharing during the total length of contact in the developed model is discussed in subsection 3.2.1. The validation of developed mathematical model with experimental AE data for the various crack lengths is presented in section 3.3. The results and discussion are given in section 3.4. In the last, the work of this chapter is summarized in section 3.5.

3.2 Mathematical model

The AE model for propagating a crack in gear is developed based on following assumptions:

a. No effect has been assumed on the AE due to pitch error, shaft misalignment, unbalance and deviation in temperature.
b. Perfect lubrication condition is assumed between the mating gears.

A relationship between an amplitude of AE and parameters related to crack propagation is developed for the gear tooth with edge crack of length, a, at the root of gear tooth as shown in Fig. 3.1.

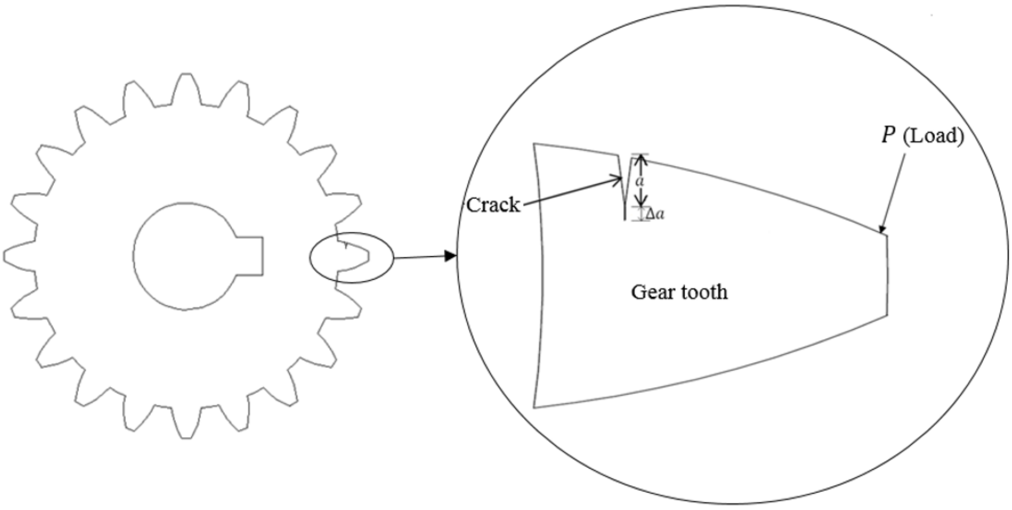

Fig. 3.1 Crack propagation in spur gear tooth

An energy release rate, E_r, which is the measure of the energy available for growth of crack extension, is defined as the rate of change in potential energy with respect to crack area, given by [127]:

$$E_r = -\frac{dE_p}{dA} \tag{3.1}$$

The strain energy, E_s, stored in the gear tooth can be given as:

$$E_s = \frac{1}{2}\, P\delta_c \tag{3.2}$$

where, P is load acting on the gear tooth and δ_c is displacement.

Using Eq. (3.2), the change in potential energy for incremental crack propagation from a to $a + \Delta a$, for the fixed displacement as shown in Fig. 3.2, is given by

$$-dE_p = \frac{\delta_c[P_a - P_{a+\Delta a}]}{2} = \frac{1}{2}\delta_c \Delta P \tag{3.3}$$

where, $\Delta P = P_a - P_{a+\Delta a}$, is the load drop accompanying with crack propagation from a to $a + \Delta a$ in gear tooth.

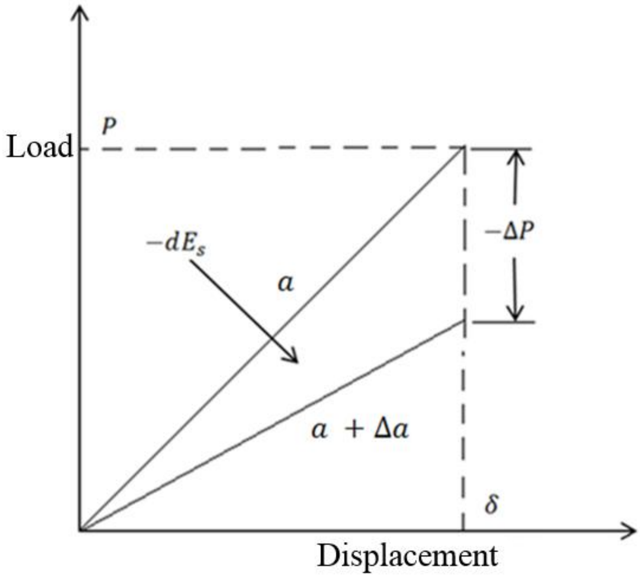

Fig. 3.2 Energy release due to crack propagation at fixed displacement [127]

Using Eqs. (3.1) and (3.3),

$$E_r = -\frac{1}{2}\frac{\delta_c \Delta P}{B\Delta a} = -\frac{1}{2}\frac{\delta_c \Delta P}{\Delta A} \tag{3.4}$$

where, B is the width of gear tooth or thickness of gear and $B\Delta a$ is the area swept out by the propagating crack i.e. ΔA.

Irwin has also established the relationship between energy release rate and compliance, as follows [127]:

$$E_r = \frac{P^2}{2B}\frac{dC_g}{da} \tag{3.5}$$

where, C_g is compliance under the applied load, P, and displacement, δ_c, given by:

$$C_g = \frac{\delta_c}{P} \tag{3.6}$$

The energy release rate of gear tooth can be determined by using Eq. (3.5). Since gear tooth is assumed as a cantilever, using beam theory, gear tooth displacement,δ_c, can be given as follows:

$$\delta_c = \frac{2}{3}\frac{Pa^3}{EI}, \text{ where } I = \frac{BL^3}{12} \tag{3.7}$$

where, E is modulus of elasticity, I is area moment of inertia.

Using Eqs. (3.5), (3.6) and (3.7) the energy release rate is

$$E_r = \frac{P^2 a^2}{BEI} \tag{3.8}$$

Hence, the energy released through the growth of crack concluded by Eq. (3.8) can be equated to that of Eq. (3.4) as follows:

$$-\frac{1}{2}\frac{\delta_c \Delta P}{\Delta A} = -\int_a^{a+\Delta a} \frac{P^2 a^2}{BEI} da \tag{3.9}$$

Since $\Delta a \ll a$ the Eq. (3.9) can be approached as follows:

$$-\frac{\delta_c \Delta P}{2\Delta A} = \frac{P^2}{3BEI}[(a+\Delta a)^3 - a^3] \approx \frac{P^2}{3BEI}(3a^2 \Delta a) \tag{3.10}$$

The relationship between energy release rate and stress intensity K_I of cracked gear tooth is given as:

$$E_g = \frac{{K_I}^2}{E} \tag{3.11}$$

Using Eqs. (3.8) and (3.11), ${K_I}^2 \approx P^2 a^2/BI$, Eq. (3.10) can be expressed as

$$-\frac{\delta_c \Delta P}{2\Delta A} \approx \frac{(\Delta a){K_I}^2}{E} \tag{3.12}$$

Putting the value of δ_c by using Eq. (3.6) and using the absolute value of ΔP,

$$\frac{(\Delta a){K_I}^2}{E} \approx \frac{\Delta P}{2\Delta A} P C_g \tag{3.13}$$

Abersek and Flasker [128] derived the stress intensity for the cracked gear tooth which is as follows:

$$K_I = \frac{6PL}{B{S_t}^2}\sqrt{\pi a}\left[\left(\cos\varphi - \frac{C}{L}\sin\varphi\right)Y_m(\alpha_c) - \frac{S_t}{6L}\sin\varphi\, Y_t(\alpha_c)\right] \tag{3.14}$$

where,

$Y_m(\alpha_c)$ and $Y_t(\alpha_c)$ are the shape factor for bending and extension respectively. The mathematical expression for the same is mentioned in Appendix D1.

S_t is the gear tooth thickness at tooth root, L is the distance between the contact point and the edge crack situated on tooth root, C is the distance between the contact point and the central line of the tooth as shown in Fig. 3.3.

φ is the pressure angle; $\varphi = tan^{-1}\left(\frac{P_y}{P_x}\right)$, $P = \sqrt{{P_x}^2 + {P_y}^2}$.

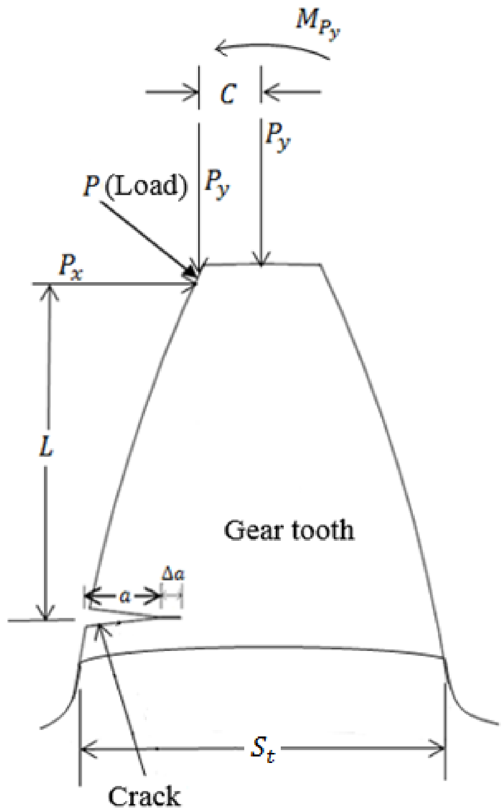

Fig. 3.3 Load and moment on gear tooth [128]

In terms of mesh stiffness of gear pair, the Eq. (3.13) can be described as follows:

$$\frac{(\Delta a){K_I}^2}{E} \approx \frac{\Delta P}{2\Delta A} P \frac{1}{k_t} \tag{3.15}$$

where k_t is the total effective mesh stiffness of a pair of involute spur gears without manufacturing error which is calculated from the following equation as given by Tian [125]:

$$k_t = \sum_{i=1}^{2} \frac{1}{\frac{1}{k_{h_i}} + \frac{1}{k_{b1_i}} + \frac{1}{k_{s1_i}} + \frac{1}{k_{a1_i}} + \frac{1}{k_{b2_i}} + \frac{1}{k_{s2_i}} + \frac{1}{k_{a2_i}}} \tag{3.16}$$

The detailed description regarding Eq. (3.16) is prescribed in Appendix D2.

Now, putting the value of P and value of k_t from Eqs. (3.14) and (3.16) respectively in Eq.(3.15)

$$\Delta P \approx \frac{12\, L\sqrt{\pi}\, a^{1/2} \Delta a K_I \Delta A\left[\left(\cos\varphi - \frac{C}{L}\sin\varphi\right) Y_m(\alpha_c) - \frac{S_t}{6L}\sin\varphi\, Y_t(\alpha_c)\right] k_t}{E B {S_t}^2} \qquad (3.17)$$

This is in line with the fracture mechanics approach [127] that SIF (stress intensity factor) is proportional to fatigue crack growth rate and it has been experienced in the above-mentioned experimental studies [84-86,88-89] that crack growth influences the AE accordingly. Hence, stress intensity will also influence to the AE accordingly when crack will propagate. Masuyama et al. [90] found that the AE energy is proportional to the SIF range, ΔK, in the experimental analysis of fatigue crack growth in a carburized gear tooth through AE technique. Desai and Gerberich [106] mentioned that the amplitude of emitted stress wave, ρ_s, should be proportional to the variation in SIF, ΔK. Since $\Delta K \propto \Delta P/B$, hence the amplitude of emitted stress wave, $\rho_s \propto \Delta P/B$. They also verified this relationship experimentally. In the perspective of infinitesimal crack propagation in gear tooth, the emitted stress wave amplitude, ρ_s, can be expressed as:

$$\rho_s = c_1\, \Delta P/B \qquad (3.18)$$

where c_1 is the constant of proportionality.

Using Eqs (3.17) and (3.18), the resulting expression is

$$\rho_s = \frac{12\, c_1 L\sqrt{\pi}\, a^{1/2} \Delta a K_I \Delta A\left[\left(\cos\varphi - \frac{C}{L}\sin\varphi\right) Y_m(\alpha_c) - \frac{S_t}{6L}\sin\varphi\, Y_t(\alpha_c)\right] k_t}{E B^2 {S_t}^2} \qquad (3.19)$$

It is clear from Eq. (3.19), that stress wave emission amplitude is influenced by parameters associated with a crack event.

Fisher et al. [129] and Baranov et al. [130] proposed the energy of AE signal. Fisher et al. [129] mentioned the energy rate of AE signal by the parameter AN where, A is amplitude and N is count rate. By using Eq. (3.18), the elastic energy rate of the AE signal is given by

$$E'_{T_c} = \rho_s t_c N \qquad (3.20)$$

where, t_c is the transducer proportionality constant.

By using Eqs. (3.19) and (3.20),

$$E'_{T_c} = \frac{12\, t_c N c_1 L\sqrt{\pi}\, a^{1/2} \Delta a K_I \Delta A\left[\left(\cos\varphi - \frac{C}{L}\sin\varphi\right) Y_m(\alpha_c) - \frac{S_t}{6L}\sin\varphi\, Y_t(\alpha_c)\right] k_t}{E B^2 {S_t}^2}$$

(3.21)

But, some part of this energy is lost due to the conversion of this energy into AE pulses and then after, some part of the energy is lost due to receiving capacity of AE instruments. Therefore, the elastic energy rate of the AE is given by

$$E'_{AE_c} = \frac{12 C_e C_m\, t_c N c_1 L\sqrt{\pi}\, a^{1/2} \Delta a K_I \Delta A\left[\left(\cos\varphi - \frac{C}{L}\sin\varphi\right) Y_m(\alpha_c) - \frac{S_t}{6L}\sin\varphi\, Y_t(\alpha_c)\right] k_t}{E B^2 {S_t}^2}$$

(3.22)

where, C_e is the part of the total elastic strain energy, mentioned in Eq. (3.21), which alters into AE pulses and C_m is the part which is received by the AE sensors/ AE measurement instruments.

Hence, the total elastic energy accumulated by the AE sensor during the particular duration ΔT is given by

$$E_{AE} = \int_0^{\Delta T} E'_{AE_c}\, dt \tag{3.23}$$

If $V(t)$ is the electrical signal which has been measured, the total energy of the AE signal is given by [as mentioned by Eq. (2.29)]

$$E_{AE'} = \int_0^{\Delta T} V^2(t)\, dt \tag{3.24}$$

It may be noted that the energy which is given in Eqs. (3.23) and (3.24) will be equal.

The rms value of AE signal during the specific duration $\Delta T$of AE signal is defined by [as mentioned by Eq. (2.29)]

$$V_{rms} = \sqrt{\frac{1}{\Delta T}\int_0^{\Delta T} V^2(t)\, dt} \tag{3.25}$$

Using Eqs. (3.23), (3.24) and (3.25), the rms value of AE signal is expressed as

$$V_{rms} = \sqrt{\frac{1}{\Delta T}\int_0^{\Delta T} E'_{AE_c}\, dt} \tag{3.26}$$

Substituting Eq. (3.22) into Eq. (3.26), the rms value of the AE signal is

$$V_{rms} = \left[\frac{1}{\Delta T}\int_0^{\Delta T} \frac{12C_eC_m\, t_cNc_1L\sqrt{\pi}\, a^{1/2}\Delta aK_I\Delta A\left[\left(\cos\varphi - \frac{C}{L}\sin\varphi\right)Y_m(\alpha_c) - \frac{S_t}{6L}\sin\varphi\, Y_t(\alpha_c)\right]k_t}{EB^2{S_t}^2}\, dt\right]^{1/2}$$

(3.27)

The energy rate of the AE (E_{AE}) will be constant if the meshing of the involute gears is stable for particular contact load, crack parameters and gear profile. Hence, by using Eq. (3.27), the relationship between AE rms and crack parameters is specified as

$$V_{rms} = \left[\frac{12\, C_eC_mt_cNc_1L\sqrt{\pi}\, a^{1/2}\Delta aK_I\Delta A\left[\left(\cos\varphi - \frac{C}{L}\sin\varphi\right)Y_m(\alpha_c) - \frac{S_t}{6L}\sin\varphi\, Y_t(\alpha_c)\right]k_t}{EB^2{S_t}^2}\right]^{1/2}$$

(3.28)

Define, $C_c = \left[12c_1C_eC_mt_c\sqrt{\pi}\right]^{1/2}$, Eq. (3.28) is expressed as

$$V_{rms} = C_c\left[\frac{a^{1/2}\Delta aK_I\Delta ANL\left[\left(\cos\varphi - \frac{C}{L}\sin\varphi\right)Y_m(\alpha_c) - \frac{S_t}{6L}\sin\varphi\, Y_t(\alpha_c)\right]k_t}{EB^2{S_t}^2}\right]^{1/2}$$

(3.29)

3.2.1 Effect of load sharing during the total length of contact

If the load sharing during the length of contact is taken into consideration, the load will be as per the LSF as described in section 2.2.1 of Chapter-2. The LSF is given by Eq. (2.35). Hence, the energy rate of the of AE generated by crack propagation due to load, p_i, and stress intensity factor, ${K_I}_i$, accordingly, mesh stiffness, ${k_t}_i$, crack propagation length, Δa_i, crack progressive area, ΔA_i, parameters, C_i, L_i, during the length of contact is expressed as follows by using Eq. (3.22):

$$E_{AE_i} = \frac{12C_eC_m\, t_cNc_1L_i\sqrt{\pi}\, a^{1/2}\Delta a_ik_i\Delta A_i\left[\left(\cos\varphi - \frac{C_i}{L_i}\sin\varphi\right)Y_m(\alpha_c) - \frac{S_t}{6L_i}\sin\varphi\, Y_t(\alpha_c)\right]k_{t_i}}{EB^2{S_t}^2}$$

(3.30)

It is clear from Eqs. (2.35) and (3.30), the value of AE will vary during the total length of contact according to LSF. The total AE evaluation during the length of contact is specified as follows:

(i) The AE generated during the TE to HPDTC.

(ii) The AE generated during the LPSTC to HPSTC.

(iii) The AE generated during the HPDTC' to TD.

Hence, the total rms value of the generated AE is calculated as follows by using Eq. (3.30):

$$V_{rms(L)} = C_c \left[\frac{1}{\theta_T} \left[\int_{\theta_{TE(1)}}^{\theta_{HPDTC(1)}} [A][B]\, d\theta + \int_{\theta_{LPSTC(1)}}^{\theta_{HPSTC(1)}} [C][D]\, d\theta + \int_{\theta_{HPDTC'(1)}}^{\theta_{TD(1)}} [E][F]\, d\theta \right] \right]^{1/2} \quad (3.31)$$

In Eq. (3.31),

$$A = LSF_{TE(1)} + \frac{\left(LSF_{HPDTC(1)} - LSF_{TE(1)}\right)}{\left(\theta_{HPDTC(1)} - \theta_{TE(1)}\right)} \left(\theta - \theta_{TE(1)}\right)$$

$$B = \frac{a^{1/2} \Delta a_d K_{I_i} \Delta A_d N L_i \left[\left(\cos\varphi - \frac{C_i}{L_i} \sin\varphi \right) Y_m(\alpha_c) - \frac{S_t}{6L_i} \sin\varphi\, Y_t(\alpha_c) \right] k_{t_d}}{E B^2 {S_t}^2}$$

$$C = LSF_{LPSTC(1)} + \frac{\left(LSF_{HPSTC(1)} - LSF_{LPSTC(1)}\right)}{\left(\theta_{HPSTC(1)} - \theta_{LPSTC(1)}\right)} \left(\theta - \theta_{LPSTC(1)}\right)$$

$$D = \frac{a^{1/2} \Delta a_s K_{I_i} \Delta A_s N L_i \left[\left(\cos\varphi - \frac{C_i}{L_i} \sin\varphi \right) Y_m(\alpha_c) - \frac{S_t}{6L_i} \sin\varphi\, Y_t(\alpha_c) \right] k_{t_s}}{E B^2 {S_t}^2}$$

$$E = LSF_{HPDTC'(1)} + \frac{\left(LSF_{TD(1)} - LSF_{HPDTC'(1)}\right)}{\left(\theta_{TD(1)} - \theta_{HPDTC'(1)}\right)} \left(\theta - \theta_{HPDTC'(1)}\right)$$

$$F = \frac{a^{1/2} \Delta a_d K_{I_i} \Delta A_d N L_i \left[\left(\cos\varphi - \frac{C_i}{L_i} \sin\varphi \right) Y_m(\alpha_c) - \frac{S_t}{6L_i} \sin\varphi\, Y_t(\alpha_c) \right] k_{t_d}}{E B^2 {S_t}^2}$$

In the Eq. (3.31), the value of parameters L_i and C_i is prescribed as follows [125]:

$$L_i = R_b[(\alpha_1 + \alpha_2) \sin\alpha_1 + \cos\alpha_1 - \cos\alpha_2] \quad (3.32)$$

$$C_i = R_b[(\alpha_1 + \alpha_2) \cos\alpha_1 - \sin\alpha_1] \quad (3.33)$$

$$K_{I_i} = \frac{6PL_i}{BS_t^2}\sqrt{\pi a}\left[\left(\cos\varphi - \frac{C_i}{L_i}\sin\varphi\right)Y_m(\alpha_c) - \frac{S_t}{6L_i}\sin\varphi\, Y_t(\alpha_c)\right] \tag{3.34}$$

where, R_b is the radius of base circle of the pinion, α_1 is angular variable and α_2 is half of the base tooth angle.

The relation between α_1 and θ is prescribed as follows [125]:

$$\alpha_1 = \theta - \frac{\pi}{2T_1} - inv\varphi + \tan\left[\arccos\left(\frac{T_1\cos\varphi}{\sqrt{(T_2+2)^2+(T_1+T_2)^2-2(T_2+2)(T_1+T_2)\cos\left(\arccos\left(\frac{T_2\cos\varphi}{T_2+2}\right)-\varphi\right)}}\right)\right] \tag{3.35}$$

where, T_1 and T_2 are the numbers of teeth of the pinion and the gear respectively. θ is the angular displacement of the pinion.

The value of α_2 is prescribed as follows [125]:

$$\alpha_2 = \frac{\pi}{2T_1} + inv\varphi \tag{3.36}$$

The value of R_b is prescribed as follows [125]:

$$R_b = \frac{T_1}{2D_p}\cos\varphi \tag{3.37}$$

where, D_p, is the diametral pitch.

The value of crack propagation length, crack progressive area and mesh stiffness are considered constant during double-tooth-pair mesh duration as $\Delta a_d, \Delta A_d, k_{t\,d}$ respectively and during single-tooth pair mesh duration as $\Delta a_s, \Delta A_s, k_{t\,s}$ respectively.

Total effective mesh stiffness is calculated as follows [125]:

$$k_{t_d} = \sum_{i=1}^{2}\frac{1}{\frac{1}{k_{h_i}}+\frac{1}{k_{b1_i}}+\frac{1}{k_{s1_i}}+\frac{1}{k_{a1_i}}+\frac{1}{k_{b2_i}}+\frac{1}{k_{s2_i}}+\frac{1}{k_{a2_i}}}$$; for double-tooth-pair mesh duration (3.38)

$$k_{t_s} = \frac{1}{\frac{1}{k_h}+\frac{1}{k_{b_{crack}}}+\frac{1}{k_{s_{crack}}}+\frac{1}{k_{a_1}}+\frac{1}{k_{b_2}}+\frac{1}{k_{s_2}}+\frac{1}{k_{a_2}}}$$; for single-tooth-pair mesh duration (3.39)

The detailed description regarding Eqs. (3.38) and (3.39) is prescribed in Appendix D2.

3.3 Experimental validation of the developed model

A mathematical model which relates the amplitude of AE to the parameters of a crack phenomenon in gear tooth is proposed. The developed mathematical model has been validated by experimental data which was extracted from the research work performed by Sentoku and Tokuda [85]. They presented experimental findings on the influence of crack length and number of cycles in generating AE of the spur gear. The experimental findings suggest that change in crack length conditions results in the change in amplitude of AE for the spur gear. Table 3.1 summarizes the test gears specifications detailed in [85]

Table 3.1: Test gears specifications [85]

No. of teeth, pinion	27
No. of teeth, gear	31
Pitch diameter, pinion (mm)	108
Pitch diameter, gear (mm)	124
Module (mm)	4
Pressure angle (°)	20
Face width (mm)	10

In order to evaluate the value of AE by the developed model, the parameters allied with Eq. (3.31) are determined and prescribed in the Table E.1 and E.2 of Appendix E.

The meshing duration of the double/single tooth pair within one mesh period (θ_d and θ_s) and the total angle of meshing (θ_T) during one mesh period is calculated by using the equations detailed in [125] which are mentioned in Appendix B2 and then after, the angular displacements for the various position during one mesh period i.e. $TE, HPDTC, LPSTC, HPSTC, HPDTC', TD$ for the different position of tooth pair during the total length of contact are calculated and mentioned in Table E.1 of Appendix E. The values of LSF for the various positions during the one mesh period i.e. $TE, HPDTC, LPSTC, HPSTC,\ HPDTC', TD$ for the tooth pair are calculated as per AGMA standard [120] for spur gears and mentioned in Table E.1 of Appendix E.

The values of k_{t_d} and k_{t_s} are calculated by using Eqs. (3.38) and (3.39) respectively and equation mentioned in Appendix D2 and the values of both are mentioned in Table E.2 of Appendix E. The value of $Y_m(\alpha_c)$ and $Y_t(\alpha_c)$ are determined from the equations which are mentioned in Appendix D1. The half of the base tooth angle of the pinion, α_2, and radius of a base circle of the pinion, R_b, is calculated by using Eqs. (3.36) and (3.37) respectively. The value of crack propagation lengths have been calculated using AutoCAD 13 by drawing tangents on the respective points belongs to particular crack length on curve between crack length and number of cycles as prescribed in [85] and measured values are mentioned in Table E.2 of Appendix E. The value of constant, c_1, is assumed to be the same as prescribed for the compact tension specimen in [106] and mentioned in Table E.1 of Appendix E. The value of, t_c, is considered as 0.95. It is assumed that the part of the total elastic strain energy which alters into AE pulses, C_e, is 95% and the part which is received by the AE sensors/ AE measurement instruments, C_m, is also 95%.

3.4 Results and discussion

The experimental findings of AE rms for different crack length have been extracted by the curve between crack length, no. of cycles and amplitude of AE as prescribed in [85]. The experimental results for effect of a crack length variation on AE rms values during the test have been given in Table 3.2. With the help of these experimental data, the influence of crack length on the generation of AE activity during meshing of spur gears is presented in Fig. 3.4, which illustrates that the change in crack length results in the change in AE rms level for the spur gear.

The value of AE rms by the developed mathematical model has been calculated by putting all values of concerned parameters, given in Table E.1 and E.2 of Appendix E. The AE rms value is calculated through developed model with different crack lengths. The results of AE rms evaluated by the developed model have been given in Table 3.2. The variation in AE rms for different crack lengths of the spur gear set is shown in Fig. 3.4. The plot shows that the change in crack length results in the change of AE rms level for the spur gear.

Table 3.2: The values of AE rms by experimental results [85] and developed model

S. No.	Crack length (mm)	AE rms by experimental investigation [85] (V)	AE rms by developed model (V)
1.	1.6	0.02871	0.0203
2.	1.8	0.03302	0.0254
3.	2.0	0.04311	0.0358
4.	2.2	0.05256	0.0456
5.	2.4	0.06103	0.0546
6.	2.6	0.06794	0.0627

The comparative plot between crack length and AE rms by developed model as well as experimental results has been plotted in Fig. 3.4. The experimental findings and results of the developed model both suggest that change in crack length results in a change in AE rms level for the spur gear and both follows almost the same trend. It can be observed that the AE rms values predicted by the developed mathematical model for different crack lengths are nearby to the AE rms values obtained from experimental investigation under the same conditions.

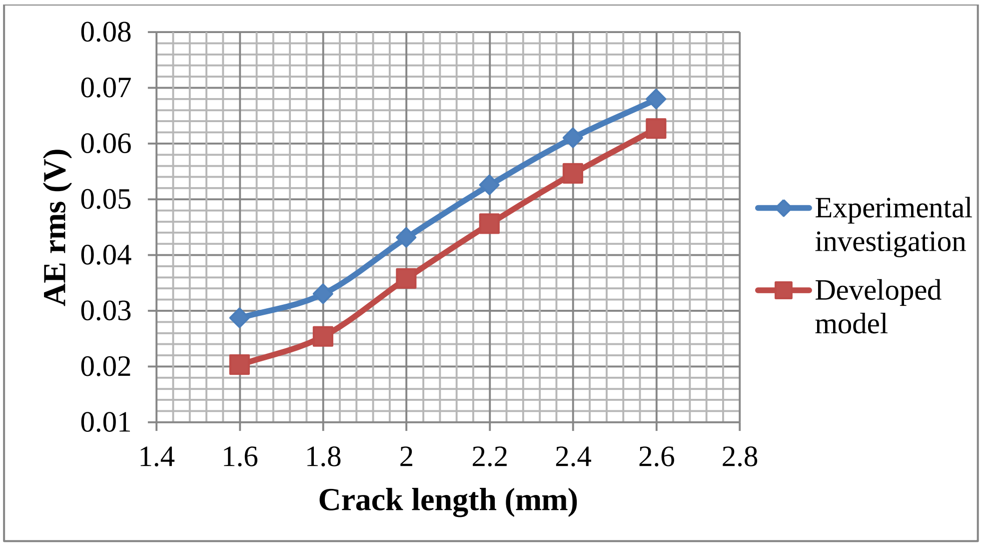

Fig. 3.4 AE rms with crack length obtained by experimental results [85] and developed model

3.5 Summary

A mathematical model to predict the AE value from crack extension in gear tooth has been developed. The relations of fracture mechanics have been implemented for the development of rapport between the amplitude of stress wave produced during crack propagation and crack parameters in spur gear. It has been postulated that crack parameters in the gear tooth viz. length of crack propagation, the progressive area swept out by the propagating crack, stress intensity and crack length affect the AE amplitude and AE rms has a square root relationship with the crack parameters. The developed model shows that AE amplitude is determined by the crack parameters and specification of gear profile. The developed relationship between gear crack parameters and AE energy level was validated on the basis of the experimental study conducted by Sentoku and Tokuda [85] and the satisfactory match has been observed.

The proposed mathematical model pronounces the theoretical base to correlate the characteristics of the AE to the crack parameters from the perspective of fracture event in gear and thus provides a base to understand the actual physical mechanism of AE during the incremental cracking in gears.

CHAPTER 4

MODELLING OF ACOUSTIC EMISSION GENERATED DUE TO PITTING ON SPUR GEAR

4.1 Introduction

Several experimental investigations have been performed which shows the capability of AE technique to fault detection of gears as detailed in Chapter-1. It has been investigated by experimental studies that if the size of defect increases, the AE level also increases. But, there is lack of mathematical model to understand the physics behind the same. In this chapter, a theoretical model is developed to establish a relationship between size of fault and energy of AE generated during gear meshing on the basis of interaction of asperities and protrusions around the fault. The mathematical model has been established using Hertzian contact approach, varying sliding velocity of gear tooth mechanism, and statistical concepts with the aid of surface topography of gear tooth having the pit of different size. The methodology used to develop the mathematical model is described in section 4.2.

The model is extended by considering the influence of three phenomena during gear mesh cycle: load sharing, lubrication and dynamic load condition as discussed in subsection of 4.2 i.e. 4.2.1, 4.2.2, and 4.2.3 respectively. The developed theoretical model is validated with an experimental study performed on IAE gear lubrication testing machine as detailed in section 4.3. The obtained experimental results are compared with results calculated by developed model and discussed in section 4.4. At the end of this chapter, the summary is presented in section 4.5.

4.2 Mathematical model of AE

The asperity and protrusion interactions influence the value of AE. Size of defect on gear tooth surface influences the size of protrusions. Hence, asperities as well as protrusions characteristics of the contact surface of the gear tooth, in presence of defect, are responsible for the generation of AE level.

The model is developed based on following assumptions:

a. The defect is considered as a pit of diameter, D, on pitch line of gear tooth surface as shown in Fig. 4.1.
b. The effect of depth of defect on AE is not considered. The defects of various diameters are considered with constant depth.
c. Only elastic deformation of asperities on the gear tooth surface is considered.
d. Only sliding contact is considered during gears mesh.
e. The effect of pitch errors, unbalance, shaft misalignment, and deviation in temperature, on the AE is not considered.

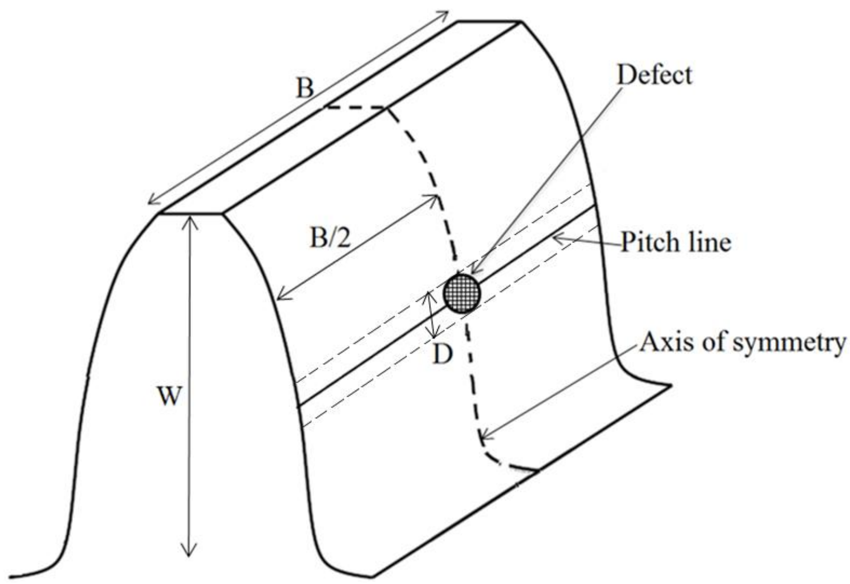

Fig. 4.1 Defect in the form of pit of diameter *D* on pitch line of gear tooth surface

The teeth surfaces of both healthy gear as well as defected gears are having asperities of different heights. Hence, for the investigation of contact between the surfaces of gear teeth, all the asperities can be considered on one surface (defected gear tooth surface) such that it is having an asperity distribution equivalent to composite asperity height distributions of both meshing surfaces of gears as per the model developed by Greenwood and Tripp [34] for the contact of surfaces. Another surface (healthy gear tooth surface) can be considered as a smooth surface. It is assumed that the heights (z) of asperities, exists on the defected gear tooth surface, varies in some statistical way and all asperities peaks are considered as spherical and have the same characteristic radius. Let the separation between healthy gear tooth surface and the reference plane in the defected gear tooth surface is d as shown in Fig. 4.2 which is constant at the point of contact of gear teeth surfaces.

A mathematical model is presented in Chapter-2 for AE generated in spur gear pair in which the model is developed by using surface topographic parameters related to healthy gear pair. The surface topographic characteristics related to defected gear pair are different which affect the AE energy and on the basis of these characteristics, this chapter presents a mathematical model for AE generated due to pitting on the spur gear. Interaction of asperities and protrusions around the defect (pit) are considered as the source of generation of AE in the developed model.

Fig. 4.2 shows the contact of healthy and defected gear teeth surfaces during the deformation of asperities and protrusions around the defect.

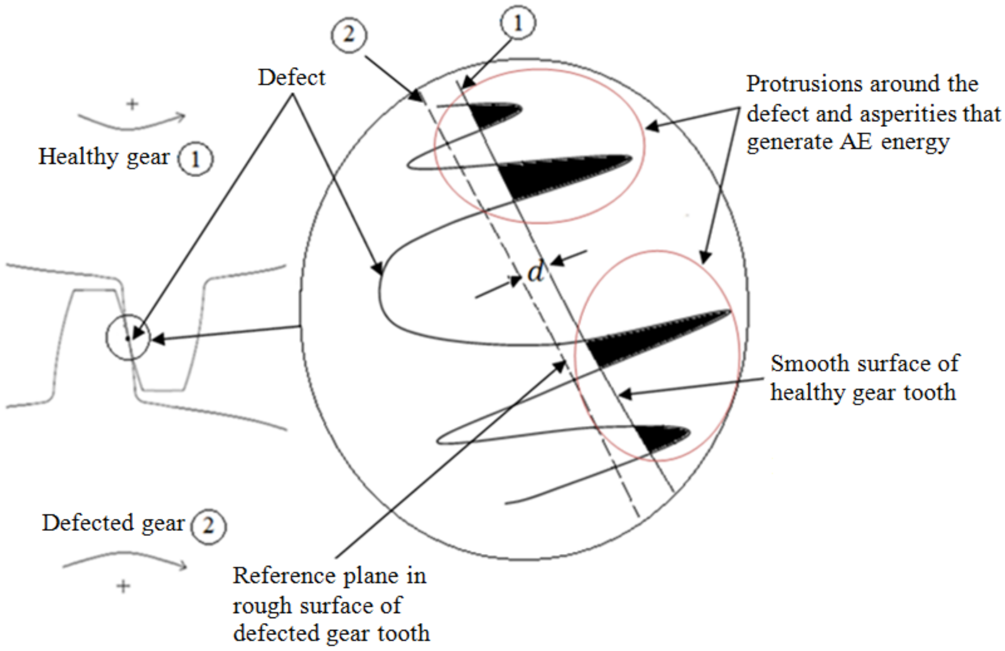

Fig. 4.2 Deformation of asperities and protrusions around the defect during contact between healthy and defected gear teeth surfaces in involute gear teeth meshing

The elastic energy rate of the AE generated due to asperities deformation during the meshing of gears is prescribed as follows:

$$E'_{AE} = \frac{3C_e C_m N_T \Delta \mathbf{r}' P \omega_1 \int_d^{\infty}(z-d)\emptyset(z)dz}{5\left[\int\left(\frac{r_s}{r_1(r_1+r_s)}\right)^{1/2} dr_1\right]\left[\int_d^{\infty}(z-d)^{1/2}\emptyset(z)dz\right]\left[\int\left[1/\left(1-R_1/R_2\sqrt{\left(\frac{R_2}{R_1}\right)^2(cos(\varphi-\alpha/2))^2+\left[(tan\,\varphi\, cos(\varphi-\alpha/2))\left\{\left(\frac{R_2}{R_1}\right)+1\right\}-sin(\varphi-\alpha/2)\right]^2}\right)\right]d\alpha\right]} \tag{4.1}$$

The mathematical description of the Eq. (4.1) is extensively described in Chapter-2 which is based on Hertzian contact approach, statistical concepts, and varying sliding velocity of gear tooth mechanism. It is clear from the Eq. (4.1); the elastic energy rate of the AE will depend on topographic characteristics of the gear tooth surface. If the value of the parameters related to the surface of gear tooth changes, the AE value will vary accordingly. It is noted that the surface topographic characteristics are different in the zone of boundary of defect due to presence of protrusions than rest of the surface of gear tooth as postulated by Tan and Mba [15] and Eftekharnejad and Mba [23] during their experimental investigation. Hence, for the calculation of the total AE, the total contact area of one pair of teeth during meshing of gears, A_c, where the asperities and protrusions deformation takes place and energy releases is considered as follows:

$$A_c = A_d + A_r \tag{4.2}$$

where, A_d is the portion of contact area of gear tooth surface which is having protrusions around the produced defect, A_r is the contact area of rest of the portion of gear tooth surface i.e. the contact area of gear tooth surface excluding the contact area A_d and the area of defect (pit) as shown in Fig. 4.3. The diameter of defect (pit) is considered as, D, on the pitch line of the gear tooth as shown in Fig. 4.3. The expressions for A_d and A_r are as follows:

$$A_r = W \times B - (A_d + \pi/4(D)^2) \tag{4.3}$$

$$A_d = \pi/4[(D + 2S)^2 - (D)^2] \tag{4.4}$$

where, W is the working depth of gear tooth, B is the face width of gear tooth and S is the distance from the boundary of defect (pit) corresponding to the area of the protrusion around the defect as shown in Fig. 4.3.

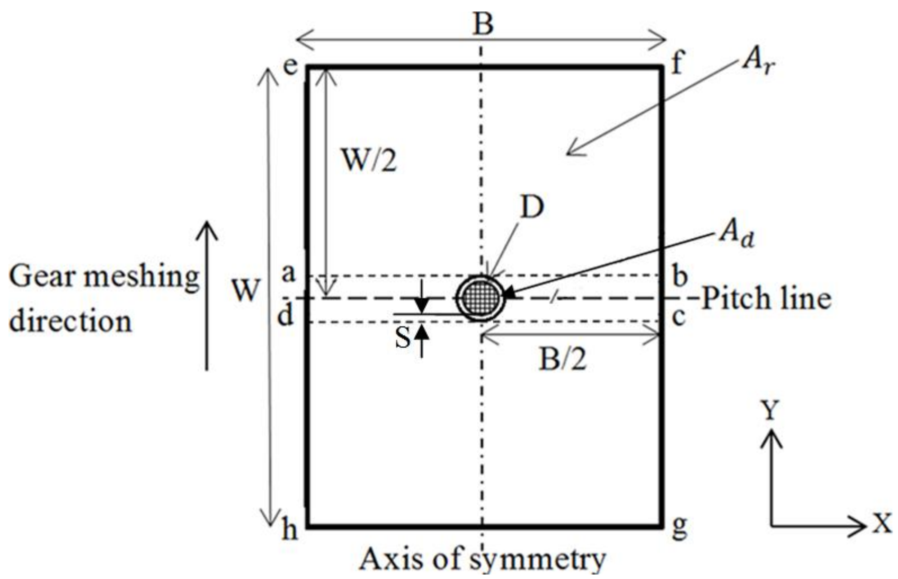

Fig. 4.3 Schematic view of gear tooth surface consists of defect in the form of pit of the diameter, *D*, on the pitch line

Hence, the elastic energy rate of the AE generated by asperities deformation in the zone of contact area of gear tooth surface which is having asperities, A_r, is calculated as follows by using Eq. (4.1):

$E'_{AE_r} =$

$$\frac{3C_eC_mN_{T_r}\Delta r' P\omega_1 \int_d^{\infty}(z-d)\emptyset(z)dz}{5\left[\int\left(\frac{r_s}{r_1(r_1+r_s)}\right)^{1/2}dr_1\right]\left[\int_d^{\infty}(z-d)^{1/2}\emptyset(z)dz\right]\left[\int\left[1/\left(1-R_1/R_2\sqrt{\left(\frac{R_2}{R_1}\right)^2(cos(\varphi-\alpha/2))^2+\left[(tan\,\varphi\,cos(\varphi-\alpha/2))\left\{\left(\frac{R_2}{R_1}\right)+1\right\}-sin(\varphi-\alpha/2)\right]^2}\right)\right]d\alpha\right]}$$

(4.5)

where, N_{T_r} is the total number of asperity contacts in the contact area, A_r, given as follows by using Eq. (2.25):

$$N_{T_r} = N_r x_g A_r N_a \int_d^{\infty} \emptyset(z)dz \qquad (4.6)$$

The stored elastic energy for protrusion interaction ($\bar{E}_{ia_d}$) around the defect on gear tooth surface can be given as follows by using Eq. (2.10):

$$\bar{E}_{ia_d} = \frac{2}{5}P(z_d - d) \qquad (4.7)$$

The total elastic energy stored due to the protrusion interaction in N_r number of revolutions of gear, E_{T_d}, can be given as follows:

$$E_{T_d} = N_r x_g\, \pi(D+S)\bar{E}_{ia_d} \qquad (4.8)$$

The mean release time of protrusion interaction during deformation can be given as follows by using Eqs. (2.15), (2.18) and, (2.20):

$$\bar{t}_d = \left[\left(\frac{r_p}{r_{1_m}(r_{1_m}+r_p)}\right)^{1/2}\right]\left[\frac{1}{\omega_1-\omega_2\sqrt{\left(\frac{R_2}{R_1}\right)^2(cos(\varphi-\alpha_m/2))^2+\left[(tan\,\varphi\,cos(\varphi-\alpha_m/2))\left\{\left(\frac{R_2}{R_1}\right)+1\right\}-sin(\varphi-\alpha_m/2)\right]^2}}\right](z_d-d)^{1/2}$$

(4.9)

where, z_d is the height of the protrusion around the defect from the mean line, r_p is the radius of the protrusion, r_{1_m} is the mean value of r_1 at DSPSTC and $r_1$at DEPSTC, α_m is the mean value of α at DSPSTC and α at DEPSTC.

Using Eqs. (4.8) and (4.9), the elastic strain energy rate released by protrusion interaction is given as follows:

$E'_{AE_d} = \frac{E_{T_d}}{\bar{t}_d} =$

$$\frac{2C_eC_mN_rx_g\pi(D+S)P\omega_1(z_d-d)}{5\left[\left(\frac{r_p}{r_{1m}(r_{1m}+r_p)}\right)^{1/2}\right]\left[(z_d-d)^{1/2}\right]\left[\left[1/\left(1-R_1/R_2\sqrt{\left(\frac{R_2}{R_1}\right)^2(cos(\varphi-\alpha_m/2))^2+\left[(tan\,\varphi\,cos(\varphi-\alpha_m/2))\left\{\left(\frac{R_2}{R_1}\right)+1\right\}-sin(\varphi-\alpha_m/2)\right]^2}\right)\right]\right]}$$

(4.10)

Hence, the total elastic strain energy accumulated by the AE sensor/ AE instrument during the specific duration ΔT is given by

$$E_{AE} = \int_0^{\Delta T} E'_{AE_r} dt + \int_0^{\Delta T_d} E'_{AE_d} dt \qquad (4.11)$$

If $V(t)$ is the electrical signal which has been measured, the total energy of the AE signals is given by [as mentioned by Eq. (2.29)]

$$E_{AE'} = \int_0^{\Delta T} V^2(t)\, dt \qquad (4.12)$$

It may be noted that the energy given in Eqs. (4.11) and (4.12) will be equal.

The rms value of AE signal during the specific duration $\Delta T$of AE signal is described by [as mentioned by Eq. (2.30)]

$$V_{rms} = \sqrt{\frac{1}{\Delta T} \int_0^{\Delta T} V^2(t)\, dt} \qquad (4.13)$$

Using Eqs. (4.11), (4.12), and (4.13), the rms value of AE signal can be expressed as

$$V_{rms} = \sqrt{\frac{1}{\Delta T} \left[\int_0^{\Delta T} E'_{AE_r} dt + \int_0^{\Delta T_d} E'_{AE_d} dt \right]} \qquad (4.14)$$

Substituting Eqs. (4.5) and (4.10) into Eq. (4.14), the rms value of the AE signal energized during the meshing of gears is

$$V_{rms} = \left[\frac{1}{\Delta T} \left\{ \int_0^{\Delta T} \left(\frac{3 C_e C_m N_{T_r} \Delta \boldsymbol{r}' P \omega_1 \int_d^{\infty} (z-d) \emptyset(z) dz}{5 \left[\int \left(\frac{r_s}{r_1 (r_1 + r_s)} \right)^{1/2} dr_1 \right] \left[\int_d^{\infty} (z-d)^{1/2} \emptyset(z) dz \right] \left[\int \left[1 / \left(1 - R_1/R_2 \sqrt{\left(\frac{R_2}{R_1} \right)^2 (\cos(\varphi - \alpha/2))^2 + \left[(\tan\varphi \cos(\varphi - \alpha/2)) \left\{ \left(\frac{R_2}{R_1} \right) + 1 \right\} - \sin(\varphi - \alpha/2) \right]^2} \right) \right] d\alpha \right]} \right) dt + \int_0^{\Delta T_d} \left(\frac{2 C_e C_m N_r x_g \pi (D+S) P \omega_1 (z_d - d)}{5 \left[\left(\frac{r_p}{r_{1m} (r_{1m} + r_p)} \right)^{1/2} \right] \left[(z_d - d)^{1/2} \right] \left[\left[1 / \left(1 - R_1/R_2 \sqrt{\left(\frac{R_2}{R_1} \right)^2 (\cos(\varphi - \alpha_m/2))^2 + \left[(\tan\varphi \cos(\varphi - \alpha_m/2)) \left\{ \left(\frac{R_2}{R_1} \right) + 1 \right\} - \sin(\varphi - \alpha_m/2) \right]^2} \right) \right] \right]} \right) dt \right\} \right]^{1/2}$$

(4.15)

The energy rate of AE, E'_{AE_r} and E'_{AE_d}, will be constant, if the sliding in the involute gears is steady during meshing of gears for particular contact load, speed, particular gear profile, and gear surface. Hence, by using Eq. (4.15), the rapport between AE rms and the gear parameters with defect (pit) based on elastic asperity contact as well as protrusion contact is specified as follows:

$$V_{rms} = \left[\frac{3C_eC_mN_{T_r}\Delta r' P\omega_1 \int_d^{\infty}(z-d)\emptyset(z)dz}{5\left[\int\left(\frac{r_s}{r_1(r_1+r_s)}\right)^{1/2}dr_1\right]\left[\int_d^{\infty}(z-d)^{1/2}\emptyset(z)dz\right]\left[\int\left[1/\left(1-R_1/R_2\sqrt{\left(\frac{R_2}{R_1}\right)^2(cos(\varphi-\alpha/2))^2+\left[(tan\,\varphi\, cos(\varphi-\alpha/2))\left\{\left(\frac{R_2}{R_1}\right)+1\right\}-sin(\varphi-\alpha/2)\right]^2}\right)\right]d\alpha\right]} + \frac{2C_eC_mN_rx_g\pi(D+S)P\omega_1(z_d-d)}{5\left[\left(\frac{r_p}{r_{1m}(r_{1m}+r_p)}\right)^{1/2}\right]\left[(z_d-d)^{1/2}\right]\left[\left[1/\left(1-R_1/R_2\sqrt{\left(\frac{R_2}{R_1}\right)^2(cos(\varphi-\alpha_m/2))^2+\left[(tan\,\varphi\, cos(\varphi-\alpha_m/2))\left\{\left(\frac{R_2}{R_1}\right)+1\right\}-sin(\varphi-\alpha_m/2)\right]^2}\right)\right]\right]}\right]^{1/2} \quad (4.16)$$

Define, $C_c = \left[\frac{3}{5}C_eC_m\right]^{1/2}$, Eq. (4.16) is expressed as

$$V_{rms} = \left[\frac{N_{T_r}\Delta r' P\omega_1 \int_d^{\infty}(z-d)\emptyset(z)dz}{\left[\int\left(\frac{r_s}{r_1(r_1+r_s)}\right)^{1/2}dr_1\right]\left[\int_d^{\infty}(z-d)^{1/2}\emptyset(z)dz\right]\left[\int\left[1/\left(1-R_1/R_2\sqrt{\left(\frac{R_2}{R_1}\right)^2(cos(\varphi-\alpha/2))^2+\left[(tan\,\varphi\, cos(\varphi-\alpha/2))\left\{\left(\frac{R_2}{R_1}\right)+1\right\}-sin(\varphi-\alpha/2)\right]^2}\right)\right]d\alpha\right]} + \frac{2N_rx_g\pi(D+S)P\omega_1(z_d-d)}{3\left[\left(\frac{r_p}{r_{1m}(r_{1m}+r_p)}\right)^{1/2}\right]\left[(z_d-d)^{1/2}\right]\left[\left[1/\left(1-R_1/R_2\sqrt{\left(\frac{R_2}{R_1}\right)^2(cos(\varphi-\alpha_m/2))^2+\left[(tan\,\varphi\, cos(\varphi-\alpha_m/2))\left\{\left(\frac{R_2}{R_1}\right)+1\right\}-sin(\varphi-\alpha_m/2)\right]^2}\right)\right]\right]}\right]^{1/2} \quad (4.17)$$

It can be noted from Eq. (4.17) that the value of AE rms is proportional to the contact load and speed and it may be determined by topographic characteristics of the gear teeth surface and specifications of gears.

4.2.1 Influence of load sharing during the total length of contact

The model is extended by considering the effect of load sharing during the total length of contact. The asperity as well as protrusion interaction is the phenomenon which is associated with local contact mechanics. The actual applied load for the deformation of asperity and protrusion is different during the mesh cycle due to load sharing during total length of contact. Hence, the value of AE generated due to deformation of asperity and protrusion by the particular load at specific local contact will vary during the mesh cycle.

The theory of load sharing of spur gears is described in section 2.2.1 of Chapter-2, in which LSF is given by Eq. (2.35) and the variation of theoretical LSF with respect to meshing angle is shown in Fig. 2.4.

Furthermore, the effect of defect with protrusion is shown in Fig. 4.4. It can be noted from Fig. 4.4, the load remains constant i.e. 3/3 (100%) of the total load during the zone of boundary of defect due to presence of protrusion when only one gear pair is in mesh between DSPSTC (defect with protrusion start point of single tooth contact at respective defect diameter) and DEPSTC (defect with protrusion end point of single tooth contact at respective defect diameter).

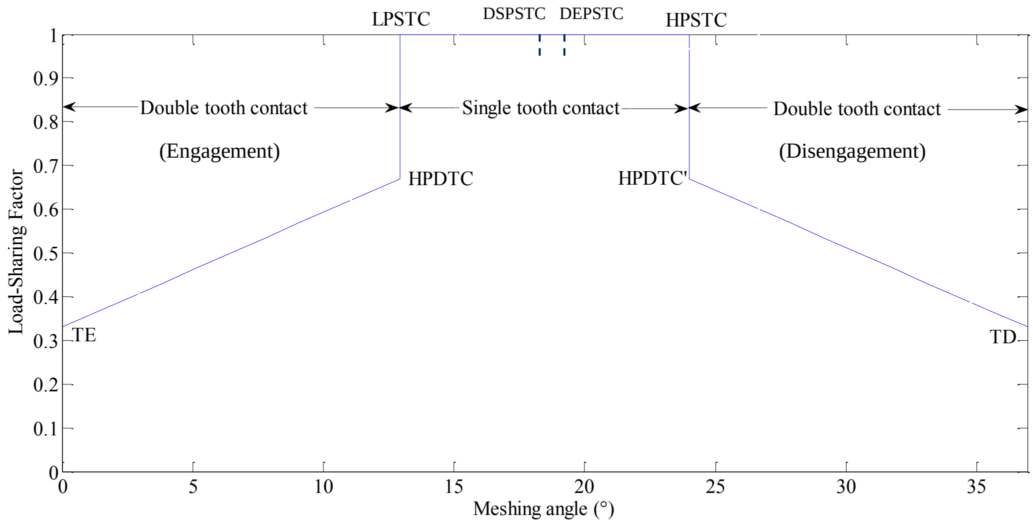

Fig. 4.4 Load Sharing Factor with meshing angle during mesh cycle including the influence of defect with protrusion

If the load sharing during the mesh cycle is taken into consideration, the load at the local contact of asperities as well as protrusions will be as per the LSF as described above. Hence, the energy rate of the of AE generated by deformation of asperities and protrusions of local contact due to load, p_i, during mesh cycle is expressed as follows by using Eqs. (4.5) and (4.10):

$$E'_{AE_{ri}} = \frac{3C_eC_mN_{T_r}\Delta \boldsymbol{r}' p_i\omega_1 \int_d^{\infty}(z-d)\emptyset(z)dz}{5\left[\int\left(\frac{r_s}{r_1(r_1+r_s)}\right)^{1/2}dr_1\right]\left[\int_d^{\infty}(z-d)^{1/2}\emptyset(z)dz\right]\left[\int\left[1/\left(1-R_1/R_2\sqrt{\left(\frac{R_2}{R_1}\right)^2(cos(\varphi-\alpha/2))^2+\left[(tan\,\varphi\, cos(\varphi-\alpha/2))\left\{\left(\frac{R_2}{R_1}\right)+1\right\}-sin(\varphi-\alpha/2)\right]^2}\right)\right]d\alpha\right]} \tag{4.18}$$

$$E'_{AE_{di}} = \frac{2C_eC_mN_rx_g\pi(D+S)p_i\omega_1(z_d-d)}{5\left[\left(\frac{r_p}{r_{1m}(r_{1m}+r_p)}\right)^{1/2}\right]\left[(z_d-d)^{1/2}\right]\left[\left[1/\left(1-R_1/R_2\sqrt{\left(\frac{R_2}{R_1}\right)^2(cos(\varphi-\alpha_m/2))^2+\left[(tan\,\varphi\, cos(\varphi-\alpha_m/2))\left\{\left(\frac{R_2}{R_1}\right)+1\right\}-sin(\varphi-\alpha_m/2)\right]^2}\right)\right]\right]} \tag{4.19}$$

It is clear from Eqs. (2.35), (4.18) and (4.19), the value of AE will vary during the total length of contact according to LSF. The total AE evaluation during the mesh cycle is described as follows:

(i) The total AE generated during the TE to HPDTC is calculated by summation of AE generated during the TE to HPDTC by new tooth pair and AE generated during the HPDTC' to TD by previous tooth pair. During this section of mesh cycle, both pairs of teeth are simultaneously engaged.

(ii) The total AE generated during the LPSTC to HPSTC by new tooth pair excluding the contact area $(\mathrm{A_d} + \pi/4(\mathrm{D})^2)$ at respective defect diameter.

(iii) The total AE generated through the contact area, A_d, i.e. area of gear tooth surface which is having protrusions around the defect (pit) as shown in Fig. 4.3 by new tooth pair during the DSPSTC to DEPSTC.

(iv) The total AE generated during the HPDTC' to TD is calculated by summation of AE generated during the HPDTC' to TD by new tooth pair and AE generated during TE to HPDTC by next tooth pair. Two pairs of teeth are again simultaneously engaged.

Hence, the total rms value of the generated AE is calculated as follows by using Eqs. (4.18) and (4.19):

$$V_{rms(F)} = C_c \left[\frac{1}{\theta_T} \left[\int_{\theta_{TE(1)}}^{\theta_{HPDTC(1)}} [A.P.B]\, d\theta + \int_{\theta_{HPDTC'(2)}}^{\theta_{TD(2)}} [C.P.D]\, d\theta + \int_{\theta_{LPSTC(1)}}^{\theta_{HPSTC(1)}} [E.P.F]\, d\theta + \int_{\theta_{DSPSTC(1)}}^{\theta_{DEPSTC(1)}} [G.P.H]\, d\theta + \int_{\theta_{HPDTC'(1)}}^{\theta_{TD(1)}} [I.P.J]\, d\theta + \int_{\theta_{TE(3)}}^{\theta_{HPDTC(3)}} [K.P.L]\, d\theta \right] \right]^{1/2} \tag{4.20}$$

In Eq. (4.20), values of $A, B, C, D, E, F, G, H, I, J, K$ and L are given by Eq. (4.20 A), (4.20 B), (4.20 C), (4.20 D), (4.20 E), (4.20 F), (4.20 G), (4.20 H), (4.20 I), (4.20 J), (4.20 K), and (4.20 L) respectively as follows:

$$A = LSF_{TE(1)} + \frac{\left(LSF_{HPDTC(1)} - LSF_{TE(1)}\right)}{\left(\theta_{HPDTC(1)} - \theta_{TE(1)}\right)}\left(\theta - \theta_{TE(1)}\right) \tag{4.20 A}$$

$$B = \frac{N_{T_{(1EH)}} \Delta \boldsymbol{r'}_{(1EH)} \omega_1 \int_d^{\infty} (z-d) \emptyset(z) dz}{\left[\int_{r_{1TE(1)}}^{r_{1HPDTC(1)}} \left(\frac{r_S}{r_1(r_1+r_S)}\right)^{1/2} dr_1\right]\left[\int_d^{\infty} (z-d)^{1/2} \emptyset(z) dz\right]\left[\int_{\alpha_{TE(1)}}^{\alpha_{HPDTC(1)}} \left[1/\left(1 - R_1/R_2 \sqrt{\left(\frac{R_2}{R_1}\right)^2 (cos(\varphi - \alpha/2))^2 + \left[(tan\,\varphi\, cos(\varphi - \alpha/2))\left\{\left(\frac{R_2}{R_1}\right) + 1\right\} - sin(\varphi - \alpha/2)\right]^2}\right)\right] d\alpha\right]} \tag{4.20 B}$$

$$C = LSF_{HPDTC'(2)} + \frac{\left(LSF_{TD(2)} - LSF_{HPDTC'(2)}\right)}{\left(\theta_{TD(2)} - \theta_{HPDTC'(2)}\right)}\left(\theta - \theta_{HPDTC'(2)}\right) \tag{4.20 C}$$

$$D = \frac{N_{T_{(2HD)}} \Delta \boldsymbol{r'}_{(2HD)} \omega_1 \int_d^{\infty} (z-d) \emptyset(z) dz}{\left[\int_{r_{1HPDTC'(2)}}^{r_{1TD(2)}} \left(\frac{r_S}{r_1(r_1+r_S)}\right)^{1/2} dr_1\right]\left[\int_d^{\infty} (z-d)^{1/2} \emptyset(z) dz\right]\left[\int_{\alpha_{HPDTC'(2)}}^{\alpha_{TD(2)}} \left[1/\left(1 - R_1/R_2 \sqrt{\left(\frac{R_2}{R_1}\right)^2 (cos(\varphi - \alpha/2))^2 + \left[(tan\,\varphi\, cos(\varphi - \alpha/2))\left\{\left(\frac{R_2}{R_1}\right) + 1\right\} - sin(\varphi - \alpha/2)\right]^2}\right)\right] d\alpha\right]} \tag{4.20 D}$$

$$E = LSF_{LPSTC(1)} + \frac{\left(LSF_{HPSTC(1)} - LSF_{LPSTC(1)}\right)}{\left(\theta_{HPSTC(1)} - \theta_{LPSTC(1)}\right)}\left(\theta - \theta_{LPSTC(1)}\right) \tag{4.20 E}$$

$$F = \frac{N_{T_{(1LH)_d}} \Delta \boldsymbol{r'}_{(1LH)} \omega_1 \int_d^{\infty} (z-d) \emptyset(z) dz}{\left[\int_{r_{1LPSTC(1)}}^{r_{1HPSTC(1)}} \left(\frac{r_S}{r_1(r_1+r_S)}\right)^{1/2} dr_1\right]\left[\int_d^{\infty} (z-d)^{1/2} \emptyset(z) dz\right]\left[\int_{\alpha_{LPSTC(1)}}^{\alpha_{HPSTC(1)}} \left[1/\left(1 - R_1/R_2 \sqrt{\left(\frac{R_2}{R_1}\right)^2 (cos(\varphi - \alpha/2))^2 + \left[(tan\,\varphi\, cos(\varphi - \alpha/2))\left\{\left(\frac{R_2}{R_1}\right) + 1\right\} - sin(\varphi - \alpha/2)\right]^2}\right)\right] d\alpha\right]} \tag{4.20 F}$$

$$G = LSF_{DSPSTC(1)} + \frac{\left(LSF_{DEPSTC(1)} - LSF_{DSPSTC(1)}\right)}{\left(\theta_{DEPSTC(1)} - \theta_{DSPSTC(1)}\right)}\left(\theta - \theta_{DSPSTC(1)}\right) \tag{4.20 G}$$

$$H = \frac{2N_r x_g \pi(D+S)\omega_1(z_d-d)}{3\left[\left(\frac{r_p}{r_{1m}(r_{1m}+r_p)}\right)^{1/2}\right]\left[(z_d-d)^{1/2}\right]\left[\left[1/\left(1-R_1/R_2\sqrt{\left(\frac{R_2}{R_1}\right)^2(\cos(\varphi-\alpha_m/2))^2+\left[(\tan\varphi\cos(\varphi-\alpha_m/2))\left\{\left(\frac{R_2}{R_1}\right)+1\right\}-\sin(\varphi-\alpha_m/2)\right]^2}\right)\right]\right]} \quad (4.20\ H)$$

$$I = LSF_{HPDTC'(1)} + \frac{\left(LSF_{TD(1)}-LSF_{HPDTC'(1)}\right)}{\left(\theta_{TD(1)}-\theta_{HPDTC'(1)}\right)}\left(\theta-\theta_{HPDTC'(1)}\right) \quad (4.20\ I)$$

$$J = \frac{N_{T_{(1HD)}}\Delta \boldsymbol{r'}_{(1HD)}\omega_1\int_d^\infty (z-d)\emptyset(z)dz}{\left[\int_{r_{1HPDTC'(1)}}^{r_{1TD(1)}}\left(\frac{r_s}{r_1(r_1+r_s)}\right)^{1/2}dr_1\right]\left[\int_d^\infty(z-d)^{1/2}\emptyset(z)dz\right]\left[\int_{\alpha_{HPDTC'(1)}}^{\alpha_{TD(1)}}\left[1/\left(1-R_1/R_2\sqrt{\left(\frac{R_2}{R_1}\right)^2(\cos(\varphi-\alpha/2))^2+\left[(\tan\varphi\cos(\varphi-\alpha/2))\left\{\left(\frac{R_2}{R_1}\right)+1\right\}-\sin(\varphi-\alpha/2)\right]^2}\right)\right]d\alpha\right]} \quad (4.20\ J)$$

$$K = LSF_{TE(3)} + \frac{\left(LSF_{HPDTC(3)}-LSF_{TE(3)}\right)}{\left(\theta_{HPDTC(3)}-\theta_{TE(3)}\right)}\left(\theta-\theta_{TE(3)}\right) \quad (4.20\ K)$$

$$L = \frac{N_{T_{(3EH)}}\Delta \boldsymbol{r'}_{(3EH)}\omega_1\int_d^\infty (z-d)\emptyset(z)dz}{\left[\int_{r_{1TE(3)}}^{r_{1HPDTC(3)}}\left(\frac{r_s}{r_1(r_1+r_s)}\right)^{1/2}dr_1\right]\left[\int_d^\infty(z-d)^{1/2}\emptyset(z)dz\right]\left[\int_{\alpha_{TE(3)}}^{\alpha_{HPDTC(3)}}\left[1/\left(1-R_1/R_2\sqrt{\left(\frac{R_2}{R_1}\right)^2(\cos(\varphi-\alpha/2))^2+\left[(\tan\varphi\cos(\varphi-\alpha/2))\left\{\left(\frac{R_2}{R_1}\right)+1\right\}-\sin(\varphi-\alpha/2)\right]^2}\right)\right]d\alpha\right]} \quad (4.20\ L)$$

and 1, 2, and 3 stands for the new tooth pair, previous tooth pair and next tooth pair respectively.

4.2.2 Influence of lubrication

In this section, the lubrication effect is presented on the developed model using the theory of load sharing of Johnson and Greenwood [121] for the asperity contact in EHL as mentioned in section 2.2.2 of Chapter-2.

If the lubrication effect is considered in the model, the AE rms of the developed model is expressed as follows using Eqs. (2.38) and (4.20):

$$V_{rms(FL)} = C_c \left[\frac{1}{\theta_T} \left[\int_{\theta_{TE(1)}}^{\theta_{HPDTC(1)}} [A.p_a.B]\, d\theta + \int_{\theta_{HPDTC'(2)}}^{\theta_{TD(2)}} [C.p_a.D]\, d\theta + \int_{\theta_{LPSTC(1)}}^{\theta_{HPSTC(1)}} [E.p_a.F]\, d\theta + \int_{\theta_{DSPSTC(1)}}^{\theta_{DEPSTC(1)}} [G.p_p.H]\, d\theta + \int_{\theta_{HPDTC'(1)}}^{\theta_{TD(1)}} [I.p_a.J]\, d\theta + \int_{\theta_{TE(3)}}^{\theta_{HPDTC(3)}} [K.p_a.L]\, d\theta \right] \right]^{1/2} \quad (4.21)$$

4.2.3 Influence of dynamic effect

In this section, the dynamic effect is presented on the developed model by using the theory of dynamic effect as described in section 2.2.3 of Chapter-2.

Hence, if the dynamic effect is also taken into consideration, the effect on AE due to dynamic factor is defined as follows by using Eqs. (2.42) and (4.21):

$$V_{rms(FL)} = C_c \left[\frac{1}{\theta_T} \left[\int_{\theta_{TE(1)}}^{\theta_{HPDTC(1)}} [A.k_v.p_a.B]\, d\theta + \int_{\theta_{HPDTC'(2)}}^{\theta_{TD(2)}} [C.k_v.p_a.D]\, d\theta + \int_{\theta_{LPSTC(1)}}^{\theta_{HPSTC(1)}} [E.k_v.p_a.F]\, d\theta + \int_{\theta_{DSPSTC(1)}}^{\theta_{DEPSTC(1)}} [G.k_v.p_P.H]\, d\theta + \int_{\theta_{HPDTC'(1)}}^{\theta_{TD(1)}} [I.k_v.p_a.J]\, d\theta + \int_{\theta_{TE(3)}}^{\theta_{HPDTC(3)}} [K.k_v.p_a.L]\, d\theta \right] \right]^{1/2} \quad (4.22)$$

4.3 Experimental validation of the model

4.3.1 Experimental setup

The experimental investigation was performed on IAE gear lubrication testing machine as described in section 2.3.1 of Chapter-2. The test gears specifications and piezoelectric transducer specifications are detailed in section 2.3.1 of Chapter-2.

In order to measure the influence of defect on the AE measurements, seeded defect tests were performed on the gear lubrication testing machine. For the seeded defect condition, a defect in the form of pit was generated on pitch line of gear tooth surface by EDM (Electrical Discharge Machining). The AE data was collected for the different diameters of seeded defect to measure the influence of size of defect on the AE level at constant load condition. The diameter of seeded defect was increased after conducting each test on the same gear. Defects of 0.5, 1.0, 1.5, 2.0 mm diameters with a constant depth of 0.5 mm were introduced on the tooth surface. The tests were conducted for the constant load condition of 1.529 kN. All the measurements were performed at 1000 rpm. The AE parameter measured was rms of the AE data.

4.3.2 AE by developed model

In order to evaluate the value of AE by the proposed model, the parameters allied with Eq. (4.22) are determined and prescribed in the Table F.1 of Appendix F. The methodology for the determination of the parameters is same as described in section 2.3.2 of Chapter-2.

The surface topography characteristics of the portion of contact area of gear tooth surface which is having protrusions around the produced defect, A_d, and the contact area of rest of the portion of gear tooth surface, A_r, as shown in Fig. 4.3 are determined experimentally by using Marsurf LD 130 which is combined contour and roughness measurement system as shown in Fig. 2.9 of Chapter-2. The specification of this experimental setup is specified in Appendix A. The surface topography of the area, A_r, of gear tooth is measured over an area of 4.0 mm^2 separately using Marsurf LD 130 and the image, depicting the surface topography of the respective area of gear tooth surface is shown in Fig. 4.5. The surface topography characteristics of the contact surface of the gear tooth consist of the asperity peak density, N_a, asperity peak radius, β, and standard deviation of asperity heights, σ. These surface topography characteristics are determined by using spectral moment method as described by McCool [124] which is detailed in Appendix B1 and MountainsMap_v7 surface imaging topography software. In order to find the characteristics of protrusion (the height of the protrusion around the defect from the mean line and the distance from the boundary of defect (pit) corresponding to the area of the protrusion around the defect as shown in Fig. 4.3) which exist in the area, A_d, of gear tooth is measured by the trace of the surface heights along a direction parallel to pitch line of gear tooth surface using Marsurf LD 130 for the different defect diameters and the images, depicting the surface trace of the same, are shown in Fig. 4.6 (a-d). The mean value of different five traces for every defect condition is considered to evaluate the characteristics of protrusions in the area,A_d. The evaluated all values of these surface topography characteristics are mentioned in Table F.1 of Appendix F.

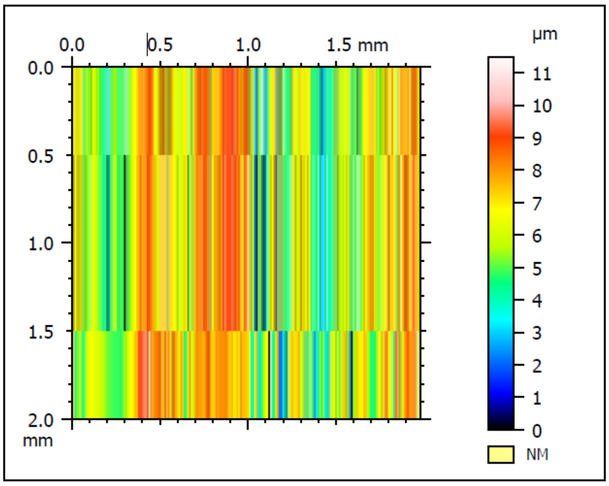

Fig. 4.5 Surface topography image comprises the average surface roughness as 1.38 µm for the gear tooth surface

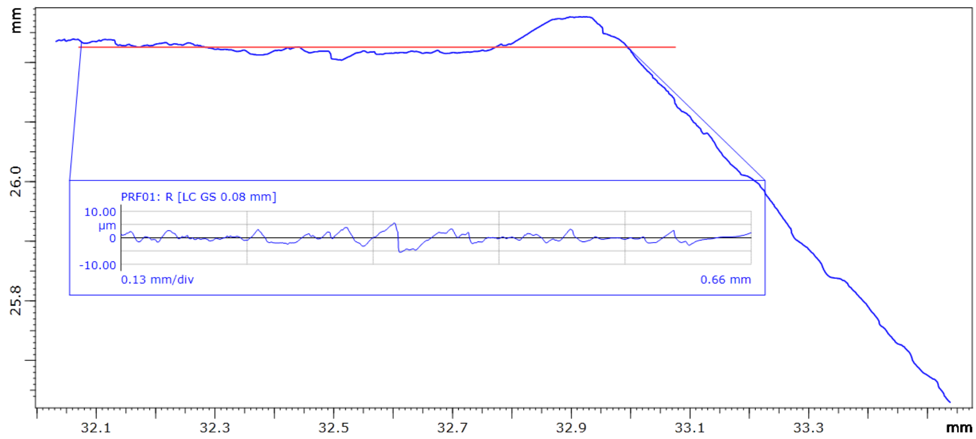
mm
26.0
25.8
PRF01: R [LC GS 0.08 mm]
10.00
µm
0
-10.00
0.13 mm/div
0.66 mm
32.1
32.3
32.5
32.7
32.9
33.1
33.3
mm

(a)

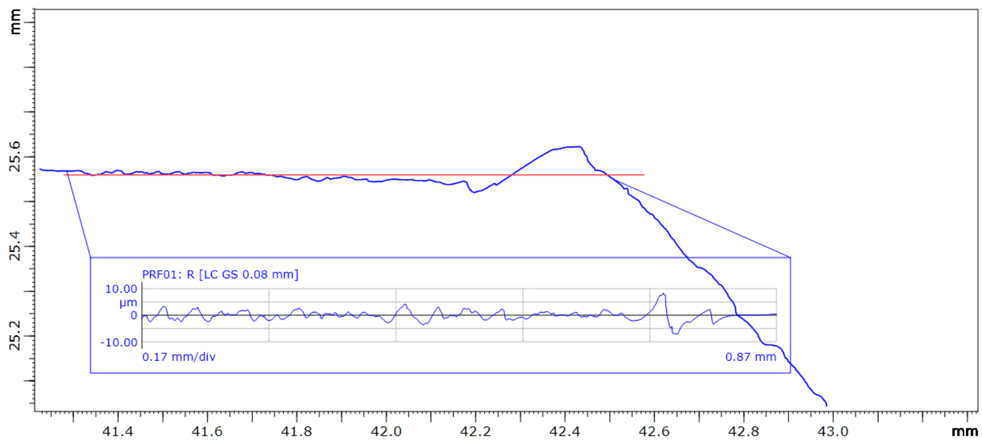
mm
25.6
25.4
25.2
PRF01: R [LC GS 0.08 mm]
10.00
µm
0
-10.00
0.17 mm/div
0.87 mm
41.4
41.6
41.8
42.0
42.2
42.4
42.6
42.8
43.0
mm

(b)

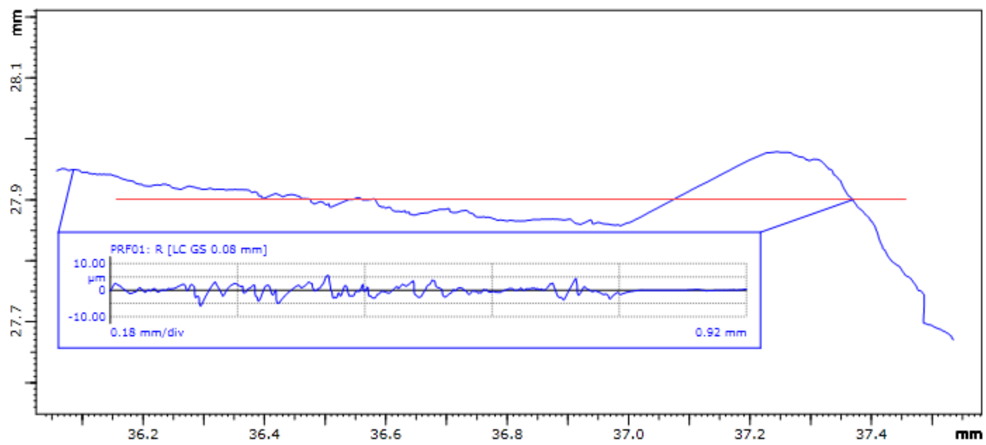
mm
28.1
27.9
27.7
PRF01: R [LC GS 0.08 mm]
10.00
µm
0
-10.00
0.18 mm/div
0.92 mm
36.2
36.4
36.6
36.8
37.0
37.2
37.4
mm

(c)

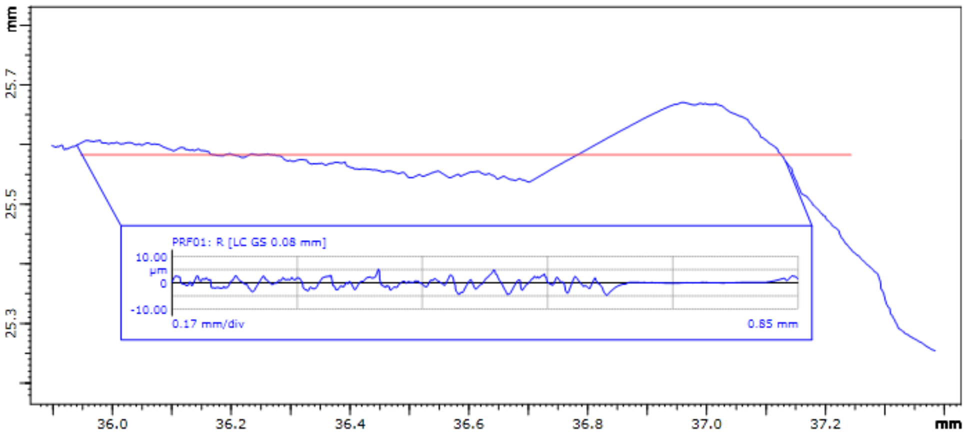

(d)

Fig. 4.6 The trace of the surface heights of the gear tooth surface for the defect (pit) diameter of (a) 0.5 mm (b) 1.0 mm (c) 1.5 mm (d) 2.0 mm

The distribution of asperity heights is considered as Gaussian distribution and the PDF is prescribed by Eq. (2.44) of Chapter-2.

The meshing duration of the double/single tooth pair within one mesh period (θ_d and θ_s) and the total angle of meshing (θ_T) during one mesh period is calculated by using the equations detailed in [125] which are mentioned in Appendix B2 and then after, the angular displacements for the various positions during one mesh period i.e. $TE, HPDTC, LPSTC, HPSTC, DSPSTC, DEPSTC, HPDTC', TD$ for the different tooth pair i.e. new, previous and next tooth pair and various defect conditions are calculated according to position and mentioned in Table F.1 of Appendix F.

The values of LSF for the various positions during the one mesh period i.e. $TE, HPDTC, LPSTC, HPSTC, DSPSTC, DEPSTC, HPDTC'$, TD for the different tooth pair i.e. new, previous and next tooth pair and various defect conditions are calculated as per AGMA standard [120] for spur gears and mentioned in Table F.1 of Appendix F.

The total number of asperity contacts during the one mesh period for the different zone of contact areas of meshing for the different tooth pair i.e. $N_{T_{(1EH)}}, N_{T_{(2HD)}}, N_{T_{(1LH)_d}}$, $N_{T_{(1HD)}}, N_{T_{(3EH)}}$ are calculated by using Eq. (4.6) for respective defect diameter by putting the values of all concerned parameters which are mentioned in Table F.1 of

Appendix F. The value of contact area, A_r and A_d, are calculated by using Eqs. (4.3) and (4.4) respectively for respective defect diameter by putting the values of all concerned parameters which are mentioned Table F.1 of Appendix F.

The dynamic factor is calculated by using Eq. (2.41), where the AGMA transmission accuracy-level number, Q_v, is considered as 6 as prescribed by [126] and mentioned in Table F.1 of Appendix F.

The separation between involute smooth flat surface of gear tooth and the reference plane of the mean peak height in the rough surface of another gear tooth, d, is calculated by using the equations described in [121] and [122] which are detailed in Appendix B3 by putting the values of all concerned parameters which are mentioned in Table F.1 of Appendix F. The value of separation, d, is calculated for the single tooth contact and double tooth contact and mentioned in Table F.1 of Appendix F. The value of PDF is calculated by using the Eq. (2.44) by putting the values of all concerned parameters which are mentioned in Table F.1 of Appendix F.

The load shared by asperities for the respective area, p_a, for the different separation condition, d, during the one mesh period is calculated using Eqs. (2.38) and (2.39) by putting the values of all concerned parameters which are mentioned in Table F.1 of Appendix F. The load shared by protrusions, p_p, due to lubrication effect is considered as half of the total contact load.

The radius of assumed plane surface during asperity contact at any point on the involute surface of gear, r_1, for the various position during one mesh period i.e. $TE, HPDTC, LPSTC, HPSTC, DSPSTC, DEPSTC,$ $HPDTC', TD$ for the different tooth pair i.e. new, previous and next tooth pair and various defect conditions are calculated by using the theoretical length of line of action of involute gear pair, AB, path of approach, AP, path of recess, PB, (referring to the Fig. 2.3 of Chapter-2), simple mathematical equations of sine law and cosine law, which are detailed in Appendix B4 , and geometry of Fig. 2.3 of Chapter-2. The obtained values of r_1 are mentioned in Table F.1 of Appendix F.

The variation of reduced radius of Hertzian curvature, $\Delta r'$, during the one mesh period for the different zone of contact areas of meshing for the different tooth pair i.e. $\Delta r'_{(1EH)}, \Delta r'_{(2HD)}, \Delta r'_{(1LH)}, \Delta r'_{(1HD)}$, $\Delta r'_{(3EH)}$ are calculated by using Eq. (2.8) of Chapter-2 by putting the values of all concerned parameters which are mentioned in Table F.1 of Appendix F.

It is assumed that the part of the total elastic strain energy which alters into AE pulses, C_e, is 95% and the part which is received by the AE sensors/ AE measurement instruments, C_m, is also 95%.

4.4 Results and discussion

To validate the developed AE model of gear, the AE data was obtained from an experimental investigation conducted on gear test rig and the AE data was evaluated by the developed model under the same conditions.

The experimental findings suggest that change in size of defect (diameter of pit) results in a change in AE rms for the spur gears. The experimental results for effect of variation of defect diameter on AE rms values at a constant speed 1000 rpm and contact load 1.529 kN during the test have been given in Table 4.1. With the help of these experimental data, the influence of defect size on the generation of AE activity is presented in Fig. 4.7, which illustrates that the increase in defect diameter resulted in an increase in AE levels.

The AE for the different defect diameter condition is calculated through developed model by putting the all values of concerned parameters, given in Table F.1 of Appendix F, at constant speed of 1000 rpm with load condition of 1.529 kN which is same as experimental investigation. The results of AE rms evaluated by the developed model have been given in Table 4.1. The variation in AE rms for different defect diameter on the spur gear set is illustrated in Fig. 4.7. The plot shows that the increase in defect size results in the increase of AE rms level for spur gear.

It can be observed that the AE rms values evaluated by the developed model are close to the AE rms values obtained from experimental investigation under the same conditions. The effect of defect size on the AE value may also be noted. The AE levels increase as pit diameter increases.

Table 4.1: Comparative results of the AE observed by experimental study and developed model due to pitting on spur gear

Type of test gears	Contact load (kN)	Diameter of seeded defect (mm)	AE rms by experimental investigation (V)	AE rms by developed model (V)
Spur	1.529	0.5	0.1257	0.1161
		1.0	0.1508	0.1314
		1.5	0.1704	0.1543
		2.0	0.2016	0.1857

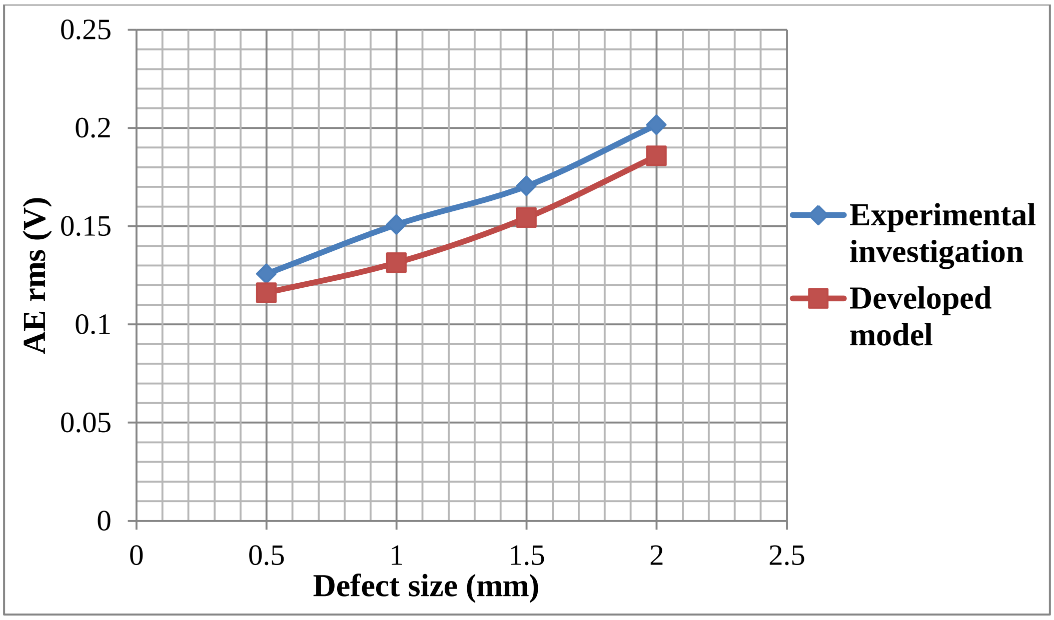

Fig. 4.7 AE rms from spur gear running with different defect size by experimental investigation and developed model

4.5 Summary

Modelling of AE generated in gears due to defect (pitting) is very intricate due to various aspects which influence the AE generation during the gear operating condition. Hence, using appropriate assumptions, related to involute gear tooth meshing, asperities and protrusions deformation process during the contact and also based upon experimental studies related to surfaces topographic characteristics, a mathematical model has been developed to predict the AE in the presence of defect engendered by asperities and protrusions interaction between the involute surfaces of gear teeth during the meshing of gear pair.

The developed theoretical model correlates AE to defect size and gear parameters which shows that the AE level in defected gear pair is influenced by the diameter of defect (pit), contact load, rotational speed, and gear teeth surface topographic characteristics. The effect of load sharing during the mesh cycle, lubrication, and dynamic load condition has been considered in the developed model. The developed theoretical relationship between AE energy level and defect size, gear parameters was validated on the basis of experimental investigation conducted on IAE gear lubricant testing machine and satisfactory results have been observed. It shows the potential of the developed model to perceive the AE value generated due to pitting on spur gear.

CHAPTER 5

MODELLING OF ACOUSTIC EMISSION GENERATED IN ROLLING ELEMENT BEARING

5.1 Introduction

In this chapter, a theoretical model is developed to understand the influence of operating parameters on energy of AE generated in rolling element bearing. The model has been developed on the basis of asperities interaction between surfaces of inner race, outer race and rolling elements of bearing using Hertzian contact approach, statistical concepts, contact load distribution in the load zone and lubrication effects. The model is extended for the defected bearing by considering the defect on inner race, outer race and rolling element to understand the physics of the influence of defect on AE. The developed model has been validated with the experimental studies.

In this chapter, the mathematical model is presented in section 5.2 for healthy bearing as well as defected bearing. The experimental validation of the developed model is given in section 5.3. The mathematical model is validated with the experimental results and discussed in section 5.4. The summary of this chapter is given in section 5.5.

5.2 Mathematical model of AE

The model is developed based on following assumptions:

a. Only elastic deformation of asperities has been considered.
b. No effect has been considered on the AE due to deviation in temperature, unbalance, and shaft misalignment.
c. Outer ring is stationary and inner ring rotates with shaft in rolling element bearing.
d. Rolling element bearing is radially loaded.

The model has been developed on the basis of Hertzian contact approach, statistical concepts, and rolling element bearing mechanics & kinematics. In rolling element bearing, asperities interaction takes place during the contact between inner-race and rolling element as well as outer-race and rolling element as shown in Fig. 5.1. For the investigation of contact between the surfaces of rolling element and races, those are having asperities with different summit heights, all deformable surface roughness can be considered on the surfaces of races such that it is having an asperity distribution equivalent to composite asperity heights distribution of the both surfaces of rolling element and races and the second surface of rolling element can be considered as smooth surface. The rough surface has been assumed to consist of asperities whose heights (z) vary in some statistical manner and all asperity summits have been considered as spherical and have the same characteristic radius. Let the separation between smooth surface of rolling element and the reference plane in the rough surface of inner race and outer race is d_i and d_o respectively as shown in Fig. 5.1.

In Chapter-2, a mathematical model is presented for AE generated in spur gear pair in which the model is developed by using mechanics & kinematics related to gear pair which affects the AE value in the spur gear pair. The mechanics & kinematics related to bearing are different which affects the AE energy in rolling element bearing. The source of generation of AE i.e. inner-race rolling element contact and outer-race rolling element contact, velocity phenomena between elements of bearing, contact load distribution in the load zone of bearing, defect mechanism in bearing contribute the model in different ways. In Fig. 5.1, the asperities interactions during inner-race rolling element contact and outer-race rolling element contact have been shown in zoomed view.

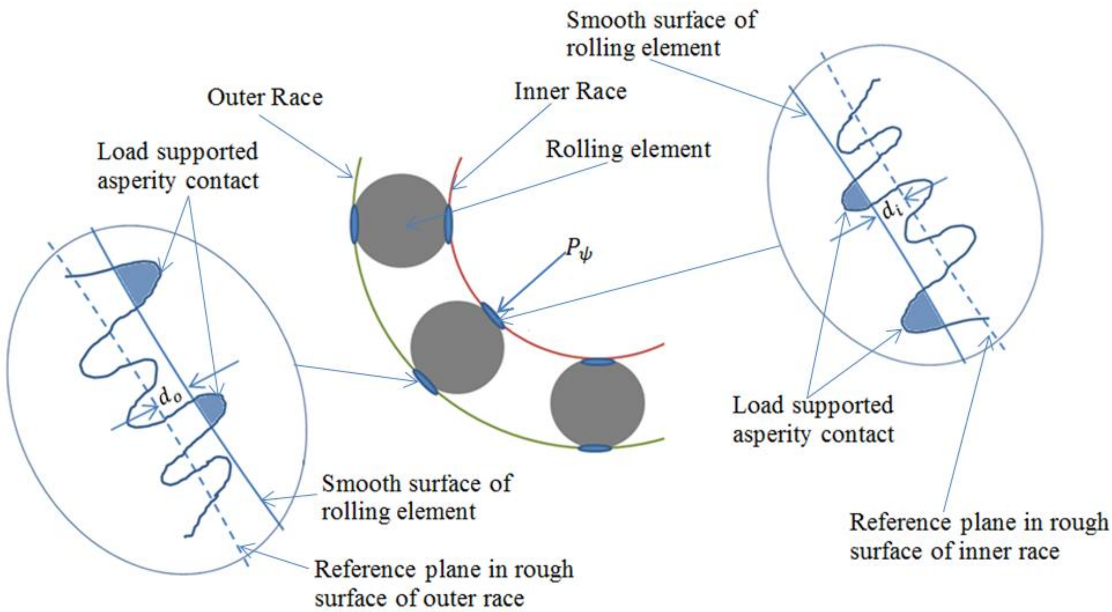

Fig. 5.1 Deformation of asperities during contact between smooth surface and rough surface in rolling element and races contact

The stored elastic energy due to asperities deformation for inner-race rolling element contact and outer-race rolling element contact E_{ei} and E_{eo} respectively is given by

$$E_{ei} = \left(\frac{9}{16}\right)^{1/3} \frac{2}{3E'^{2/3} {r'_i}^{1/3}} \int {F_r}^{2/3} \mathrm{dF_r} \ = \frac{2}{5} F_r \delta_i \tag{5.1}$$

$$E_{eo} = \left(\frac{9}{16}\right)^{1/3} \frac{2}{3E'^{2/3} {r'_o}^{1/3}} \int {F_r}^{2/3} \mathrm{dF_r} \ = \frac{2}{5} F_r \delta_o \tag{5.2}$$

where, F_r is the radial load, δ_i and δ_o are the deformation of asperity at the point of contact for inner-race rolling element contact and outer-race rolling element contact respectively which can be expressed as $\delta_i = z - d_i$ and $\delta_o = z - d_o$, r'_i and r'_o are the reduced radii of Hertzian curvature for inner-race rolling element contact and outer-race rolling element contact respectively, E' is the Hertzian contact modulus. The expressions for δ_i/δ_o, r'_i/r'_o, and E' are prescribed in Appendix G.

Since, maximum deformation depends upon the value of z, the stored mean elastic energy of asperities contact for the inner-race rolling element contact, $\bar{E}_{ei}$, and outer-race rolling element contact, $\bar{E}_{eo}$, is given by

$$\bar{E}_{ei} = \frac{\int_{d_i}^{\infty}\left(\frac{2}{5}F_r\delta_i\right)\emptyset(z)_i\mathrm{dz}}{\int_{d_i}^{\infty}\emptyset(z)_i\mathrm{dz}} = \frac{\frac{2}{5}F_r\int_{d_i}^{\infty}(z-d_i)\emptyset(z)_i\mathrm{dz}}{\int_{d_i}^{\infty}\emptyset(z)_i\mathrm{dz}} \tag{5.3}$$

$$\bar{E}_{eo} = \frac{\int_{d_o}^{\infty}\left(\frac{2}{5}F_r\delta_o\right)\emptyset(z)_o\mathrm{dz}}{\int_{d_o}^{\infty}\emptyset(z)_o\mathrm{dz}} = \frac{\frac{2}{5}F_r\int_{d_o}^{\infty}(z-d_o)\emptyset(z)_o\mathrm{dz}}{\int_{d_o}^{\infty}\emptyset(z)_o\mathrm{dz}} \tag{5.4}$$

where, z is the random variable for the heights of asperity summits which varies randomly, $\emptyset(z)_i$ and $\emptyset(z)_o$ are probability density function of the asperity heights for inner-race rolling element contact and outer-race rolling element contact respectively.

If there are N_{ai} and N_{ao} asperities in the unit contact area of inner-race rolling element contact and outer-race rolling element contact during load zone respectively, the number of such asperity contacts in this area, n_i and n_o, is given by

$$n_i = N_{ai}\int_{d_i}^{\infty}\emptyset(z)_i\mathrm{dz} \tag{5.5}$$

$$n_o = N_{ao}\int_{d_o}^{\infty}\emptyset(z)_o\mathrm{dz} \tag{5.6}$$

Thus, the total elastic energy stored due to the asperity contacts in N_{r_b} number of revolutions of bearing for the inner-race rolling element contact, E_{Ti}, and outer-race rolling element contact, E_{To}, is as follows:

$$E_{Ti} = N_{r_b}rA_{ci}n_i\bar{E}_{ei} \tag{5.7}$$

$$E_{To} = N_{r_b}rA_{co}n_o\bar{E}_{eo} \tag{5.8}$$

where, r is the total number of rolling elements in the load zone of bearing, A_{ci} and A_{co} are the total apparent contact area between inner-race and rolling element as well as outer-race and rolling element in the load zone respectively.

Substitute the value of $\bar{E}_{ei}$ and $\bar{E}_{eo}$ from Eqs. (5.3) and (5.4) respectively and the value of n_i and n_o from Eqs. (5.5) and (5.6) respectively into Eqs. (5.7) and (5.8) respectively

$$E_{Ti} = \frac{2}{5}N_{r_b}rA_{ci}N_{ai}F_r\int_{d_i}^{\infty}(z-d_i)\emptyset(z)_i\mathrm{dz} \tag{5.9}$$

$$E_{To} = \frac{2}{5}N_{r_b}rA_{co}N_{ao}F_r\int_{d_o}^{\infty}(z-d_0)\emptyset(z)_o\mathrm{dz} \tag{5.10}$$

Now, the time for the asperity deformation has been calculated by considering the relative velocities in rolling element bearing. For this purpose, assume the relative velocity between inner-race rolling element and outer-race rolling element is v_{ri} and v_{ro} respectively. The time required for deformation and release of distinct asperity contact through a zone of the Hertzian radius is evaluated as follows [44]:

$$t'_i = \frac{a_i}{v_{ri}}, \qquad \text{for inner-race rolling element contact} \quad (5.11)$$

$$t'_o = \frac{a_o}{v_{r0}}, \qquad \text{for outer-race rolling element contact} \quad (5.12)$$

where, a_i and a_o are the Hertzian radius of the resultant circular asperity contact area for inner-race rolling element contact and outer-race rolling element contact respectively and given as follows:

$$a_i = \left(\frac{3F_r r'_i}{4E\prime}\right)^{1/3} \quad (5.13)$$

$$a_o = \left(\frac{3F_r r'_o}{4E\prime}\right)^{1/3} \quad (5.14)$$

In rolling element bearing mechanism, the angular velocity of the rolling element is obtained by the following equation [131-133]:

$$\omega_r = \frac{(v_r)}{D_e/2} \quad (5.15)$$

where, v_r is the linear velocity of rolling element, D_e is the pitch diameter.

The linear velocity of rotating inner ring at the point of contact between inner race and rolling element, a′, as shown in Fig. 5.2, is expressed as follows [131-133]:

$$v_i = \frac{\omega_i D_i}{2} \quad (5.16)$$

where, ω_i is angular velocity of inner ring or shaft, D_i is the diameter of inner-race rolling element contact.

At the point of contact between outer race and rolling element, b′, as shown in Fig. 5.2, the linear velocity of stationary outer ring is zero. Hence, the linear velocity of rotating element is expressed as follows [131-133]:

$$v_r = \frac{v_i}{2} = \frac{\omega_i D_i}{4} \quad (5.17)$$

Hence, the magnitude of relative velocity between inner-race and rolling element as well as outer-race and rolling element is expressed as follows:

$$v_{ri} = v_{ro} = \frac{\omega_i D_i}{4} \tag{5.18}$$

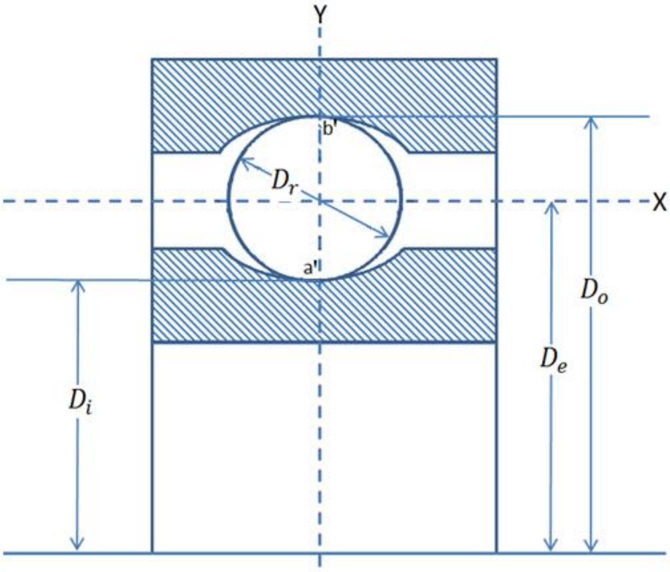

(i)

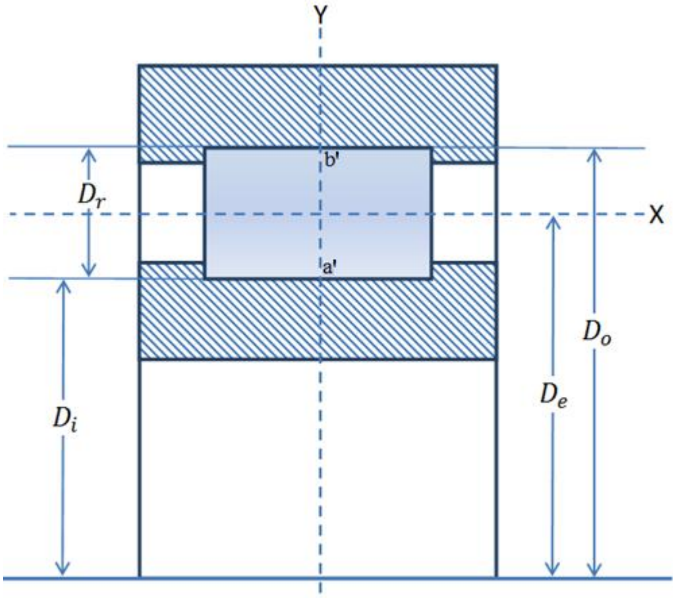

(ii)

Fig. 5.2 Geometrical characteristics of rolling element bearing (i) ball bearing (ii) cylindrical roller bearing

Substitute the value of a_i and v_{ri} from Eqs. (5.13) and (5.18) respectively into Eq. (5.11) and the value of a_o and v_{ro} from Eqs. (5.14) and (5.18) respectively into Eq. (5.12), the total time is expressed, for the inner-race rolling element contact and outer-race rolling element contact, as follows:

$$t'_i = \frac{(\delta_i r'_i)^{1/2}}{\frac{\omega_i D_i}{4}} \tag{5.19}$$

$$t'_o = \frac{(\delta_o r'_0)^{1/2}}{\frac{\omega_i D_i}{4}} \tag{5.20}$$

Since, maximum deformation, δ_i and δ_o, depends upon the value of z, the mean release time of asperity contact during deformation is given as follows for the inner-race rolling element contact and outer-race rolling element contact respectively:

$$\overline{t'_\iota} = \frac{(r'_i)^{1/2}\int_{d_i}^{\infty}(z-d_i)^{1/2}\emptyset(z)_i\mathrm{dz}}{\frac{\omega_i D_i}{4}\int_{d_i}^{\infty}\emptyset(z)_i\mathrm{dz}} \tag{5.21}$$

$$\overline{t'_o} = \frac{(r'_0)^{1/2}\int_{d_o}^{\infty}(z-d_o)^{1/2}\emptyset(z)_o\mathrm{dz}}{\frac{\omega_i D_i}{4}\int_{d_0}^{\infty}\emptyset(z)_o\mathrm{dz}} \tag{5.22}$$

The rate of total elastic strain energy released by asperities deformation for the rolling element bearing is evaluated by adding the rate of elastic strain energy released by asperities deformation for the inner-race rolling element contact (using Eqs. (5.9) and (5.21)) and the rate of elastic strain energy released by asperities deformation for the outer-race rolling element contact (using Eqs. (5.10) and (5.22))] as follows:

$$E'_T = \frac{E_{Ti}}{\overline{t'_\iota}} + \frac{E_{To}}{\overline{t'_0}} = \frac{1}{10}\omega_i D_i N_{r_b} r F_r\left[\frac{A_{ci}N_{ai}\int_{d_i}^{\infty}(z-d_i)\emptyset(z)_i\mathrm{dz}\int_{d_i}^{\infty}\emptyset(z)_i\mathrm{dz}}{(r'_i)^{1/2}\int_{d_i}^{\infty}(z-d_i)^{1/2}\emptyset(z)_i\mathrm{dz}} + \frac{A_{co}N_{ao}\int_{d_o}^{\infty}(z-d_0)\emptyset(z)_o\mathrm{dz}\int_{d_0}^{\infty}\emptyset(z)_o\mathrm{dz}}{(r'_0)^{1/2}\int_{d_o}^{\infty}(z-d_o)^{1/2}\emptyset(z)_o\mathrm{dz}}\right] \tag{5.23}$$

But, some part of this energy is lost due to conversion of this energy into AE pulses and then after, some part of the energy is lost due to receiving capacity of AE instruments. Therefore, the elastic energy release rate of the AE is given by

$$E'_{AE} = \frac{1}{10} C_e C_m \omega_i D_i N_{r_b} r F_r \left[\frac{A_{ci} N_{ai} \int_{d_i}^{\infty} (z-d_i) \emptyset(z)_i \mathrm{dz} \int_{d_i}^{\infty} \emptyset(z)_i \mathrm{dz}}{(r'_i)^{1/2} \int_{d_i}^{\infty} (z-d_i)^{1/2} \emptyset(z)_i \mathrm{dz}} + \frac{A_{co} N_{ao} \int_{d_o}^{\infty} (z-d_0) \emptyset(z)_o \mathrm{dz} \int_{d_0}^{\infty} \emptyset(z)_o \mathrm{dz}}{(r'_0)^{1/2} \int_{d_o}^{\infty} (z-d_o)^{1/2} \emptyset(z)_o \mathrm{dz}} \right] \tag{5.24}$$

where, C_e is the part of the total elastic strain energy, mentioned in Eq. (5.23), which alters into AE pulses and C_m is the part which is received by the AE sensors/AE measurement instruments.

Hence, the total elastic strain energy accumulated by the AE sensor/AE instrument during the specific duration ΔT is given by [as mentioned by Eq. (2.28)]

$$E_{AE} = \int_0^{\Delta T} E'_{AE} \mathrm{dt} \tag{5.25}$$

If $V(t)$ is the electrical signal which has been measured, the total energy of the AE signals is given by [as mentioned by Eq. (2.29)]

$$E_{AE'} = \int_0^{\Delta T} V^2(t)\, \mathrm{dt} \tag{5.26}$$

It may be noted that the energy given in Eqs. (5.25) and (5.26) will be equal.

The rms value of AE signal during the specific duration ΔT of AE signal is described by [as mentioned by Eq. (2.30)]

$$V_{\mathrm{rms}} = \sqrt{\frac{1}{\Delta T} \int_0^{\Delta T} V^2(t)\, \mathrm{dt}} \tag{5.27}$$

Using Eqs. (5.25), (5.26), and (5.27), the rms value of AE signal is expressed as follows:

$$V_{\mathrm{rms}} = \sqrt{\frac{1}{\Delta T} \int_0^{\Delta T} E'_{AE} \mathrm{dt}} \tag{5.28}$$

Substituting Eq. (5.24) into Eq. (5.28), the rms value of the AE signal energized by the asperity interactions during the bearing operation is expressed as follows:

$$V_{\text{rms}} = \left[\frac{1}{\Delta T}\int_0^{\Delta T}\frac{1}{10}C_e C_m \omega_i D_i N_{r_b} r F_r \left[\frac{A_{ci}N_{ai}\int_{d_i}^{\infty}(z-d_i)\phi(z)_i\mathrm{dz}\int_{d_i}^{\infty}\phi(z)_i\mathrm{dz}}{(r'_i)^{1/2}\int_{d_i}^{\infty}(z-d_i)^{1/2}\phi(z)_i\mathrm{dz}} + \frac{A_{co}N_{ao}\int_{d_o}^{\infty}(z-d_0)\phi(z)_o\mathrm{dz}\int_{d_0}^{\infty}\phi(z)_o\mathrm{dz}}{(r'_0)^{1/2}\int_{d_o}^{\infty}(z-d_o)^{1/2}\phi(z)_o\mathrm{dz}}\right]\mathrm{dt}\right]^{1/2}$$

(5.29)

The rate of elastic strain energy released by asperities deformation (E'_T) will be constant and accordingly the energy rate of the AE (E'_{AE}) will also be constant, if the relative motion between the elements of bearing is steady during the bearing operation for particular contact load, rotational speed and particular bearing specification, characteristics of surface of bearing elements. Hence, by Eq. (5.29), the relationship between AE rms and the bearing operational parameters based on elastic asperity contact is specified as follows:

$$V_{\text{rms}} = \left[\frac{1}{10}C_e C_m \omega_i D_i N_{r_b} r F_r \left[\frac{A_{ci}N_{ai}\int_{d_i}^{\infty}(z-d_i)\phi(z)_i\mathrm{dz}\int_{d_i}^{\infty}\phi(z)_i\mathrm{dz}}{(r'_i)^{1/2}\int_{d_i}^{\infty}(z-d_i)^{1/2}\phi(z)_i\mathrm{dz}} + \frac{A_{co}N_{ao}\int_{d_o}^{\infty}(z-d_0)\phi(z)_o\mathrm{dz}\int_{d_0}^{\infty}\phi(z)_o\mathrm{dz}}{(r'_0)^{1/2}\int_{d_o}^{\infty}(z-d_o)^{1/2}\phi(z)_o\mathrm{dz}}\right]\right]^{1/2}$$

(5.30)

Define,$C_c = \left[\frac{1}{10}C_e C_m\right]^{1/2}$, Eq. (5.30) is expressed as follows:

$$V_{\text{rms}} = C_c\left[\omega_i D_i N_{r_b} r F_r \left[\frac{A_{ci}N_{ai}\int_{d_i}^{\infty}(z-d_i)\phi(z)_i\mathrm{dz}\int_{d_i}^{\infty}\phi(z)_i\mathrm{dz}}{(r'_i)^{1/2}\int_{d_i}^{\infty}(z-d_i)^{1/2}\phi(z)_i\mathrm{dz}} + \frac{A_{co}N_{ao}\int_{d_o}^{\infty}(z-d_0)\phi(z)_o\mathrm{dz}\int_{d_0}^{\infty}\phi(z)_o\mathrm{dz}}{(r'_0)^{1/2}\int_{d_o}^{\infty}(z-d_o)^{1/2}\phi(z)_o\mathrm{dz}}\right]\right]^{1/2} \quad (5.31)$$

It can be noted from Eq. (5.31) that the value of AE rms is proportional to the contact load and rotational velocity of inner ring or shaft and it can be determined by topographic characteristics of the surface of bearing elements i.e. inner race, outer race, rolling element and specifications/profile of bearing.

5.2.1 Influence of contact load distribution during the load zone

The contact load between rolling elements and races are unequally distributed in the load zone for a rolling element bearing due to its geometry. The asperity interaction is the phenomenon which is related to local contact mechanics and the actual applied load for the deformation of asperities will be different during the contact between rolling element and raceways due to load distribution in the load zone. Hence, the value of AE generated due to deformation of asperities by the specific load at particular local contact will vary in the load zone. The model is extended by considering the influence of load distribution in the load zone of bearing.

The radial load, F_r, radial clearance, Δ_r, and angular speed of inner ring or shaft, ω_i, influence the internal load distribution of rolling element bearing. The theoretical radial contact load, F_ψ, received by each rolling element at angle ψ during the loading zone $[-\psi_l,\ \psi_l]$, as shown in Fig. 5.3, is expressed as follows [134,135]:

$$F_\psi = F_{\max}\left(1 - \frac{1}{2\epsilon}(1 - \cos\psi)\right)^{3/2} \tag{5.32}$$

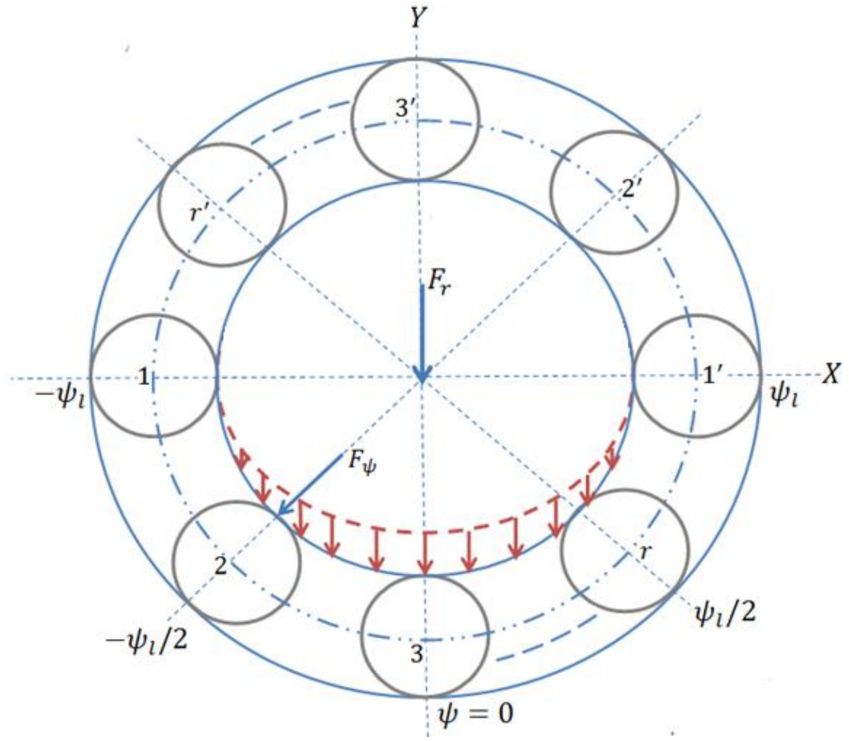

Fig. 5.3 Radial load distribution for $\epsilon = 0.5$, $\Delta_r = 0$ [135]

The Eq. (5.32) estimates the fraction of the total radial load which acts between a race and rolling element at the localized contact point at angle ψ.

where, $F_{\max}$ is the maximum load (at $\psi = 0$) and expressed as follows [134, 135]:

$$F_{\max} = \frac{F_r}{N_e J_r(\epsilon)} \tag{5.33}$$

where N_e is the total number of rolling elements in bearing and $J_r(\epsilon)$ indicates the radial integral evaluated at ϵ, which is evaluated by the following expression [134, 135]:

$$J_r(\epsilon) = \frac{1}{2\pi}\int_{-\psi_l}^{\psi_l}\left(1 - \frac{1}{2\epsilon}(1 - \cos\psi)\right)^{3/2} \cos\psi \, \mathrm{d}\psi \tag{5.34}$$

and ϵ is the dimensionless load parameter which defines the state of load in rolling element bearing and given as follows [134, 135]:

$$\epsilon = \frac{1}{2}\left(1 - \frac{\Delta_r}{\delta_r}\right) \tag{5.35}$$

where, Δ_r and δ_r are radial clearance and radial shift respectively in the rolling element bearing. The value of ϵ defines the number of rolling elements to be loaded and rest of rolling elements to lose contact with raceways. In the present modelling, the value of ϵ is considered as 0.5 (Δ_r= 0), hence load is distributed on half of the rolling elements during the loading zone i.e. [$-\psi_l$,ψ_l] as shown in Fig. 5.3.

If the load distribution in the load zone is taken into consideration, the load at the local contact of asperities will be as per the Eq. (5.32) as described above. Hence, the energy rate of the AE generated by deformation of asperities of local contact due to load, F_ψ, for the particular rolling element and races contact is expressed as follows by using Eq. (5.24):

$$E'_{AE_\psi} = \frac{1}{10} C_e C_m \omega_i D_i N_{r_b} F_\psi \left[\frac{A_{ci} N_{ai} \int_{d_i}^{\infty} (z-d_i)\emptyset(z)_i \mathrm{dz} \int_{d_i}^{\infty} \emptyset(z)_i \mathrm{dz}}{(r'_i)^{1/2} \int_{d_i}^{\infty} (z-d_i)^{1/2} \emptyset(z)_i \mathrm{dz}} + \frac{A_{co} N_{ao} \int_{d_o}^{\infty} (z-d_0)\emptyset(z)_o \mathrm{dz} \int_{d_0}^{\infty} \emptyset(z)_o \mathrm{dz}}{(r'_0)^{1/2} \int_{d_o}^{\infty} (z-d_o)^{1/2} \emptyset(z)_o \mathrm{dz}} \right] \tag{5.36}$$

It is clear from Eqs. (5.32) and (5.36), the value of AE will vary in the load zone. The total elastic energy rate evaluation in the load zone of bearing is calculated by summation of AE generated in the load zone by a rolling element and AE generated in the load zone by its complementary element (i.e. rolling element opposite to each other) as shown in Fig. 5.3.

Hence, the total rms value of the generated AE is calculated as follows by using Eq. (5.36):

$$V_{rms(F)} = \left[\frac{1}{\psi_T} \left[\int_{-\psi_l}^{\psi_l} \left[\left(E'_{AE_\psi} \right)_1 \right] d\psi + \int_{\psi_l}^{-\psi_l} \left[\left(E'_{AE_\psi} \right)_{1'} \right] d\psi + \int_{-\psi_l/2}^{\psi_l} \left[\left(E'_{AE_\psi} \right)_2 \right] d\psi + \int_{-\psi_l/2}^{-\psi_l} \left[\left(E'_{AE_\psi} \right)_{2'} \right] d\psi + \int_{0}^{\psi_l} \left[\left(E'_{AE_\psi} \right)_3 \right] d\psi + \int_{-\psi_l}^{0} \left[\left(E'_{AE_\psi} \right)_{3'} \right] d\psi + \int_{\psi_l/2}^{\psi_l} \left[\left(E'_{AE_\psi} \right)_4 \right] d\psi + \int_{\psi_l/2}^{-\psi_l} \left[\left(E'_{AE_\psi} \right)_{4'} \right] d\psi + \cdots upto\ r^{th}\ element \right] \right]^{1/2} \tag{5.37}$$

where, $\left(E'_{AE_\psi} \right)_1$ and $\left(E'_{AE_\psi} \right)_{1'}$ are the energy rate of AE generated by deformation of asperities during contact between races and rolling element number 1 and $1'$ respectively as shown in Fig. 5.3. Similarly, $\left(E'_{AE_\psi} \right)_2$ and $\left(E'_{AE_\psi} \right)_{2'}$, $\left(E'_{AE_\psi} \right)_3$ and $\left(E'_{AE_\psi} \right)_{3'}$, and upto r^{th} rolling element are also defined as shown in Fig. 5.3.

It is also noted that the contact load at an angle ψ, F_ψ, is transferred from the inner ring to outer ring by rolling element, consequently, the fraction of this load, xF_ψ , will occur between outer race and rolling element at the localized contact point at angle ψ. Where, x is the fractional constant.

Hence, for the static equilibrium of a rolling element bearing, the total rms value of the generated AE is expressed as follows by using

Eqs. (5.32), (5.33), (5.36), and (5.37) and simple rule of definite integral:

$$V_{\mathrm{rms(F)_b}} = C_c\left[\frac{1}{\psi_T}\left[\int_{-\psi_l}^{\psi_l}\left[\frac{\omega_i D_i N_{r_b} r F_r\left(1-\frac{1}{2\epsilon}(1-\cos\psi)\right)^{3/2}}{N_e J_r(\epsilon)}\left[\frac{A_{ci}N_{ai}\int_{d_i}^{\infty}(z-d_i)\emptyset(z)_i\mathrm{dz}\int_{d_i}^{\infty}\emptyset(z)_i\mathrm{dz}}{(r'_i)^{1/2}\int_{d_i}^{\infty}(z-d_i)^{1/2}\emptyset(z)_i\mathrm{dz}} + \frac{xA_{co}N_{ao}\int_{d_o}^{\infty}(z-d_0)\emptyset(z)_o\mathrm{dz}\int_{d_0}^{\infty}\emptyset(z)_o\mathrm{dz}}{(r'_0)^{1/2}\int_{d_o}^{\infty}(z-d_o)^{1/2}\emptyset(z)_o\mathrm{dz}}\right]\right]\mathrm{d}\psi\right]\right]^{1/2} \tag{5.38}$$

5.2.2 Influence of lubrication

The researchers presented the experimental study in which they explained that the importance of lubrication in AE generation in bearing [136, 137]. In EHL, the thickness of the lubricating film plays an important role in the contact zone for the AE generation due to asperities interaction. In this section, the lubrication effect is presented on the developed model using the theory of load sharing of Johnson and Greenwood [121] for the asperity contact in EHL as mentioned in section 2.2.2 of Chapter-2.

Since, the main source of AE is asperity interactions during bearing operation. The load given by Eq. (2.38) is responsible for the deformation of the asperities and generation of AE accordingly which is the fraction of total radial load held by bearing and it is expressed as follows:

$$p_a = F_r y \tag{5.39}$$

where, y is the fractional constant for the load due to lubrication effect. Hence, if the lubrication effect is considered in the proposed model, the effect on AE due to load shared by asperities is defined as follows using Eqs. (2.38), (5.38), and (5.39):

$$V_{\mathrm{rms(FL)_b}} = C_c\left[\frac{1}{\psi_T}\left[\int_{-\psi_l}^{\psi_l}\left[\frac{\omega_i D_i N_{r_b} r F_r y\left(1-\frac{1}{2\epsilon}(1-\cos\psi)\right)^{3/2}}{N_e J_r(\epsilon)}\left[\frac{A_{ci}N_{ai}\int_{d_i}^{\infty}(z-d_i)\emptyset(z)_i\mathrm{dz}\int_{d_i}^{\infty}\emptyset(z)_i\mathrm{dz}}{(r'_i)^{1/2}\int_{d_i}^{\infty}(z-d_i)^{1/2}\emptyset(z)_i\mathrm{dz}}+\frac{xA_{co}N_{ao}\int_{d_o}^{\infty}(z-d_0)\emptyset(z)_o\mathrm{dz}\int_{d_0}^{\infty}\emptyset(z)_o\mathrm{dz}}{(r'_0)^{1/2}\int_{d_o}^{\infty}(z-d_o)^{1/2}\emptyset(z)_o\mathrm{dz}}\right]\right]\mathrm{d}\psi\right]\right]^{1/2} \quad (5.40)$$

5.2.3 Model of AE for rolling element bearing with defect

The model is extended for the effect of a defect in the load zone of bearing. The defect is considered as detailed in the experimental study for the bearing defect diagnosis by AE conducted by [67] and [70]. In a defected bearing, defects at different locations (inner race, outer race, and rolling element) during the load zone have been shown in Fig. 5.4. The length of defect is l_i, l_o and l_r and width of defect is w_i, w_o and w_r when defect exists on inner race, outer race and rolling element respectively. The angle subtended by the defect on the centre of bearing is $\theta_{d_i}, \theta_{d_0}, \theta_{d_{ri}}$, and $\theta_{d_{r0}}$ when defect exist on inner race, outer race, rolling element when contact with inner race, and rolling element when contact with outer race respectively.

It is clear from the Eq. (5.24); the elastic energy rate of the AE will depend on the topographic characteristics of the surface of bearing elements. If the value of the parameters related to surface changes, the AE will vary accordingly. It is noted that the surface topographic characteristics will be different in the zone of defect due to presence of different surface roughness and protrusions than rest of the surface of bearing elements [67, 70]. The influence of surface roughness in the zone of generated defect is relatively higher than the rest of the asperities or surface roughness of bearing element in generation of AE and the value of parameters of AE vary accordingly [67]. Hence, the total elastic energy rate of the AE can be evaluated by addition of energy rate generated in the zone of defected area and energy rate generated in the rest of the area in bearing.

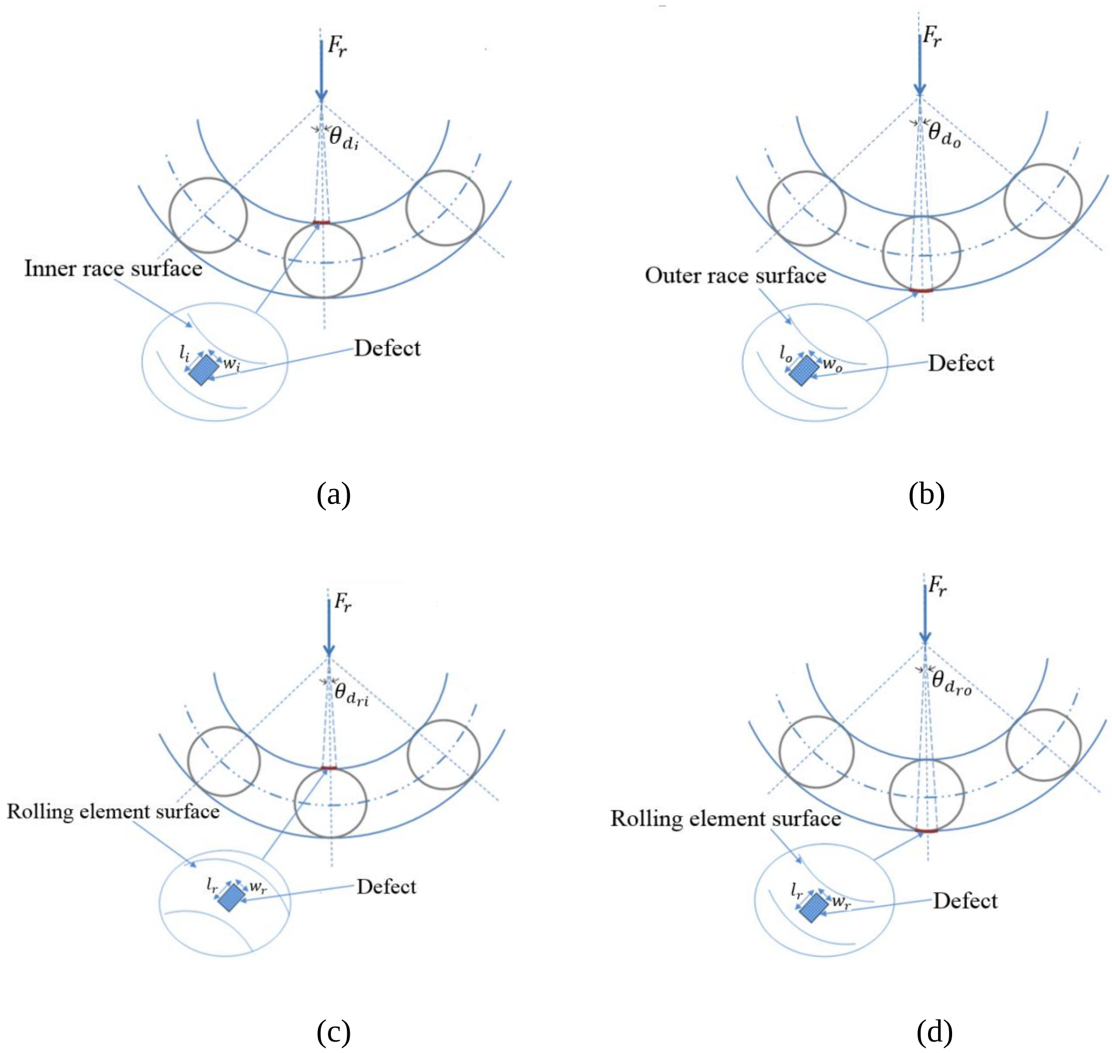

Fig. 5.4 Schematic of rolling element bearing components with an (a) inner race defect (b) outer race defect(c) rolling element defect during contact with inner race (d) rolling element defect during contact with outer race

The total rms value of the generated AE is expressed as follows by incorporating the effect of defect exists on inner race by using Eq. (5.40):

$$V_{rms(FL)_{b_i}} = C_c\left[\frac{1}{\psi_T}\left[\int_{-\psi_l}^{\psi_l}\left[\frac{\omega_i D_i N_{r_b} r F_r y\left(1-\frac{1}{2\epsilon}(1-\cos\psi)\right)^{3/2}}{N_e J_r(\epsilon)}\left[\frac{(A_{ci}-A_{di})\, N_{ai}\int_{d_i}^{\infty}(z-d_i)\emptyset(z)_i dz \int_{d_i}^{\infty}\emptyset(z)_i dz}{(r'_i)^{1/2}\int_{d_i}^{\infty}(z-d_i)^{1/2}\emptyset(z)_i dz} + \frac{x A_{co} N_{ao}\int_{d_o}^{\infty}(z-d_o)\emptyset(z)_o dz \int_{d_o}^{\infty}\emptyset(z)_o dz}{(r'_o)^{1/2}\int_{d_o}^{\infty}(z-d_o)^{1/2}\emptyset(z)_o dz}\right]\right] d\psi + \int_{\psi_{dsi}}^{\psi_{dei}}\left[\frac{\omega_i D_i N_{r_b} r F_r y\left(1-\frac{1}{2\epsilon}(1-\cos\psi)\right)^{3/2}}{N_e J_r(\epsilon)}\left[\frac{A_{di}\, N_{ai_d}\int_{d_{id}}^{\infty}(z-d_{id})\emptyset(z)_{id} dz \int_{d_{id}}^{\infty}\emptyset(z)_{id} dz}{(r'_{id})^{1/2}\int_{d_{id}}^{\infty}(z-d_{id})^{1/2}\emptyset(z)_{id} dz}\right]\right] d\psi\right]\right]^{1/2} \tag{5.41}$$

The total rms value of the generated AE is expressed as follows by incorporating the effect of defect exists on outer race by using Eq. (5.40):

$$V_{rms(FL)_{b_o}} = C_c\left[\frac{1}{\psi_T}\left[\int_{-\psi_l}^{\psi_l}\left[\frac{\omega_i D_i N_{r_b} r F_r y\left(1-\frac{1}{2\epsilon}(1-\cos\psi)\right)^{3/2}}{N_e J_r(\epsilon)}\left[\frac{A_{ci}\, N_{ai}\int_{d_i}^{\infty}(z-d_i)\emptyset(z)_i dz \int_{d_i}^{\infty}\emptyset(z)_i dz}{(r'_i)^{1/2}\int_{d_i}^{\infty}(z-d_i)^{1/2}\emptyset(z)_i dz} + \frac{(A_{co}-A_{do}) x N_{ao}\int_{d_o}^{\infty}(z-d_0)\emptyset(z)_o dz \int_{d_0}^{\infty}\emptyset(z)_o dz}{(r'_o)^{1/2}\int_{d_o}^{\infty}(z-d_o)^{1/2}\emptyset(z)_o dz}\right]\right] d\psi + \int_{\psi_{dso}}^{\psi_{deo}}\left[\frac{\omega_i D_i N_{r_b} r F_r y\left(1-\frac{1}{2\epsilon}(1-\cos\psi)\right)^{3/2}}{N_e J_r(\epsilon)}\left[\frac{x A_{do} N_{ao_d}\int_{d_{od}}^{\infty}(z-d_{0d})\emptyset(z)_{od} dz \int_{d_{od}}^{\infty}\emptyset(z)_{od} dz}{(r'_{od})^{1/2}\int_{d_{od}}^{\infty}(z-d_{od})^{1/2}\emptyset(z)_{od} dz}\right]\right] d\psi\right]\right]^{1/2} \tag{5.42}$$

The total rms value of the generated AE is expressed as follows by incorporating the effect of defect exists on rolling element by using Eq. (5.40):

$$V_{rms(FL)_{b_r}} =$$

$$C_c \left[\frac{1}{\psi_T} \left[\int_{-\psi_l}^{\psi_l} \left[\frac{\omega_i D_i N_{r_b} F_r y \left(1 - \frac{1}{2\epsilon}(1 - \cos\psi)\right)^{3/2}}{N_e J_r(\epsilon)} \left[\frac{(r A_{ci} - A_{dr}(D_i/D_r))\, N_{ai} \int_{d_i}^{\infty} (z - d_i) \emptyset(z)_i dz \int_{d_i}^{\infty} \emptyset(z)_i dz}{(r'_i)^{1/2} \int_{d_i}^{\infty} (z - d_i)^{1/2} \emptyset(z)_i dz} + \right.\right.\right.\right.$$

$$\left.\left. \frac{(r A_{co} - A_{dr}(D_o/D_r)) x N_{ao} \int_{d_o}^{\infty} (z - d_o) \emptyset(z)_o dz \int_{d_0}^{\infty} \emptyset(z)_o dz}{(r'_o)^{1/2} \int_{d_o}^{\infty} (z - d_o)^{1/2} \emptyset(z)_o dz} \right]\right] d\psi +$$

$$\int_{\psi_{dsri}}^{\psi_{deri}} \left[\frac{(D_i/D_r) \omega_i D_i N_{r_b} r F_r y \left(1 - \frac{1}{2\epsilon}(1 - \cos\psi)\right)^{3/2}}{N_e J_r(\epsilon)} \left[\frac{A_{dr}\, N_{ari_d} \int_{d_{rid}}^{\infty} (z - d_{rid}) \emptyset(z)_{rid} dz \int_{d_{rid}}^{\infty} \emptyset(z)_{rid} dz}{(r'_{rid})^{1/2} \int_{d_{rid}}^{\infty} (z - d_{rid})^{1/2} \emptyset(z)_{rid} dz} \right] \right] d\psi +$$

$$\left. \left. \int_{\psi_{dsro}}^{\psi_{dero}} \left[\frac{(D_o/D_r) \omega_i D_i N_{r_b} r F_r y \left(1 - \frac{1}{2\epsilon}(1 - \cos\psi)\right)^{3/2}}{N_e J_r(\epsilon)} \left[\frac{x A_{dr} N_{aro_d} \int_{d_{rod}}^{\infty} (z - d_{rod}) \emptyset(z)_{rod} dz \int_{d_{rod}}^{\infty} \emptyset(z)_{rod} dz}{(r'_{rod})^{1/2} \int_{d_{rod}}^{\infty} (z - d_{rod})^{1/2} \emptyset(z)_{rod} dz} \right] \right] d\psi \right] \right]^{1/2}$$

(5.43)

It can be noted from Eqs. (5.41), (5.42), and (5.43), that the size of defect influences the AE rms energy level which also observed by the experimental investigation conducted by researchers that if the size of defect increases, the AE level also increases.

5.3 Experimental validation of the developed model

To validate the developed AE model of rolling element bearing, experimental data was extracted from the research work performed by Al-Ghamd and Mba [67]. They presented experimental findings on the influence of speed and load in generating AE for operating the radially loaded cylindrical roller bearing. The characteristics of the test bearing (Split Cooper, type 01C/40GR), AE sensor (piezoelectric type) and defects are mentioned in [67]. The experimental findings suggest that change in load and speed condition results in a change in AE rms for the bearing. Typically, AE rms values increase with increasing load, speed and size of defect in bearing. Table 5.1 summarizes the test bearing specifications as prescribed by [67].

Table 5.1: Test bearings specifications

Parameters	**Value**
No. of rolling elements	10
Internal (bore) diameter (mm)	40
External diameter (mm)	84
Diameter of rolling element (mm)	12
Diameter of rolling element centres (pitch diameter) (mm)	66

In order to evaluate the value of AE by the proposed model, the parameters allied with Eqs. (5.40) and (5.42) are determined and prescribed in the Table H.1 of Appendix H. The bearing of same specifications as mentioned in [67] has been considered, inspite of this the surface characteristics may be different. The methodology for the determination of the parameters is same as described in section 2.3.2 of Chapter-2.

The surface topography characteristics of the contact surface of the bearing elements i.e. inner race, outer race and rolling element are determined experimentally by using Marsurf LD 130 which is combined contour and roughness measurement system. The specification of this experimental setup is specified in Appendix A. The surface topography of the bearing elements is measured over an area of 4.0 mm^2 using Marsurf LD 130 as shown in Fig. 2.9 of Chapter-2. The images, depicting the surface topography of the bearing elements, are shown in Fig. 5.5. The surface topography characteristics of the contact surface of the bearing elements consist of the asperity peak density, N_a, asperity peak radius, β, and standard deviation of asperity heights, σ. These surface topography characteristics are determined by using spectral moment method as described by McCool [124] which is detailed in Appendix B1 and MountainsMap_v7 surface imaging topography software. The evaluated values of these surface topography characteristics are mentioned in Table H.1 of Appendix H.

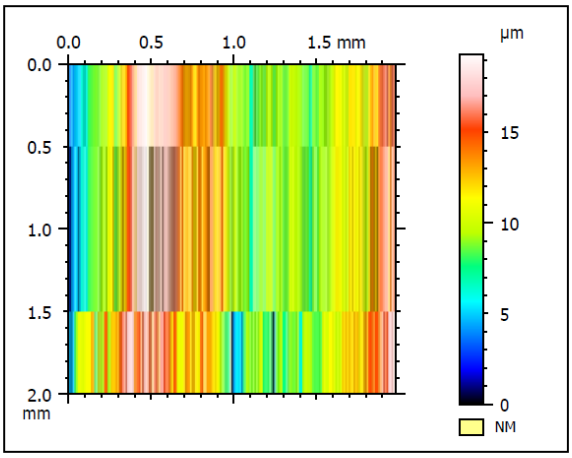

(a)

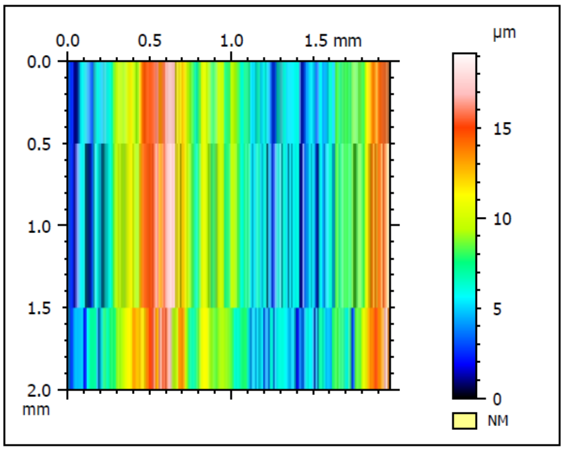

(b)

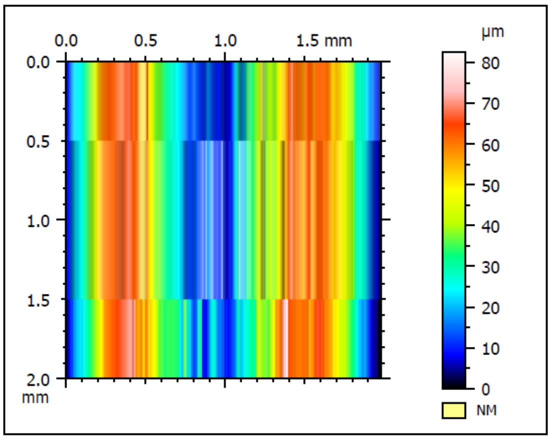

(c)

Fig. 5.5 Surface topography image of test area of surface of (a) inner race (b) outer race (c) defected area of outer race

The distribution of asperity heights is considered as Gaussian distribution and the PDF is prescribed by Eq. (2.44) of Chapter-2.

The total angle of rotation of bearing during load zone is 180°. The values of diameter of inner-race rolling element contact, D_i, and diameter of outer-race rolling element contact, D_o, are determined with the help of test bearings specifications given in Table 5.1. The width of race is considered as 16 mm. The value of dimensionless load parameter, ϵ, is determined by using Eq. (5.35) , by considering the value of radial clearance, Δ_r, as zero. The value of radial integral, $J_r(\epsilon)$, is determined by using Eq. (5.34). These all calculated values are mentioned in Table H.1 of Appendix H.

The separation between smooth surface of rolling element and the reference plane of the mean peak height in the rough surface of inner race and outer race, d_i and d_o respectively, are calculated by using the equations described in [121] and [122] which are detailed in Appendix B3 by putting the values of all concerned parameters which are mentioned in Table H.1 of Appendix H. The value of PDF is calculated by using the Eq. (2.44) by putting the values of all concerned parameters which are mentioned in Table H.1 of Appendix H.

The load shared by asperities for the respective area, p_a, for the different separation condition, d_i and d_o, is calculated by using Eqs. (2.38) and (2.39) by putting the values of all concerned parameters which are mentioned in Table H.1 of Appendix H. The pressure viscosity coefficient of the lubrication is considered as 2.2×10^{-8} m^2/N. The specification of lubrication is mentioned in Table H.1 of Appendix H.

The reduced radius of Hertzian curvature for inner-race rolling element contact, r'_i, and outer race-rolling element contact, r'_0, are calculated by using Eq. (G.6) and (G.7) respectively by putting the values of all concerned parameters which are mentioned in Table H.1 of Appendix H.

It is assumed that the part of the total elastic strain energy which alters into AE pulses, C_e, is 95% and the part which is received by the AE sensors/ AE measurement instruments, C_m , is also 95%. The fractional constant for the contact load at an angle, x, is assumed as

0.95 and fractional constant for the radial load due to lubrication effect, y, is determined by using Eqs. (2.38), (2.39), and (5.39).

5.4 Results and discussion

5.4.1 Results of validation of the model for the influence of load on AE

Al-Ghamd and Mba [67] presented the experimental study for the defect-free condition and defect on the outer race of the bearing. The experimental results for effect of load variation on AE rms values at a constant speed (2000 rpm and 1000 rpm for experiments of bearing with no defect and bearing with defect on outer race respectively) during the test have been given in Table 5.2. With the help of these experimental data, the influence of load on the generation of AE activity is presented in Fig. 5.6 and Fig. 5.7 for healthy bearing and bearing with defect on outer race respectively which illustrates that the increase in load resulted in an increase in AE levels.

The AE is calculated through developed model by putting all values of concerned parameters, given in Table H.1 of Appendix H, at constant speed with different load which is same as experimental investigation. The results of AE rms evaluated by the developed model have been given in Table 5.2. The variation in AE rms for different load condition is illustrated in Fig. 5.6 and Fig. 5.7 for healthy bearing and bearing with defect on outer race respectively. The plot shows that the increase in load results in the increase of AE rms levels.

It can be observed that the AE rms values evaluated by the developed model are close to the AE rms values obtained from experimental investigation under the same conditions.

Table 5.2: The values of AE rms by experimental results [67] and developed model at constant speed

Location of defect in bearing	Load (kN)	AE rms by experimental investigation [67] (V)	AE rms by developed model (V)
No defect	0.1	0.01	0.0087
	4.43	0.0365	0.0311
	8.86	0.0525	0.0462
Defect on outer race	0.1	0.039	0.0334
	4.43	0.052	0.0458
	8.86	0.06	0.0524

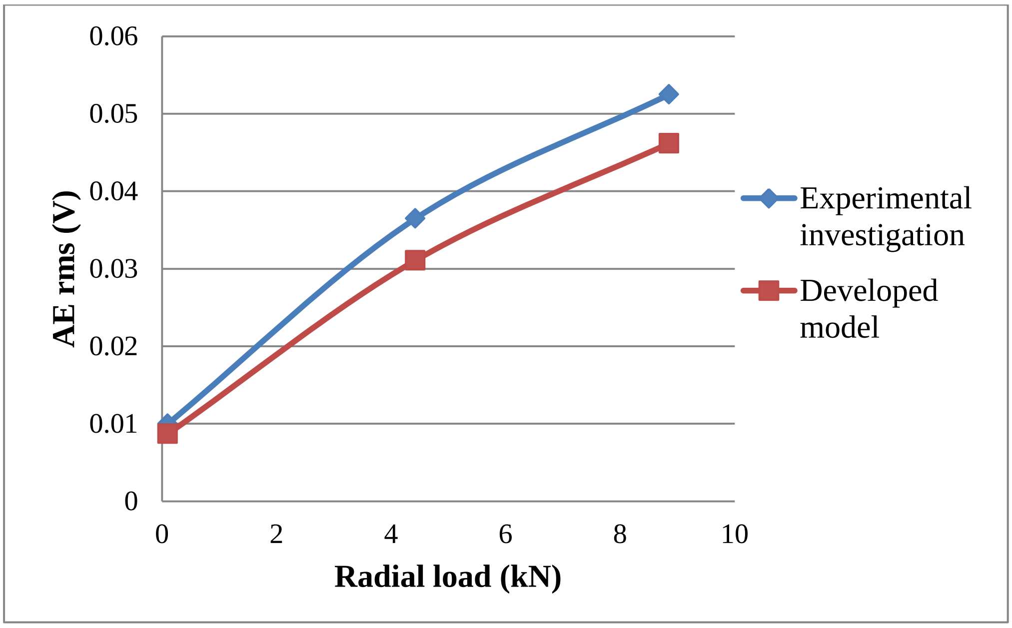

Fig. 5.6 AE rms from bearing with no defect running at different loads by experimental investigation [67] and developed model

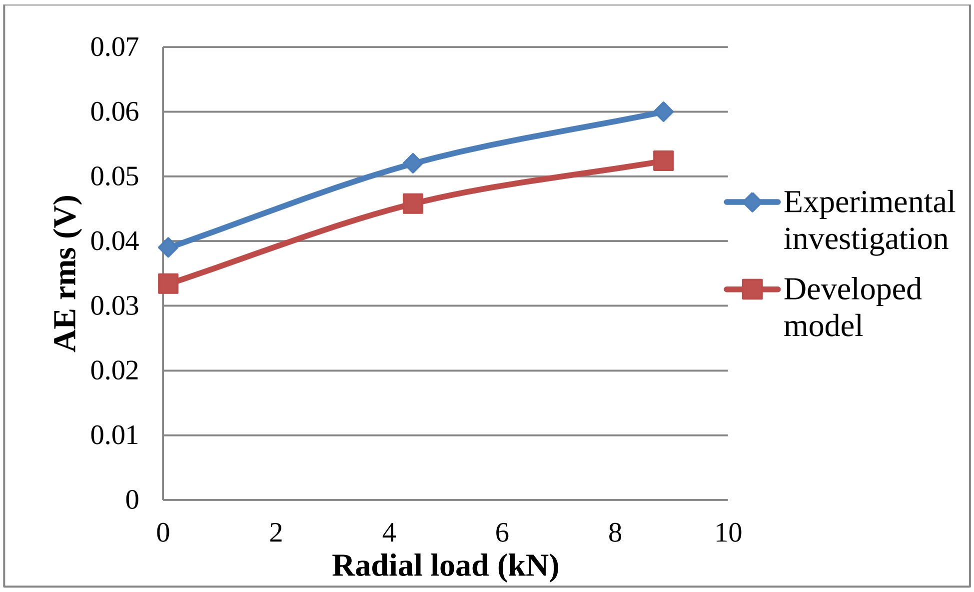

Fig. 5.7 AE rms from bearing with defect on outer race running at different loads by experimental investigation [67] and developed model

5.4.2 Results of validation of the model for the influence of speed on AE

Al-Ghamd and Mba [67] presented the values of AE rms by conducting the experiments for different speed at constant load for the defect-free condition and defect on the outer race of the bearing. The results of an experimental study for effect of rotational speed variation on AE rms values at a constant load (8.86 kN) during the test have been presented in Table 5.3. These data of AE rms and speed from Table 5.5 were used to plot Fig. 5.8 and Fig. 5.9 for healthy bearing and bearing with defect on outer race respectively. The plot shows that the increase in speed results in the increase of AE rms level for roller bearing.

The AE is evaluated through developed model by putting all values of concerned parameters, given in Table H.1 of Appendix H, at constant load with different speeds which is same as experimental investigation. The results of AE rms evaluated by the developed model have been given in Table 5.3. The variation in AE rms for different speed condition is illustrated in Fig. 5.8 and Fig. 5.9 for healthy bearing and bearing with defect on outer race respectively. The plot shows that the increase in speed results in the increase of AE rms levels.

It can be observed that the AE rms values evaluated by the developed model are nearby the AE rms values obtained from experimental investigation under the same conditions.

Table 5.3: The values of AE rms by experimental results [67] and developed model at constant load

Location of defect in bearing	Rotational speed (rpm)	AE rms by experimental investigation [67] (V)	AE rms by developed model (V)
No defect	600	0.0078	0.0067
	1000	0.024	0.0202
	2000	0.057	0.0462
	3000	0.073	0.0649
Defect on outer race	600	0.034	0.0281
	1000	0.062	0.0524
	2000	0.28	0.239
	3000	0.50	0.449

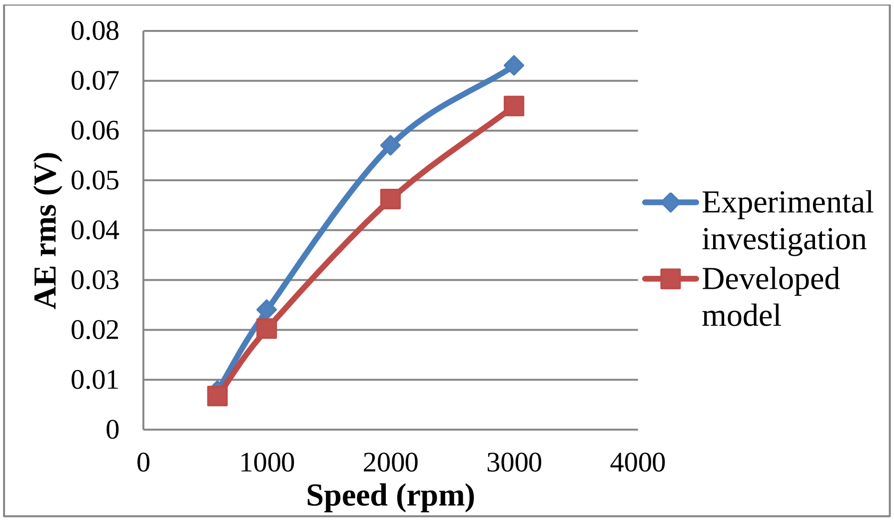

Fig. 5.8 AE rms from bearing with no defect running at different rotational speeds by experimental investigation [67] and developed model

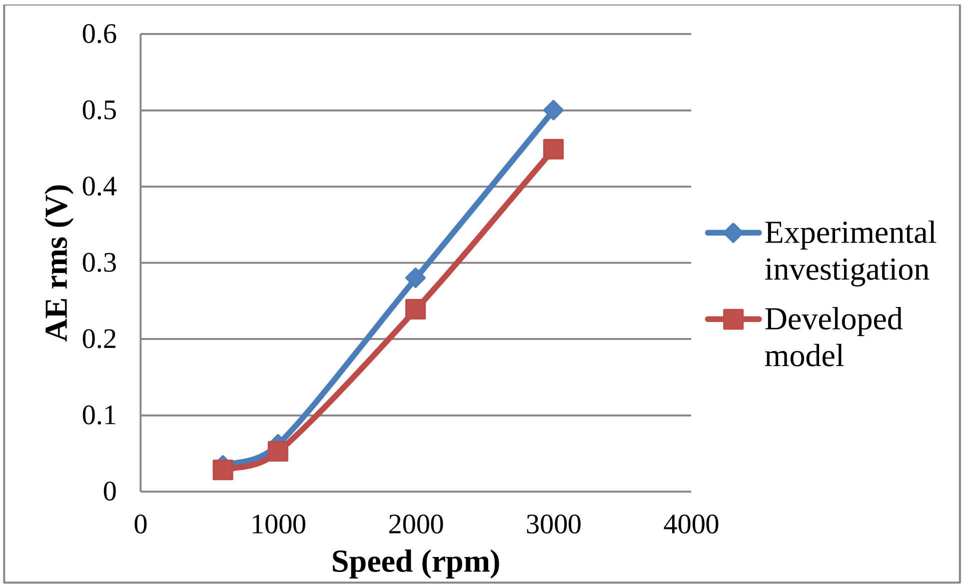

Fig. 5.9 AE rms from bearing with defect on outer race running at different rotational speeds by experimental investigation [67] and developed model

5.5 Summary

Modelling of AE in bearings is very intricate due to various aspects which influence the bearing operation process. Hence, using appropriate assumptions, related to rolling element bearing and asperities deformation process during asperity contact and also based upon experimental studies accomplished by researchers, a mathematical model has been developed to predict the AE engendered by asperity interaction between the surfaces of elements of bearing during bearing operation.

The developed model correlates AE to bearing operating parameters which demonstrates that the level of AE is influenced by the load, rotational speed, defect size, number of asperity contacts, bearing element surface topographic characteristics and specifications/profile of bearing. The model has been developed by considering the effect of contact load distribution in the load zone, lubrication effect, and influence of presence of defect in the load zone which play the vibrant role in generating of the AE during the bearing operation. The developed model was validated on the basis of experimental studies conducted by Al-Ghamd and Mba [67] and satisfactory results have been observed. It shows the potential of the developed model to perceive the AE generated during the bearing operation.

CHAPTER 6

CONCLUSIONS AND SCOPE FOR FUTURE WORK

6.1 Conclusions

The present thesis has accomplished an in-depth research and investigations on the theoretical models of AE generated in spur gear pair and rolling element bearing to identify the physics of generated AE.

In this section, the conclusions of the developed theoretical models of AE generated in spur gear pair and rolling element bearing are discussed. These mathematical models are developed for the healthy spur gear pair, the spur gear pair with crack, the spur gear pair with pitting, and healthy as well as defected rolling element bearing. The conclusions of this research work are summarized as follows:

1. A theoretical model has been developed to predict the AE engendered by asperity interaction between the involute surfaces of gear teeth during mesh in healthy condition. The developed model correlates AE to gear operating parameters i.e. load, speed, number of asperity contacts, gear teeth surface topographic characteristics and specifications/profile of gears.
2. A mathematical model has been developed to predict the AE energy generated from crack propagation in a gear tooth. This model forms the rapport between AE energy and crack parameters in the gear tooth viz. the length of crack propagation, progressive area swept out by the propagating crack, stress intensity, and crack length.
3. A mathematical model has been developed to predict the AE energy, in the presence of defect (pit), engendered by asperities and protrusions interaction between the involute surfaces of

gear teeth during the meshing of gear pair. The developed theoretical model correlates AE to defect size and gear parameters i.e. contact load, rotational speed, gear teeth surface topographic characteristics and specifications of gears.

4. A mathematical model has been developed to measure the AE generated by asperity interaction between the surfaces of bearing elements i.e. inner race, outer race and rolling element of bearing during bearing operation in healthy as well as defected condition. The developed model establishes the relationship between energy of AE and bearing operating parameters i.e. load, rotational speed, number of asperity contacts, bearing element surface topographic characteristics, specifications/profile of bearing, and defect characteristics.

Hence, the overall conclusion is that the proposed mathematical models pronounce the theoretical base to correlate the characteristics of the AE to the operational parameters related to spur gear pair and rolling element bearing. The developed models provide a base to understand the actual mechanism of AE generated during the gear and bearing operation in healthy as well as defected condition. The developed models were validated on the basis of experimental studies and satisfactory results have been observed. It shows the potential of the developed models to perceive the energy of AE generated during the gear and bearing operation which is the significant factor in the condition monitoring of spur gear and rolling element bearing.

6.2 Future work recommendations

There are several related research topics that have not been included in the present thesis, or that they have been simply remarked without performing a deep analysis, which constitutes interesting and promising scope for future work as follows:

- The mathematical modelling of AE generated in helical gear pair may be considered as scope for future work. It is found in the literature that the AE level is different in helical gear pair than spur gear pair. Hence, this modeling will be very useful to understand the physics behind the same.

- The mathematical modelling may be explored for the planetary gears.
- The mathematical modelling of AE generated in thrust bearing is promising research topic.
- The mathematical modelling of AE generated due to various types of defect in gears and bearings such as spall, missing tooth, scuffing, shaft misalignment etc may be considered as future work.

Appendix A

The Marsurf LD 130 is including nanometer range measurements, high measuring and positioning speeds, innovative probe system with bionic probe arm design with magnetic mounting and automatic probe arm recognition. The specification of this experimental setup is as follows:

Table A.1: Specifications of Marsurf LD 130

Resolution	0.8 nm
Start of traversing length (in X)	0.1 mm
End of traversing length (in X)	130 mm
Positioning speed	0.02 mms-1 to 200 mms-1
Measuring speed	0.02 mms-1 to 10 mms-1; For roughness measurements 0.1 mms-1 to 0.5 mms-1 is recommended
Measuring range mm	13 mm (100 mm Tastarm) 26 mm (200 mm Tastarm)
Traversing lengths	0.1 mm - 130 mm or 260 mm
Measuring force (N)	0.5 mN to 30 mN, adjustable

Appendix B

Appendix B1

McCool [124] defined a statistical technique to find out the surface topography characteristics of a three dimensional rough surface which is based on spectral moments i.e. m_o, m_2 and m_4 of a single arbitrary two dimensional trace of the surface. The spectral moments are specified as [124]:

$$m_o = AVG[(z^2)] \tag{B.1}$$

$$m_2 = AVG\left[\left(\frac{\partial z}{\partial x}\right)^2\right] \tag{B.2}$$

$$m_4 = AVG\left[\left(\frac{\partial^2 z}{\partial x^2}\right)^2\right] \tag{B.3}$$

where, $z(x)$ specifies the two dimensional trace of surface heights along the arbitrary x or y direction of the three dimensional rough surface. The surface topography characteristics are evaluated as:

$$N_a = \left(\frac{m_4}{m_2}\right)/6\pi\sqrt{3} \tag{B.4}$$

$$\beta = 0.375\left(\frac{\pi}{m_4}\right)^{0.5} \tag{B.5}$$

$$\sigma = 0.375\left(1 - \frac{0.8968}{\gamma}\right)^{0.5} {m_o}^{0.5} \tag{B.6}$$

where, $\gamma = m_o m_4/{m_2}^2$ is bandwidth parameter.

Appendix B2

The meshing duration of the double/single tooth pair within one mesh period is calculated by using the following equations detailed in [125]:

$$\theta_d = tan\left[arccos\left(\frac{T_1 cos\alpha}{T_1+2}\right)\right] - \frac{2\pi}{T_1} - tan\left[arccos\left(\frac{T_1 cos\alpha}{\sqrt{(T_2+2)^2+(T_1+T_2)^2-2(T_2+2)(T_1+T_2)cos\left(arccos\left(\frac{T_2 cos\alpha}{T_2+2}\right)-\alpha\right)}}\right)\right] \tag{B.7}$$

$$\theta_s = \frac{2\pi}{T_1} - \theta_d \tag{B.8}$$

where, θ_d is the angular displacement during the meshing of two pairs of teeth simultaneously, θ_s is the angular displacement during the meshing of single pair of teeth, T_1 and T_2 are the numbers of teeth of the pinion and the gear respectively.

The total angle of meshing, θ_T, during one mesh period is calculated as follows:

$$\theta_T = 2\theta_d + \theta_s \tag{B.9}$$

Appendix B3

The separation between involute smooth flat surface of gear tooth and the reference plane of the mean peak height in the rough surface of another gear tooth, d, is calculated by using following equations given in [121]:

$$\frac{d}{\sigma} = 1.4\frac{s}{\sigma\prime} - 0.9 \tag{B.10}$$

$$\frac{\bar{h}}{\sigma\prime} = \frac{s}{\sigma\prime} + F_1(s/\sigma') \tag{B.11}$$

$$\sigma \simeq 0.7\sigma' \tag{B.12}$$

To keep simplicity, following relationship is proposed in [121]

$$\frac{s}{\sigma\prime} \simeq \frac{d}{\sigma} \simeq \frac{\bar{h}}{\sigma\prime} \tag{B.13}$$

where, $\bar{h}$ is the oil film thickness between the actual two rough surfaces, s is the separation between the contacting smooth surface and the reference plane of mean level of the surface, and σ' is the standard deviation of surface

The oil film thickness, $\bar{h}$, in the EHD regime is calculated by using following equation given in [122]

$$\frac{\bar{h}}{R_e} = \frac{1.95(\eta_0 U\alpha_0)^{8/11}(E_e)^{1/11}}{(R_e)^{7/11}(P_l)^{1/11}} \tag{B.14}$$

where, η_0 is the viscosity of lubricant

U is the rolling velocity and given as, $U = \frac{U_1+U_2}{2}$

α_0 is the pressure viscosity coefficient

R_e is the effective radius and given as, $R_e = \frac{1}{\frac{1}{R_1}+\frac{1}{R_2}}$

E_e is the effective modulus of elasticity and given as,

$$E_e = \frac{1}{\frac{1}{2}\left(\frac{1-\nu_1{}^2}{E_1} + \frac{1-\nu_2{}^2}{E_2}\right)}$$

P_l is the load per unit length

Appendix B4

The theoretical length of line of action of involute gear pair, AB, path of approach, AX, path of recess, XB, (referring to the Fig. 2.3), and simple mathematical equations of sine law and cosine law are given as follows:

$$\mathrm{AB} = \mathrm{AX} + \mathrm{XB} =$$

$$\sqrt{(R_a)^2 - (R_1)^2 cos^2\varphi} + \sqrt{(R_b)^2 - (R_2)^2 cos^2\varphi} - (R_1 + R_2) sin\varphi \quad \text{(B.15)}$$

where, R_1= pitch circle radius of pinion, R_2= pitch circle radius of gear, R_a= addendum circle radius of pinion, R_b = addendum circle radius of gear.

$$\frac{sinA}{a} = \frac{sinB}{b} = \frac{sinC}{c} \quad \text{(B.16)}$$

$$a^2 = b^2 + c^2 - 2bc.cosA \quad \text{(B.17)}$$

where, a, b, c are the sides of triangle and A, B, C are the opposite angles of respective side of the triangle.

Appendix C

Table C.1: The parameters of the developed model of AE generated in involute spur gear pair

Name of parameter	Value	Name of parameter	Value
Gear type	Standard involute spur teeth	$LSF_{LPSTC(1)}$	1
Material	Steel	$LSF_{HPSTC(1)}$	1
μ	1.4 µm	$\theta_{HPDTC'(1)}$	24°
σ	0.2 µm	$\theta_{TD(1)}$	36.9359°
β	400.0 µm	$LSF_{HPDTC'(1)}$	0.67
N_a	40×10^7 asperities/m^2	$LSF_{TD(1)}$	0.33
θ_T	36.9359°	$\theta_{TE(3)}$	0°
k_v	1.1537	$\theta_{HPDTC(3)}$	12.9359°
R_1	37.5 mm	$LSF_{TE(3)}$	0.33
R_2	40.0 mm	$LSF_{HPDTC(3)}$	0.67
φ	20°	$N_{T_{(1EH)}}$	7.2471×10^3
AB	21.9946 mm	$N_{T_{(2HD)}}$	7.2471×10^3
AX	11.0612 mm	$N_{T_{(1LH)}}$	6.1911×10^3
XB	10.9335 mm	$N_{T_{(1HD)}}$	7.2471×10^3
Lubricant type	Mobilgear 627	$N_{T_{(3EH)}}$	7.2471×10^3

ρ at 15.6°C	0.89 Kg/l	$\Delta r'_{(1EH)}$	8.6411e-11 m
η_0 at 40°C	100 cSt	$\Delta r'_{(2HD)}$	2.0778e-10 m
η_0 at 100°C	12 cSt	$\Delta r'_{(1LH)}$	1.8709e-10 m
α_0	2.2× 10^{-8} m^2/N	$\Delta r'_{(1HD)}$	2.0778e-10 m
τ	44.0°C	$\Delta r'_{(3EH)}$	8.6411e-11 m
$d_{(10.78\ \mathrm{Nm})}$	0.504 µm	$r_{1TE(1)}$	0.03528 m
$d_{(26.95\ \mathrm{Nm})}$	0.465 µm	$r_{1HPDTC(1)}$	0.03639 m
$d_{(53.9\ \mathrm{Nm})}$	0.437 µm	$r_{1HPDTC(2)}$	0.03905 m
$d_{(64.68\ \mathrm{Nm})}$	0.430 µm	$r_{1TD(2)}$	0.04250 m
$d_{(80.85\ \mathrm{Nm})}$	0.421 µm	$r_{1LPSTC(1)}$	0.03639 m
$d_{(107.8\ \mathrm{Nm})}$	0.411 µm	$r_{1HPSTC(1)}$	0.03905 m
$p_{a_{(d=0.505\ \mu m)}}$	8.3880 N	$r_{1HPDTC'(1)}$	0.03905 m
$p_{a_{(d=0.465\ \mu m)}}$	15.7856 N	$r_{1TD(1)}$	0.04250 m
$p_{a_{(d=0.437\ \mu m)}}$	24.0980 N	$r_{1TE(3)}$	0.03528 m
$p_{a_{(d=0.430\ \mu m)}}$	26.7195 N	$r_{1HPDTC(3)}$	0.03639 m
$p_{a_{(d=0.421\ \mu m)}}$	30.4689 N	$\alpha_{TE(1)}$	0°
$p_{a_{(d=0.411\ \mu m)}}$	35.1878 N	$\alpha_{HPDTC(1)}$	12.9359°
$\theta_{TE(1)}$	0°	$\alpha_{HPDTC(2)}$	24°
$\theta_{HPDTC(1)}$	12.9359°	$\alpha_{TD(2)}$	36.9359°
$LSF_{TE(1)}$	0.33	$\alpha_{LPSTC(1)}$	12.9359°

$LSF_{HPDTC(1)}$	0.67	$\alpha_{HPSTC(1)}$	24°
$\theta_{HPDTC(2)}$	24°	$\alpha_{HPDTC'(1)}$	24°
$\theta_{TD(2)}$	36.9359°	$\alpha_{TD(1)}$	36.9359°
$LSF_{HPDTC(2)}$	0.67	$\alpha_{TE(3)}$	0°
$LSF_{TD(2)}$	0.33	$\alpha_{HPDTC(3)}$	12.9359°
$\theta_{LPSTC(1)}$	12.9359°	C_e	0.95
$\theta_{HPSTC(1)}$	24°	C_m	0.95

Appendix D

Appendix D1

Abersek and Flasker [128] detailed the expression of shape factor of cracked gear tooth for bending, $Y_m(\alpha_c)$, and extension , $Y_t(\alpha_c)$, as follows:

$$Y_t(\alpha_c) = 1.1215 - 0.231\alpha_c + 10.55(\alpha_c)^2 - 21.72(\alpha_c)^3 + 30.39(\alpha_c)^4 \tag{D.1}$$

$$Y_m(\alpha_c) = Y_t(\alpha_c) - 3.6\alpha_c(0.333 + 0.066m_1 + 0.0286m_2) \tag{D.2}$$

$$m_1 = \frac{1}{Y_t(\alpha_c)}[2\alpha Y'_t(\alpha_c) + 8.33Y^*_t(\alpha_c)] - 4 \tag{D.3}$$

$$m_2 = 5.554Y_t(\alpha_c) - \frac{1}{Y_t(\alpha_c)}\left[13.884Y^*_t(\alpha_c) + \frac{10}{3}\alpha_c Y'_t(\alpha_c)\right] + \frac{5}{3} \tag{D.4}$$

$$Y^*_t(\alpha_c) = 0.6289 - 0.17248\alpha_c + 5.9213(\alpha_c)^2 - 10.705(\alpha_c)^3 + 31.568(\alpha_c)^4 - 67.476(\alpha_c)^5 + 139.13(\alpha_c)^6 - 146.68(\alpha_c)^7 + 92.355(\alpha_c)^8 \tag{D.5}$$

where, $\alpha_c = \frac{a}{S}$

Appendix D2

Tian [125] has detailed the equation for total effective mesh stiffness for each pair of meshing teeth as follows:

$$k_{t,i} = \frac{1}{\frac{1}{k_{h,i}}+\frac{1}{k_{b1,i}}+\frac{1}{k_{s1,i}}+\frac{1}{k_{a1,i}}+\frac{1}{k_{b2,i}}+\frac{1}{k_{s2,i}}+\frac{1}{k_{a2,i}}} \quad , \ i = 1, 2 \tag{D.6}$$

where, $i = 1$, for the first pair of meshing teeth when there are two pairs of teeth meshing, $i = 2$, for the second pair.

For the single-tooth-pair meshing duration, the total effective mesh stiffness, when cracked tooth exists on the pinion, can be calculated from the following equation as given by Tian [125]:

$$k_{t_{crack}} = \frac{1}{\frac{1}{k_h}+\frac{1}{k_{b_{crack}}}+\frac{1}{k_{s_{crack}}}+\frac{1}{k_{a_1}}+\frac{1}{k_{b_2}}+\frac{1}{k_{s_2}}+\frac{1}{k_{a_2}}} \tag{D.7}$$

For the double-tooth-pair meshing duration, the total effective mesh stiffness can be calculated from the following equation as given by Tian [125]:

$$k_t = \sum_{i=1}^{2} \frac{1}{\frac{1}{k_{h,i}}+\frac{1}{k_{b1,i}}+\frac{1}{k_{s1,i}}+\frac{1}{k_{a1,i}}+\frac{1}{k_{b2,i}}+\frac{1}{k_{s2,i}}+\frac{1}{k_{a2,i}}} \tag{D.8}$$

where, $i = 1$ for the first pair of meshing teeth when cracked tooth exists on the pinion and $i = 2$ for the second pair.

In above mentioned Eqs., k_h is Hertzian-contact stiffness, k_b is bending stiffness, k_s is shear stiffness and k_a is axial compressive stiffness. These all stiffness can be calculated by following equations as given by Tian [125]:

$$k_h = \frac{\pi EB}{4(1-\nu^2)} \tag{D.9}$$

$$\frac{1}{k_b} = \int_{-\alpha_1}^{\alpha_2} \frac{3[1+\cos\alpha_1\{(\alpha_2-\alpha)sin\alpha-cos\alpha\}]^2(\alpha_2-\alpha)\cos\alpha}{2EB[\sin\alpha+(\alpha_2-\alpha)\cos\alpha]^3} d\alpha \tag{D.10}$$

$$\frac{1}{k_s} = \int_{-\alpha_1}^{\alpha_2} \frac{1.2(1+\nu)(\alpha_2-\alpha)\cos\alpha(\cos\alpha_1)^2}{EB[\sin\alpha+(\alpha_2-\alpha)\cos\alpha]} d\alpha \tag{D.11}$$

$$\frac{1}{k_a} = \int_{-\alpha_1}^{\alpha_2} \frac{(\alpha_2-\alpha)\cos\alpha(\sin\alpha_1)^2}{2EB[\sin\alpha+(\alpha_2-\alpha)\cos\alpha]} d\alpha \tag{D.12}$$

$$\frac{1}{k_{b_{crack}}} = \int_{-\alpha_1}^{\alpha_2} \frac{12[1+\cos\alpha_1\{(\alpha_2-\alpha)sin\alpha-cos\alpha\}]^2(\alpha_2-\alpha)\cos\alpha}{EB\left[\sin\alpha_2-\frac{q}{R_{b1}}\sin\nu+\sin\alpha+(\alpha_2-\alpha)\cos\alpha\right]^3} d\alpha \tag{D.13}$$

$$\frac{1}{k_{s_{crack}}} = \int_{-\alpha_1}^{\alpha_2} \frac{2.4(1+\nu)(\alpha_2-\alpha)\cos\alpha(\cos\alpha_1)^2}{EB\left[\sin\alpha_2-\frac{q}{R_{b1}}\sin\nu+\sin\alpha+(\alpha_2-\alpha)\cos\alpha\right]} d\alpha \tag{D.14}$$

$$\alpha_2 = \frac{\pi}{2T_1} + inv\emptyset \tag{D.15}$$

$$\alpha'_2 = \frac{\pi}{2T_2} + inv\emptyset \tag{D.16}$$

$$\alpha_{1,1} = \theta_1 - \frac{\pi}{2T_1} - inv\emptyset + tan\left[arccos\left(\frac{T_1 cos\emptyset}{\sqrt{(T_2+2)^2+(T_1+T_2)^2-2(T_2+2)(T_1+T_2)cos\left(arccos\left(\frac{T_2 cos\emptyset}{T_2+2}\right)-\emptyset\right)}}\right)\right] \tag{D.17}$$

$$\alpha'_{1,1} = tan\left[arccos\left(\frac{T_2 cos\emptyset}{T_2+2}\right)\right] - \frac{\pi}{2T_2} - inv\emptyset - \frac{T_1}{T_2}\theta_1 \tag{D.18}$$

$$\alpha_{1,2} =$$

$$\theta_1 + \frac{3\pi}{2T_1} - inv\emptyset +$$

$$tan\left[arccos\left(\frac{T_1 cos\emptyset}{\sqrt{(T_2+2)^2+(T_1+T_2)^2-2(T_2+2)(T_1+T_2)cos\left(arccos\left(\frac{T_2 cos\emptyset}{T_2+2}\right)-\emptyset\right)}}\right)\right] \quad \text{(D.19)}$$

$$\alpha'_{1,2} = tan\left[arccos\left(\frac{T_2 cos\emptyset}{T_2+2}\right)\right] - \frac{5\pi}{2T_2} - inv\emptyset - \frac{T_1}{T_2}\theta_1 \quad \text{(D.20)}$$

where, E, is the Young's modulus, ν is the Poisson's ratio, v is intersection angle between the crack and the central line of the tooth, q is the depth of crack which exists at the root of the pinion, R_{b1} is the radius of base circle of pinion, α_2 and α'_2 are the half tooth angles on the base circle of the pinion and the gear, respectively. $\alpha_{1,1}$ and $\alpha'_{1,1}$ are the corresponding to the angle α_1 of the pinion and gear for the first pair of meshing teeth respectively, $\alpha_{1,2}$ and $\alpha'_{1,2}$ are the corresponding to the angle α_1 of the pinion and gear for the second pair of meshing teeth respectively, θ_1 is the angular displacement of the pinion.

Appendix E

Table E.1: The parameters of the developed model of AE generated by crack propagation in spur gear

Name of parameter	Value	Name of parameter	Value
Gear type	Standard involute spur teeth	θ_{LPSTC}	8.6027°
Material	Steel	θ_{HPSTC}	13.3334°
θ_T	21.9360°	LSF_{LPSTC}	1
R_1	54.0 mm	LSF_{HPSTC}	1
R_2	62.0 mm	$\theta_{HPDTC'}$	13.3334°
$\emptyset$	20°	θ_{TD}	21.9360°
E	228GPa	$LSF_{HPDTC'}$	0.67
B	10.0 mm	LSF_{TD}	0.33
S	5.9043 mm	Load,P,	16.9 kN
R_b	50.7434 mm	Module, m,	4 mm
θ_{TE}	0°	c_1	7.2519 $\mathrm{mm}^2/\mathrm{Nsec}^2$
θ_{HPDTC}	8.6027°	t_c	0.95
LSF_{TE}	0.33	N	50/min
LSF_{HPDTC}	0.67	C_e, C_m	0.95, 0.95

Table E.2: The values of total effective mesh stiffness for various crack length

Crack length (mm)	Crack propagation length (mm)	total effective mesh stiffness during double-tooth-pair meshing 10^8 N/m	total effective mesh stiffness during single-tooth-pair meshing 10^8 N/m
1.6	0.0009407	8.110,7.694	4.819
1.8	0.001109	8.101,7.596	4.767
2.0	0.00147	8.091,7.494	4.719
2.2	0.00175	8.076,7.390	4.658
2.4	0.00195	8.067,7.284	4.605
2.6	0.00210	8.029,7.175	4.534

Appendix F

Table F.1: The parameters of the developed model of AE generated due to pitting on spur gear

Name of parameter	Value	Name of parameter	Value
Gear type	Standard involute spur teeth	$\mathrm{LSF}_{\mathrm{HPDTC}'(1)}$	0.67
Material	Steel	$LSF_{TD(1)}$	0.33
μ	1.38 µm	$\theta_{TE(3)}$	0°
σ	0.2 µm	$\theta_{HPDTC(3)}$	12.9359°
β	62.0 µm	$LSF_{TE(3)}$	0.33
N_a	260×10^7 asperities/ m^2	$LSF_{HPDTC(3)}$	0.67
θ_T	36.9359°	$r_{1TE(1)}$	35.28 mm
k_v	1.1537	$r_{1HPDTC(1)}$	36.39 mm
R_1	37.5 mm	$r_{1HPDTC(2)}$	39.05 mm
R_2	40.0 mm	$r_{1TD(2)}$	42.50 mm
φ	20°	$r_{1LPSTC(1)}$	36.39 mm
AB	21.9946 mm	$r_{1HPSTC(1)}$	39.05 mm
AX	11.0612 mm	$r_{1DSPSTC(1)}{}_{(D=0.5mm)}$	37.28 mm
XB	10.9335 mm	$r_{1DEPSTC(1)}{}_{(D=0.5mm)}$	37.72 mm
Lubricant type	Mobilgear 627	$r_{1DSPSTC(1)}{}_{(D=1.0mm)}$	37.09 mm
ρ at 15.6°C	0.89 Kg/l	$r_{1DEPSTC(1)}{}_{(D=1.0mm)}$	37.95 mm
η_0 at 40°C	100 cSt	$r_{1DSPSTC(1)}{}_{(D=1.5mm)}$	36.90 mm

η_0 at 100°C	12 cSt	$r_{1DEPSTC(1)}{}_{(D=1.5mm)}$	38.20 mm
α_0	2.2× 10^{-8} m^2/N	$r_{1DSPSTC(1)}{}_{(D=2.0mm)}$	36.72 mm
τ	41.0°C	$r_{1DEPSTC(1)}{}_{(D=2.0mm)}$	38.46 mm
D	0.5,1.0,1.5 ,2.0 mm	$r_{1HPDTC'(1)}$	0.03905 m
$d_{(53.9Nm)}$	0.539 µm ,0.506 µm	$r_{1TD(1)}$	0.04250 m
$\theta_{TE(1)}$	0°	$r_{1TE(3)}$	0.03528 m
$\theta_{HPDTC(1)}$	12.9359°	$r_{1HPDTC(3)}$	0.03639 m
$LSF_{TE(1)}$	0.33	$\alpha_{TE(1)}$	0°
$LSF_{HPDTC(1)}$	0.67	$\alpha_{HPDTC(1)}$	12.9359°
$\theta_{HPDTC(2)}$	24°	$\alpha_{HPDTC(2)}$	24°
$\theta_{TD(2)}$	36.9359°	$\alpha_{TD(2)}$	36.9359°
$LSF_{HPDTC(2)}$	0.67	$\alpha_{LPSTC(1)}$	12.9359°
$LSF_{TD(2)}$	0.33	$\alpha_{HPSTC(1)}$	24°
$\theta_{LPSTC(1)}$	12.9359°	$\alpha_{DSPSTC(1)}{}_{(D=0.5mm)}$	17.5582°
$\theta_{HPSTC(1)}$	24°	$\alpha_{DEPSTC(1)}{}_{(D=0.5mm)}$	19.3777°
$LSF_{LPSTC(1)}$	1	$\alpha_{DSPSTC(1)}{}_{(D=1.0\,mm)}$	16.6485°
$LSF_{HPSTC(1)}$	1	$\alpha_{DEPSTC(1)}{}_{(D=1.0\,mm)}$	20.2875°
$\theta_{DSPSTC(1)}{}_{(D=0.5mm)}$	17.5582°	$\alpha_{DSPSTC(1)}{}_{(D=1.5mm)}$	15.7387°
$\theta_{DEPSTC(1)}{}_{(D=0.5mm)}$	19.3777°	$\alpha_{DEPSTC(1)}{}_{(D=1.5mm)}$	21.1972°
$\theta_{DSPSTC(1)}{}_{(D=1.0\,mm)}$	16.6485°	$\alpha_{DSPSTC(1)}{}_{(D=2.0\,mm)}$	14.8290°
$\theta_{DEPSTC(1)}{}_{(D=1.0\,mm)}$	20.2875°	$\alpha_{DEPSTC(1)}{}_{(D=2.0\,mm)}$	22.1070°
$\theta_{DSPSTC(1)}{}_{(D=1.5mm)}$	15.7387°	$\alpha_{HPDTC'(1)}$	24°
$\theta_{DEPSTC(1)}{}_{(D=1.5mm)}$	21.1972°	$\alpha_{TD(1)}$	36.9359°
$\theta_{DSPSTC(1)}{}_{(D=2.0\,mm)}$	14.8290°	$\alpha_{TE(3)}$	0°
$\theta_{DEPSTC(1)}{}_{(D=2.0\,mm)}$	22.1070°	$\alpha_{HPDTC(3)}$	12.9359°

$LSF_{DSPSTC(1)}{}_{(D=0.5,1.0,1.5,2.0\ mm)}$	1	C_e	0.95
$LSF_{DEPSTC(1)}{}_{(D=0.5,1.0,1.5,2.0\ mm)}$	1	C_m	0.95
$\theta_{HPDTC'(1)}$	24°	$z_d{}_{(D=0.5,1.0,1.5,2.0\ mm)}$	0.05,0.06,0.08,0.105 mm
$\theta_{TD(1)}$	36.9359°	$S_{(D=0.5,1.0,1.5,2.0\ mm)}$	0.21,0.22,0.28,0.32 mm

Appendix G

1. The probability of making contact at any particular asperity of height, z, during inner-race rolling element contact and outer-race rolling element contact is expressed as follows:

$$P\ (z > d_i) = \int_{d_i}^{\infty} \emptyset(z)_i \mathrm{dz} \tag{G.1}$$

$$P\ (z > d_o) = \int_{d_o}^{\infty} \emptyset(z)_o \mathrm{dz} \tag{G.2}$$

2. The stored elastic energy (E_e) for the asperities contact between the surfaces of inner-race rolling element and outer-race rolling element can be given by:

$$E_e = \int F_r \mathrm{d}\delta \tag{G.3}$$

3. Expression for δ_i and δ_o are given as follows:

$$\delta_i = \left(\frac{9{F_r}^2}{16E'^2 {r'}_i}\right)^{1/3} \tag{G.4}$$

$$\delta_o = \left(\frac{9{F_r}^2}{16E'^2 {r'}_o}\right)^{1/3} \tag{G.5}$$

4. Expression for ${r'}_i$ and ${r'}_o$ are given as follows:

$$\frac{1}{{r'}_i} = \frac{1}{r_b} + \frac{1}{r_{si}} \tag{G.6}$$

$$\frac{1}{{r'}_o} = \frac{1}{r_b} + \frac{1}{r_{so}} \tag{G.7}$$

where, r_{si} and r_{so} are radii of spherical asperity for inner-race rolling element contact and outer-race rolling element contact respectively and r_b is the radius of rolling element during asperity contact.

5. Expression for E' is given as follows:

$$\frac{1}{E'} = \frac{1-{\nu_1}^2}{E_1} + \frac{1-{\nu_2}^2}{E_2} \tag{G.8}$$

E_1, E_2, are the Yong's modulus and ν_1, ν_2, are the Poisson's ratios of the materials of races (inner race/outer race) and rolling element respectively.

Appendix H

Table H.1: The parameters of the developed model of AE generated in rolling element bearing

Name of parameter	Value	Name of parameter	Value
D_i	54 mm	N_{ai}	240×10^7 asperities/m^2
D_o	78 mm	μ_i	1.70 μm
D_e	66 mm	σ_i	0.20 μm
D_r	12 mm	β_i	65.0 μm
ψ_T	180°	N_{ao}	220×10^7 asperities/m^2
ψ_l	90°	μ_o	1.76 μm
$-\psi_l$	- 90°	σ_o	0.21 μm
N_r	0.5	β_o	78.0 μm
r	5	N_{ao_d}	320×10^7 asperities/m^2
ϵ	0.5	μ_{od}	4.7 μm
N	10	σ_{od}	0.23 μm
r_b	6 mm	β_{od}	53.0 μm
A_{ci}	1357.71 mm^2	A_{do}	157.5 mm^2
A_{co}	1961.14 mm^2	ψ_{dso}	0°
Lubricant type	Exxon Ronex MP	ψ_{deo}	14.45°
η_0 at 40°C	115 cSt	C_e	0.95
α_0	2.2×10^{-8} m^2/N	C_m	0.95

REFERENCES

[1] Miller R.K., Hill E.V.K., Moore P.O., (2005) Non-destructive testing handbook, Acoustic emission testing, vol. 6. 3rd ed. American Society for Non-destructive Testing, Columbus, USA.

[2] Pao Y.H., Gajewski R.R., Ceranoglu A.N., (1979) Acoustic emission and transient waves in an elastic plate, J. Acoust. Soc. Am., 65(1), 96-105.

[3] Tandon N., Choudhury A., (1999) A review of vibration and acoustic measurement methods for the detection of defects in rolling element bearings, Tribology International, 32, 469-480.

[4] Condition monitoring and diagnostic of machines, (2007) Acoustic emission-general guidelines, ISO22096.

[5] Loutas T.H., Roulias D., Pauly E., Kostopoulos V., (2011) The combined use of vibration, acoustic emission and oil debris on-line monitoring towards a more effective condition monitoring of rotating machinery, Mechanical Systems and Signal Processing, 25, 1339-1352.

[6] Mba D., Bannister R.H., (1999) Condition monitoring of low-speed rotating machinery using stress waves: Part 1 and Part 2, Proceedings of the Institute of Mechanical Engineers, 213 (Part E), 153-185.

[7] Holroyd T., Randall N., (1993) The use of acoustic emission for machine condition monitoring, British Journal of Non-Destructive Testing, 35 (2), 75-78.

[8] Mba D., (2001) The detection of shaft-seal rubbing in large-scale turbines using acoustic emission, In: Proceedings of the 14th International Congress on Condition Monitoring and Diagnostic Engineering Management (COMADEM'2001), Manchester, UK, pp. 21-28, ISBN:0080440363.

[9] Mba D., (2002) Applicability of acoustic emissions to monitoring the mechanical integrity of bolted structures in

low speed rotating machinery: case study, NDT and E International, 35 (5), 293-300.

[10] Mba D., Cooke A., Roby D., Hewitt G., (2003) Opportunities offered by acoustic emission for shaft-seal rubbing in power generation turbines; a case study sponsored by the British Institute of NDT, In: Proceedings of the International Conference on Condition Monitoring, Oxford, UK, pp. 280-286, ISBN:1901892174.

[11] Rao R.B.K.N., Mba D., (2006) Development of acoustic emission technology for condition monitoring and diagnosis of rotating machines: bearings, pumps, gearboxes, engines, and rotating structures, Shock Vib Dig, 38, 3-16.

[12] Qu Y., He D., Yoon J., Van H.B., Bechhoefer E., and Zhu J., (2014) Gearbox tooth cut fault diagnostics using acoustic emission and vibration sensors - A comparative study, Sensors,14, 1372-1393.

[13] Qu Y., Van H.B., He D., Yoon J., Bechhoefer E., and Zhu J., (2013) Gearbox fault diagnostics using AE sensors with low sampling rate, Journal of Acoustic Emission, 31, 67- 90.

[14] Prieto S., (2006) A Bearing test-rig for extreme operating conditions, MsC thesis, School of Mechanical Engineering, Cranfield University.

[15] Tan C.K., Mba D., (2005) Identification of the acoustic emission source during a comparative study on diagnosis of a spur gearbox, Tribology International, 38, 469-480.

[16] Toutountzakis T., Mba D., (2003) Observations of acoustic emission activity during gear defect diagnosis, NDT&E International, 36, 471-477.

[17] Hamzah R.I., Mba D., (2009) The influence of operating condition on acoustic emission (AE) generation during meshing of helical and spur gear, Tribology International, 42, 3-14.

[18] Tan C.K., Irving P., Mba D., (2007) A comparative experimental study on the diagnostic and prognostic

capabilities of acoustic emission, vibration and spectrometric oil analysis for spur gears, Mechanical Systems and Signal Processing, 21, 208-233.

[19] Tandon N., Mata S., (1999) Detection of defects in gears by acoustic emission measurements, J. Acoustic Emission, 19, 23-27.

[20] Tan C., Mba D., (2005) Correlation between acoustic emission activity and asperity contact during meshing of spur gears under elastohydrodynamic lubrication, Ttibol. Lett., 20, 63-67.

[21] Hamzah R.I., Mba D., (2007) Acoustic emission and specific film thickness for operating spur gears, Journal of Tribology, 129, 860-867.

[22] Vicuna C.M., (2014) Effects of operating conditions on the acoustic emissions (AE) from planetary gearboxes, Applied Acoustics, 77, 150-158.

[23] Eftekharnejad B., Mba D., (2009) Seeded fault detection on helical gears with acoustic emission, Applied Acoustics, 70, 547-555.

[24] Hamzah R.I., Al-Balushi K.R., Mba D., (2008) Observations of acoustic emission under conditions of varying specific film thickness for meshing spur and helical gears, Journal of Tribology, 130, 021506-1-12.

[25] Hamel M., Addali A., Mba D., (2014) Investigation of the influence of oil film thickness on helical gear defect detection using acoustic emission, Applied Acoustics, 79, 42-46.

[26] Boness R.J., McBride S.L., Sobczyk M., (1990) Wear studies using acoustic emission techniques, Tribology International, 23, 291-295.

[27] Boness R.J., McBride S.L., (1991) Adhesive and abrasive wear studies using acoustic emission techniques, Wear, 149, 41-53.

[28] Benabdallah H.S., Aguilar D.A., (2008) Acoustic emission and its relationship with friction and wear for sliding contact,

Tribology Transactions, 51,738-747.

[29] Lingard S., Yu C.W., Yau C.F., (1993) Sliding wear studies using acoustic emission, Wear, 162–164, 597-604.

[30] Hanchi J., Klamecki B.E., (1991) Acoustic emission monitoring of the wear process, Wear, 145, 1-27.

[31] Sun J., Wood R.J.K., Wang L., Care I., Powrie H.E.G., (2005) Wear monitoring of bearing steel using electrostatic and acoustic emission techniques, Wear, 259, 1482-1489.

[32] Price E.D., Lees A.W., Friswell M.I., (2005) Detection of severe sliding and pitting fatigue wear regimes through the use of broadband acoustic emission, J Eng Tribol, I Mech E, Part J, 219, 85-98.

[33] Greenwood J.A., Williamson J.B.P., (1966) Contact of nominally flat surfaces, Proceedings of the Royal Society of London, Series A, 295, 300-319.

[34] Greenwood J.A., Tripp J.H., (1970) The contact of two nominally flat surfaces, Proc. Instn. Mech. Engrs., 185, 625-633.

[35] Gupta P.K., Cook N.H., (1972) Statistical analysis of mechanical interaction of rough surfaces, Journal of Lubrication Technology, Trans. Am. Soc. mech. Engrs., 19-26.

[36] Archard J.F., (1957) Elastic deformation and the laws of friction, Proc. R. Soc. A, 243,190-205.

[37] Archard J.F., (1959) The temperature of rubbing surfaces, Wear, 2, 438-455.

[38] Iwaki A., Mori M., (1958) On the distribution of surface roughness when two surfaces are pressed together, Bull. J.S.M.E., 1, 329-337.

[39] Kimura Y., (1970) Estimation of the number and the mean area of real contact points on the basis of surface profiles, Wear, 15, 47-55.

[40] Ling F.F., (1958) On asperity distributions of metallic surfaces, J. Appl. Phys., 29, 1168-1174.

[41] Mikic B., (1971) Analytical studies of contact of nominally flat surfaces; effect of previous loading, J. Lubric. Technology, Trans. Am. Soc. mech. Engrs., 451-456.

[42] Thomas T.R., Probert S.D., (1970) Establishment of contact parameters from surface profiles, J. Phys. D: Appl. Phys., 3, 277-289.

[43] Whitehouse D.J., Archard J.F., (1970) Properties of random surfaces of significance in their contact, Proc. R. Soc. A., 316, 97-121.

[44] Baranov V.M., Kudryavtsev E.M., Sarychev G.A., (1997) Modelling of parameters of acoustic emission under sliding friction of solids, Wear, 202,125-133.

[45] Fan Y., Gu F., Ball A., (2010) Modelling acoustic emissions generated by sliding friction, Wear, 268, 811-815.

[46] Bosia F., Pugno N., Lacidogna G., Carpinteri A., (2008) Mesoscopic modelling of acoustic emission through an energetic approach, International Journal of Solids and Structures, 45, 5856-5866.

[47] Saini D.P., Park Y.J., (1996) A quantitative model of acoustic emissions in orthogonal cutting operations, Journal of Materials Processing Technology, 58, 343-350.

[48] Rogers L.M., (1979) The application of vibration signature analysis and acoustic emission source location to on-line condition monitoring of anti-friction bearings, Tribol Int., 12(2), 51-59.

[49] Yoshioka T., Fujiwara T., (1982) A new acoustic emission source locating system for the study of rolling contact fatigue, Wear, 81,183-6.

[50] Yoshioka T., Fujiwara T., (1984) Application of acoustic emission technique to detection of rolling bearing failure, In: Dornfield DA, editor, Acoustic emission monitoring and analysis in manufacturing, ASME, New York, 55-75.

[51] Holroyd T.J., Randall N., (1993) Use of acoustic emission for machine condition monitoring, British Journal of Non-

Destructive Testing, 35 (2), 75-78.

[52] Mathews J.R., (1983) Acoustic Emission, Gordon and Breach Science Publishers Inc., New York, (ISSN0730-7152).

[53] Tandon N., Nakra B.C., (1990) Defect detection in rolling element bearings by acoustic emission method, J Acoustic Emission, 9(1), 25-8.

[54] Kakishima H., Nagatomo T., Ikeda H., Yoshioka T., Korenaga A., (2000) Measurement of acoustic emission and vibration of rolling bearings with an artificial defect, QR of RTRI, 41(3),127-130.

[55] Smith J.D., (1982) Vibration monitoring of bearings at low speeds, Tribol Int., 139-144.

[56] McFadden P.D., Smith J.D., (1984) Acoustic emission transducer for the vibration monitoring of bearings at low speeds, Proc IMechE, 198(C8), 127-130.

[57] Bansal V., Gupta B.C., Prakash A., Eshwar V.A., (1990) Quality inspection of rolling element bearing using acoustic emission technique, J Acoustic Emission, 9(2),142-146.

[58] Tan C.C., (1990) Application of acoustic emission to the detection of bearing failures, In: Proceedings, Tribology Conference, Institution of Engineers, Brisbane, Australia, 110-114.

[59] Yoshioka T., (1992) Detection of rolling contact subsurface fatigue cracks using acoustic emission technique, J Soc Tribol Lubr Eng, 49(4), 303-308.

[60] Elforjani M., Mba D., (2008) Monitoring the onset and propagation of natural degradation process in a slow speed rolling element bearing with acoustic emission, Journal of Vibration and Acoustics, 130(4),041013-1-14.

[61] Elforjani M., Mba D., (2009) Natural mechanical degradation measurements in slow speed bearings, Engng Fail Anal., 16(I), 521-32.

[62] Elforjani M., Mba D., (2010) Accelerated natural fault diagnosis in slow speed bearings with Acoustic Emission,

Engineering Fracture Mechanics, 77, 112-127.
[63] Bagnoli S., Capitani R., Citti P., (1988) Comparison of accelerometer and acoustic emission signals as diagnostic tools in assessing bearing damage, In: Proceedings of 2nd International Conference on Condition Monitoring, London, p.p.117-25.
[64] Tavakoli M.S., (1991) Bearing fault detection in the acoustic emission frequency range, In: Proceedings of Noise Conference, USA: INCE, p.p.79-86.
[65] Hawman M.W., Galinatis W.S., (1988) Acoustic emission monitoring of rolling element bearings, In: Proceedings of Ultrasonic Symposium, IEEE, p.p.885-9.
[66] Smulders A., Loob C., (1994) Machine condition monitoring using multi-parameter measurement, In: Proceedings of Condition Monitoring and Diagnostic Engineering Management Conference, New Delhi, p.p.147-53.
[67] Al-Ghamd A.M., Mba D., (2006) A comparative experimental study on the use of acoustic emission and vibration analysis for bearing defect identification and estimation of defect size, Mech. Syst. Signal Process, 20,1537-1571.
[68] Choudhury A., Tandon N., (2000) Application of acoustic emission technique for the detection of defects in rolling element bearings, Tribology International, 33, 39-45.
[69] Al-Dossary S., Hamzah R.I., Mba D., (2009) Observations of changes in acoustic emission waveform for varying seeded defect sizes in a rolling element bearing, Applied Acoustics, 70, 58-81.
[70] Morhain A., Mba D., (2003) Bearing defect diagnosis and acoustic emission, Journal of Engineering Tribology, Institution of Mechanical Engineering, 217(4) (Part J), 257-272.
[71] Mba D., (2003) Acoustic emissions and monitoring bearing health, Tribology Transactions, 46(3), 447-451.

[72] Mba D., (2008) The use of acoustic emission for estimation of bearing defect size, J Fail. Anal. And Preven., 8,188-192.

[73] Mirhadizadeh S.A., Moncholi E.P., Mba D., (2010) Influence of operational variables in a hydrodynamic bearing on the generation of acoustic emission, Tribol. Int., 43, 1760-1767.

[74] Harsha S.P., Nataraj C., Kankar P.K., (2006) The effect of ball waviness on nonlinear vibration associated with rolling element bearings, International Journal of Acoustics and Vibrations, 11 (2), 56-66.

[75] Kankar P.K., Sharma S.C., Harsha S.P., (2012) Nonlinear vibration signature analysis of a rotor bearing system due to race imperfections, Journal of Computational Nonlinear Dynamics, 7 (1), 011014.

[76] Bhavaraju K.M., Kankar P.K., Sharma S.C., Harsha S.P., (2010) A comparative study on bearings faults classification by artificial neural networks and self-organizing maps using wavelets, International Journal of Engineering Science and Technology, 2 (5),1001-1008.

[77] Toutountzakis T., Tan C. K., Mba D., (2005) Application of acoustic emission to seeded gear fault detection, NDT&E International, 38, 27-36.

[78] Elforjani M., Mba D., Muhammad A., Sire A., (2012) Condition monitoring of worm gears, Applied Acoustics, 73, 859-863.

[79] Singh A., Houser D.R., Vijayakar S., (1996) Early detection of gear pitting, power transmission and gearing conference, ASME DE-vol. 88, 673-8.

[80] Sentoku H., (1998) AE in tooth surface failure process of spur gears, J Acoust Emission,16(1-4), S19-S24.

[81] Siores E., Negro A.A., (1997) Condition monitoring of a gear box using acoustic emission testing, Mater Eval, 183-7.

[82] Scruby C.B., (1987) An introduction to acoustic emission, Journal of Physics E: Scientific Instruments, 20(8), 946.

[83] Gerberich W.W., Hartbower C.E., (1967) Some observations

on stress wave emission as a measure of crack growth, Int. J. Fract. Mech., 3(3), 185-92.

[84] Singh A., Houser D.R., Vijayakar S., (1999) Detecting gear tooth breakage using acoustic emission: a feasibility and sensor placement study, Journal of Mechanical Design, 121,587-93.

[85] Sentoku H., Tokuda T., (1995) AE in bending fatigue process of carburizing spur gears, Transactions of the Japan Society of Mechanical Engineers Series C, 61 (582), 417-21.

[86] Sentoku H., Yamato H., (1997) AE source location in bending fatigue process of carburizing spur gear, Transactions of the Japan Society of Mechanical Engineers Series C, 63 (611), 2526-31.

[87] Pullin R., Clarke A., Eaton M.J., Holford K.M., Evans S.L., McCory J. P., (2010) Detection of cracking in gear teeth using acoustic emission, Applied Mechanics and Materials, 24-25, 45-50.

[88] Obata Y., Kobayashi H., Aoki K.I., (1989) Evaluation of fatigue crack growth rate of carburized gear by acoustic emission technique, Journal of Acoustic Emission, 8 (1-2),5145-48. Special Supplement - Extended Summaries of Papers to be presented at the World Meeting on Acoustic Emission, Charlotte, North Carolina, USA, 1989.

[89] Miyachika K., Oda S., Koide T., (1995) Acoustic emission of bending fatigue process of spur gear teeth, Journal of Acoustic Emission,13, 47-53.

[90] Masuyama T., Inoue K., Kato M., (1994) Acoustic emission during fatigue crack growth in carburized gear tooth, Nippon Kikai Gakkai Ronbunshu, C Hen/Transactions of the Japan Society of Mechanical Engineers, Part C, 60(575), 2456-61.

[91] Moriwaki T., (1980) Detection for cutting tool fracture by acoustic emission measurement, Annals of the CIRP, 29(1), 35-40.

[92] Yu J., Ziehl P., Zarate B., Caicedo J., (2011) Prediction of fatigue crack growth in steel bridge components using acoustic emission, Journal of Constructional Steel Research, 67, 1254-60.

[93] Elforjani M., Mba D., (2009) Detecting natural crack initiation and growth in slow speed shafts with the acoustic emission technology, Engineering Failure Analysis, 16, 2121-29.

[94] Raad A., Zhang F., Randall B., Sidahmed M., (2003) On the comparison of the use of AE and vibration analysis for early gear fault detection, In: Proceedings of the 8th Western Pacific Acoustics Conference, Melbourne, Australia.

[95] Yu J., Ziehl P. , Zarate B., Caicedo J., (2011) Prediction of fatigue crack growth in steel bridge components using acoustic emission, Journal of Constructional Steel Research, 67, 1254-1260.

[96] Sinclair A.C.E., Connors D.C.C., (1977) Acoustic emission analysis during fatigue crack growth in steel, Materials Science and Engineering, 28, 263-73.

[97] Ohira T., Kishi T., Horiuchi R., (1980) Acoustic emission during fatigue crack propagation in structural materials, International Acoustic Emision Symposium, 5, 137-45.

[98] Kohn D.H., Ducheyne P., Awerbuch J., (1992) Acoustic emission during fatigue of TI-6AL-4V incipient fatigue crack detection limits and generalized data analysis methodology, Journal of Materials Science, 27, 3133-42.

[99] Bassim M.N., Lawrence S.S., Liu C.D., (1994) Detection of the onset of fatigue crack growth in rail steels using acoustic emission, Engineering Fracture Mechanics, 47(2), 207-14.

[100] Berkovits A., Fang D., (1995) Study of fatigue crack characteristics by acoustic emission, Engineering Fracture Mechanics, 51(3), 401-16.

[101] Oh K.H., Jung C.K., Yang Y.C., Han K.S., (2004) Acoustic emission behavior during fatigue crack propagation in 304

stainless steel, Key Engineering Materials, 261-263,1325-30.

[102] Chen H.L., Choi J.H., (2004) Acoustic emission study of fatigue cracks in materials used for AVLB, Journal of Nondestructive Evaluation, 23(4), 133-51.

[103] Choi J., Luo J.J., Daniel I.M., (2000) Analysis of acoustic emission waveforms from propagating fatigue crack, Review of Progress in Quantitative Nondestructive Evaluation, 19, 351-8.

[104] Lysak M.V., (1996) Development of the theory of acoustic emission by propagating cracks in terms of fracture mechanics, Engineering Fracture Mechanics, 55(3), 443-52.

[105] Diei E.N., Dornfeld D.A., (1987) A model of tool fracture generated acoustic emission during machining, J. Manuf. Sci. Eng., 109, 227-33.

[106] Desai J.D., Gerberich W.W., (1975) Analysis of incremental cracking by the stress-wave emission technique, Engineering Fracture Mechanics, 7 (1), 153-65.

[107] Malen K., Bolin L., (1974) A theoretical estimate of acoustic emission stress amplitudes, Phys. Stat. Sol. B, 61, 637-45.

[108] Ono K., (1979) Acoustic emission arising from plastic deformation and fracture, Fundamentals of Acoustic Emission, K. Ono, ed., University of California, Los Angeles,168-207.

[109] Sano K., Fujimoto K., (1979) Microscopic aspects of fracture and acoustic emission in metals, Fundamentals of Acoustic Emission, K. Ono, ed., University of California, Los Angeles, 131- 64.

[110] Harris D.Q., Dunegan H.L., (1974) Continuous monitoring of fatigue-crack growth by acoustic-emission techniques, Experimental Mechanics, 14, 71-81.

[111] Lindley T.C., Palmer I.G., Richards C.E., (1978) Acoustic emission monitoring of fatigue crack growth, Materials Science and Engineering, 32, 1-15.

[112] Ebeling C.E., (2013) An Introduction to Reliability and

Maintainability Engineering, 16th ed., McGraw Hill Education, New Delhi, India.

[113] Bhushan B., (2001) Modern Tribology Handbook, CRC Press LLC, Florida, USA.

[114] Maugis D., (2000) Contact, Adhesion and Rupture of Elastic Solid, Springer, New York.

[115] Johnson K. L., (1985) Contact Mechanics, Cambridge University Press, Cambridge.

[116] Litvin F.L., Fuentes A., (2004) Gear Geometry and Applied Theory, 2nd ed., Cambridge University Press, New York.

[117] Dooner D.B., (2012) Kinematic Geometry of Gearing, 2nd ed., John Wiley & Sons, United Kingdom.

[118] Sfantos G.K., Spitas V.A., Costopoulos T.N., Papadopoulos G.A., (2003) Load sharing of spur gears in mesh an analytical and experimental study, Technical Report, National Tech. Univ. Athens, No. TR-SM-0303.

[119] Spitas V., Papadopoulos G.A., Spitas C., Costopoulos T., (2009) Experimental investigation of load sharing in multiple gear tooth contact using the stress-optical method of caustics, Strain,1-7.

[120] American national standard, (1988) Fundamental rating factors and calculation methods for involute spur and helical gear teeth, American Gear Manufacturers Association (AGMA) Standard, ANSI/AGMA 2001-B88, 11-14.

[121] Johnson K.L., Greenwood J.A., Poona S.Y., (1972) A simple theory of asperity contact in elastohydrodynamic lubrication, Wear, 19, 91-108.

[122] Seireg A.A., (1998) Friction and Lubrication in Mechanical Design, Marcel Dekker, Inc, New York.

[123] Dowson D., Higginson G.R., (1977) Elastohydrodynamic Lubrication, 1st ed. Pergamon Press, Oxford.

[124] McCool J.I., (1987) Relating profile instrument measurements to the functional performance of rough surfaces, J Tribol., 109(2), 264-70.

[125] Tian X.H., (2004) Dynamic simulation for system response of gearbox including localized gear faults, Master's Thesis, University of Alberta, Edmonton, Alberta, Canada.

[126] Childs P., (2004) Mechanical Design, 2nd ed. Elsevier, Oxford.

[127] Anderson T.L., (2005) Fracture Mechanics: Fundamentals and Applications, CRC Press, Taylor & Francis Group, Boca Raton.

[128] Abersek B., Flasker J., (1994) Stress intensity factor for cracked gear tooth, Theoretical and Applied Fracture Mechanics, 20, 99-104.

[129] Fisher R.M., Lally L.S., (1967) Microplasticity detected by an acoustic technique, Canad. J. Phys., 63(1), 63-81.

[130] Baranov V., Kudryavtsev E., Sarychev G., Schavelin V., (2007) Acoustic Emission in Friction, Elsevier, UK.

[131] Philips G.J., (1979) Bearing performance investigations through speed ratio measurements, ASLE Transactions, 22(4), 307-314.

[132] Harris T.A., (2001) Rolling Bearing Analysis, 4th ed. John Wiley & Sons, Inc., New York (USA).

[133] Hamrock B.J., Anderson W.J., (1983) Rolling Element Bearings, Lewis Research Centre, Ohio, NSA Reference Publication 1105.

[134] Harris T.A., Kotzalas M.N., (2007) Rolling Bearing Analysis: Essential Concepts of Bearing Technology, CRC Press, Taylor & Francis Group, New York.

[135] Machado C., Guessasma M., Bellenger E., (2015) Electromechanical modeling by DEM for assessing internal ball bearing loading, Mechanism and Machine Theory, 92, 338-355.

[136] Miettinen J., Andersson P., (2000) Acoustic emission of rolling bearings lubricated with contaminated grease, Tribology International, 33, 777-787.

[137] Oh H., Azarian M.H., Morillo C., Pecht M., Rhem E., (2015)

Failure mechanisms of ball bearings under lightly loaded, non-accelerated usage conditions, Tribology International, 81, 291-299.

LIST OF PUBLICATIONS

International Journals

1. Sharma R. B., Parey A., Tandon N., Modelling of acoustic emission generated in involute spur gear pair, *Journal of Sound and Vibration*, 393 (2017) 353-373.
2. Sharma R. B., Parey A., Modelling of acoustic emission generated by crack propagation in spur gear, *Engineering Fracture Mechanics*, 182 (2017) 215-228.
3. Sharma R. B., Parey A., Modelling of acoustic emission generated in rolling element bearing, *Applied Acoustics*, (In Press) https://doi.org/10.1016/j.apacoust.2017.07.015.
4. Sharma R. B., Parey A., Modelling of acoustic emission generated due to pitting in spur gear, *Engineering Failure Analysis*, 86 (2018) 1-20.

Conference Proceedings

1. Sharma R. B., Parey A., Condition monitoring of gearbox using experimental investigation of acoustic emission technique, *Procedia Engineering*, 173 (2017) 1575-1579.

International Conferences

1. Sharma R. B., Parey A., A novel technique based on statistical parameters using acoustic emissions for the detection of incipient gear fault, *12thInternational Conference on Vibration Problems*, IIT Guwahati, India, 14-15 December 2015.
2. Sharma R. B., Parey A., Diagnosis of fault advancement in gearbox by application of entropy measures on acoustic emission signal, *6th International Congress on Computational Mechanics and Simulation (ICCMS-2016)*, IIT Bombay, Powai, Maharashtra, India, 27th June-1st July 2016.

3. Sharma R. B., Parey A., Gear fault diagnosis using probability density function and entropy measures for gear acoustic emission signal, *11th International Conference on Vibrations in Rotating Machinery (VIRM-11),* The Institution of Mechanical Engineers, University of Manchester, UK, 13-15 September 2016.
4. Sharma R. B., Parey A., Condition monitoring of gearbox using experimental investigation of acoustic emission technique, *11th International Symposium on Plasticity and Impact Mechanics (IMPLAST-2016),* IIT Delhi, India, 11-14 December 2016.